Space-time dynamics of runoff generation in a snowmelt-dominated montane catchment

by

Russell Smith

A THESIS SUBMITTED IN PARTIAL FULFILLMENT OF
THE REQUIREMENTS FOR THE DEGREE OF

DOCTOR OF PHILOSOPHY

in

The Faculty of Graduate Studies

(Geography)

THE UNIVERSITY OF BRITISH COLUMBIA

(Vancouver)

October 2011

Abstract

Runoff source area dynamics are controlled by the interaction of processes influencing the dynamics of water inputs at the soil surface and processes influencing vertical versus lateral flux partitioning at or below the soil surface coupled with variability in connectivity between runoff generating areas. These issues are investigated for the snowmelt-dominated Cotton Creek Experimental Watershed in southeast British Columbia, Canada. First, the controls on midwinter snowmelt are investigated. Accumulated snowmelt during the midwinter period of 2007 with nearly continuous subzero air temperatures comprised between 3% and 27% of the total snowfall. This, and other circumstantial evidence, supports the hypothesis that soil heat flux generated the midwinter snowmelt. Early-winter soil hydrothermal conditions and midwinter meteorological conditions are important controls on the midwinter melt dynamics. Second, the influences of soil hydraulic conductivity (K_s) and water input dynamics on the formation of transient perched shallow groundwater via percolation-excess processes are investigated. The results suggest that the initiation depth and maximum water table level vary according to and can be predicted by an interplay between the K_s profile and the maximum water input intensity during an event. At sites where K_s does not decrease gradually with depth, water input intensity does not appear to influence the depth of groundwater initiation. Last, seasonal variation in the spatial controls on the occurrence, timing, and persistence of shallow groundwater response are examined. The K_s of the soil at 75 cm depth is a first-order control on the distribution of sites that generate shallow groundwater response versus sites that experience only deep percolation. Upslope contributing area and slope gradient are first-order controls on the persistence of shallow groundwater response during peak flow, recession flow, and low flow periods, and runoff source areas expand and contract throughout these periods according to an interplay between catchment wetness and the spatial patterns of topographic convergence. However, controls on the space-time distribution and rates of snowmelt, and controls on vertical versus lateral flux partitioning in the soil overwhelm the importance of topographic convergence during early spring freshet periods.

Preface

Chapters 3 to 5 of this dissertation were written as independent manuscripts and will be submitted for publication in peer-reviewed journals, but are modified herein to conform to formatting and content requirements and to avoid redundancies. I am the lead author of all three chapters. I led all phases of development for each chapter including conceptualization, designing and implementing the research approach, collecting and analyzing the data, and reporting the results. My supervisors, R. D. (Dan) Moore and Markus Weiler, both provided suggestions and guidance for each of these phases of development, as well as manuscript revision. Other specific contributions from my co-authors are outlined below.

Chapter 3

This chapter was co-authored by Dan Moore, Markus Weiler, Mike Novak, and Dave Gluns. Dan Moore provided guidance for the statistical analyses, Mike Novak conducted the soil heat flux modelling, and Dave Gluns contributed to collection of meteorological data.

Chapter 4

This chapter was co-authored by Dan Moore, Markus Weiler, and Gerald Flerchinger. Gerald Flerchinger developed the Soil Heat and Water (SHAW) model and further modified the model for application in this chapter. He also provided guidance for applying the model.

Chapter 5

This chapter was co-authored by Dan Moore, Markus Weiler, and Georg Jost. Dan Moore provided guidance for the statistical analyses. Georg Jost contributed to designing the research approach and to data collection.

Table of contents

List of tables

List of figures

Acknowledgments

I am grateful to the generous support and contributions from many people in helping this dissertation become realized. First, I would like to thank my supervisors, Dan Moore and Markus Weiler, for their roles in guiding me throughout my PhD and for their keen interest in my work. In particular, I thank Dan Moore for accepting me into the doctoral program at UBC Geography, and Markus Weiler for helping me join the Cotton Creek Experimental Watershed (CCEW) project. I would like to thank Sean Fleming and Roger Beckie for their guiding efforts as members of my research committee. Thanks also to my other co-authors Georg Jost, Dave Gluns, Mike Novak, and Gerald Flerchinger for their valuable contributions to my work.

I would like to give a special thanks to everyone who contributed "hard labour" in the field and the laboratory including Georg Jost, Dave Gluns, Pascal Szeftel, Michelle Sawka, Gerard Lohmann, Ryan Thoren, Nils Illchman, Natalie Stafl, Maria Staudinger, Fabian Nippgen, Nicolas Teichrob, Selina Agbayani, Kyle Terry, Roger Hodson, Stephanie Ewen, Vojtech Prilesky, Andres Varhola, Amy O'Neil, and Dan Moore. Thank you to Marwan Hassan for moral support throughout my PhD. Thanks also to Younes Alila and Kim Green for initiating the CCEW project; to Dianna Allen, Nicholas Coops, Harry Verwoerd, Jerry Maedel, Vincent Kujala, and Julie Ranada for equipment support; to Eric Leinberger for cartographic support; and to Daniel Henke for statistical support.

Thank you to the following partners for providing valuable funding and/or logistical support: Tembec Inc., B.C. Ministry of Forests and Range, Forest Investment Account – Forest Sciences Program (grant nos. Y062294, Y081214), Kalesnikoff Lumber Co. Ltd., Alberta Pacific Forest Industries Inc., Natural Sciences and Engineering Research Council of Canada, Mathematics of Information Technology and Complex Systems Network of Centres of Excellence, Sustainable Forest Management Network, and the University of Zürich.

I extend my thanks to my personal mentors, Rob Scherer and Georg Jost, for guidance and friendship throughout my career as a hydrologist, and to other colleagues for their friendship and support including Klemens Rosin, Pascal Szeftel, Joe Shea, Jason Leach, John Richards, Elisa Scordo, Yeganeh Asadian, Joel Trubilowicz, Bill Floyd, Axel Anderson, Rich McCleary, Kim Green, and the entire H2K group at the University of Zürich.

Last, but not least, I would like to thank my family and friends for their continual interest in my work and their support. In particular, I am forever grateful and indebted to my lovely wife, Laura, for her inexhaustible patience, encouragement, sacrifice, and financial support throughout this arduous doctoral process, and to our wonderful daughter, Erin, who brought so much joy to my life during the most difficult days of this endeavor.

To

Laura and Erin Smith

1 Introduction

Understanding runoff generation processes and streamflow source area dynamics is important for predicting streamflow quantity, quality, and timing, and for assessing the potential impacts of land use and climate changes on water resources [*Beschta et al.*, 2000; *Stewart*, 2009; *Stewart et al.*, 2005]. Stochastic and lumped runoff modelling approaches are widely used for flow prediction; however, these approaches do not provide answers related to source area dynamics and are unable to account for changing initial and boundary conditions influencing runoff generation processes. For these reasons, process-based runoff modelling is necessary to answer more spatially and process-specific questions. Process-based runoff models are built upon a conceptualization of the physical environment that considers both hydrology and geomorphology. Several hydrogeomorphic runoff conceptual models have been developed for rainfall conditions [*Dunne and Black*, 1970a; b; *Freeze*, 1972; *Hewlett and Hibbert*, 1963; 1967; *Sidle et al.*, 2000]; however, water inputs occurring in mountainous catchments are more spatially variable under snowmelt conditions than under rainfall conditions. This added spatial complexity complicates conceptualization of snowmelt runoff processes. In particular, topographic and geologic controls on flow path convergence and hydrologic connectivity (the extent and responsiveness of a laterally contiguous path of hydrologically responsive hillslope) might be of lower importance than meteorological controls on water input patterns in determining runoff source area dynamics during snowmelt [*Boyer et al.*, 1995; 1997; 2000; *Deng et al.*, 1994; *Kuras et al.*, 2008]. As a result, the existing rainfall runoff conceptual models might not appropriately represent snowmelt runoff source area dynamics and cannot be readily applied to snowmelt-dominated mountainous catchments without further development.

Few researchers have empirically investigated hillslope and catchment level runoff source area dynamics resulting from spatially variable snowmelt. Several studies have investigated localized physiographic influences on snow processes and hydrologic response [*Dunne and Black*, 1971; *Harms and Chanasyk*, 1998; *Laudon et al.*, 2004; *Price and Hendrie*, 1983], but these did not investigate, in detail, issues of hillslope

hydrologic connectivity between source areas and streams, and they did not account for the cumulative effects of spatially variable physiography on streamflow dynamics. A few studies have investigated spatio-temporal variability in soil water states and resulting streamflow dynamics under snowmelt conditions [*Grant et al.*, 2004; *McNamara et al.*, 2005; *Monteith et al.*, 2006a; b], but they were conducted at sites with limited topographic variability and spatial extent. Moreover, it appears that only a few studies have investigated the influences of hillslope geomorphic variability on hillslope hydrologic connectivity under snowmelt conditions and within catchments having topographic variability sufficient to generate substantial asynchronous melt [*Deng et al.*, 1994; *Jencso et al.*, 2009; *Kuras et al.*, 2008]. As snowmelt constitutes a much greater source of water supply in temperate regions than does rainfall, there exists a great need to develop an improved conceptualization of snowmelt runoff source area dynamics to not only improve the conceptual understanding, but also to refine process-based numerical representation of snowmelt-dominated hydrologic systems.

The following sections comprise a review of the literature focused on runoff generation in snowmelt-dominated montane catchments to identify key knowledge gaps, which are then used to frame the research objectives. The chapter concludes with an outline of the dissertation.

1.1 Processes controlling runoff source area dynamics

Runoff source area dynamics are controlled by the interaction of processes controlling the space-time variability of water inputs at the soil surface and processes controlling the vertical versus lateral partitioning of water flux at or below the soil surface. The following sections review rainfall and snowmelt water input dynamics, runoff generation mechanisms, and hillslope hydrologic connectivity in an effort to clearly understand each component of the system of processes controlling runoff source area dynamics.

1.1.1 Water inputs

Mountainous topography can significantly influence the spatial distribution of rainfall [*Goodrich et al.*, 1995; *Guan et al.*, 2005; *Linderson*, 2003; *Shoji and Kitaura*, 2006]; however, some studies indicate that the spatial variability of rainfall decreases with increasing event magnitude [*Linderson*, 2003; *Taupin*, 1997], which limits the impact of rainfall distribution on streamflow response. Forest canopies can further increase the spatial variability of rainwater inputs to the soil surface through interception processes, but the spatial scale of variability is small (e.g. <10 m correlation length for throughfall distribution) [*Keim et al.*, 2005; *Staelens et al.*, 2006] and likely averaged in space in terms of its influence on catchment processes. Moreover, its influence quickly diminishes once the canopy interception capacity is reached during an event [*Keim et al.*, 2005; *Molicova and Hubert*, 1994; *Staelens et al.*, 2006]. As a result, the influence of rainfall distribution on runoff source area dynamics is more relevant to large catchments (e.g. >15000 ha based on reported correlation lengths for rainfall distribution of >14 km) [*Guan et al.*, 2005; *Lloyd*, 2005; *Shoji and Kitaura*, 2006].

In contrast to rainfall inputs, snowmelt inputs can exhibit significant and systematic spatial variability, even within an individual hillslope, particularly in continental climatic areas with complex mountainous topography and highly variable snow water equivalent (SWE), vegetation, and meteorological distributions [*Anderton et al.*, 2002; *Carey and Woo*, 2001; *Erxleben et al.*, 2002; *Leydecker et al.*, 2001; *Sommerfeld et al.*, 1994; *Williams et al.*, 1999]. This potentially large variability in the location, timing, intensity, and total volume of water inputs from snowmelt are the primary factors making snowmelt runoff processes different and more complex than rainfall runoff processes, as they introduce issues of hydrologic connectivity between source areas and streams, and issues of synchronization and desynchronization.

The spatio-temporal distribution of snowmelt inputs is controlled by the spatial distribution of snow accumulation coupled with the spatio-temporal distribution of snowpack energy exchanges. Snow accumulation patterns depend on the distribution of

precipitation, incident solar radiation, longwave radiation, air temperature, vapor density gradient, and wind turbulence [*Balk and Elder*, 2000; *Berris and Harr*, 1987; *Cline*, 1997; *Winkler et al.*, 2005], as they determine the amount and form (solid or liquid) of precipitation and the amount of sublimation. During snowmelt, meteorological conditions govern the amounts of melt and sublimation/evaporation by influencing the energy exchanges between the snowpack, underlying soil, and atmosphere. Moreover, the variability in meteorological conditions accumulates through time due to snowpack energy storage and metamorphism. Large spatial variability in these processes causes differential snowmelt amounts, rates, and timing, which vary with the physiographic properties of the landscape, including slope, aspect, elevation, hillslope shading, wind exposure, and vegetation cover [*Balk and Elder*, 2000; *Berris and Harr*, 1987; *Jost et al.*, 2007; *Jost et al.*, 2009; *Toews and Gluns*, 1986; *Winkler et al.*, 2005]. Forest cover, for instance, reduces incoming solar radiation, reduces sensible and latent heat exchanges, increases incoming longwave radiation to the snowpack, and increases sublimation/evaporation via increased canopy interception. In regions where melt is dominated by net radiation, seasonal melt begins earlier and typically occurs at higher rates at sites with high insolation (e.g. south-facing sites in the northern hemisphere) [*Jost et al.*, 2007; *Toews and Gluns*, 1986] and at sites lacking forest cover [*Anderton et al.*, 2002; *Daly et al.*, 2000; *Hock*, 1999; *Marks et al.*, 2002; *Winkler et al.*, 2005]. Where melt is dominated by the turbulent fluxes of sensible and latent heat, open sites with higher wind speeds experience higher melt rates than those with forest cover [*Berris and Harr*, 1987].

1.1.2 Runoff generation mechanisms

The spatial organization and timing of runoff generation mechanisms are also important controls on runoff source area dynamics. The most commonly documented rapid stormflow generation mechanisms in temperate forested catchments include saturation overland flow (including return flow), throughflow from a perched water table, groundwater flow, and preferential flow. Other mechanisms like infiltration-excess overland flow, flow through bedrock, and channel interception can often be reliably

discounted as contributing minimally to stormflow. Soil infiltration capacities in forested areas are almost always too high and water input rates too low to generate infiltration-excess overland flow. Exceptions include disturbed sites such as logging roads and locations where soil freezing reduces the infiltration capacity due to the presence of ice-filled soil pores [*Dunne and Black*, 1971; *Laudon et al.*, 2004; *Stadler et al.*, 1996; *Stein et al.*, 1994]; however, frozen soils often either begin to thaw once the snowpack is sufficiently deep or quickly thaw upon contact with meltwater [*Iwata and Hirota*, 2005; *Lindstrom et al.*, 2002]. Flow through bedrock, particularly via fractures, is known to contribute to baseflow conditions, but significant contributions to stormflow have not been readily observed; however, bedrock flow has also not been extensively studied [*Montgomery et al.*, 2002; *Montgomery et al.*, 1997]. Although channel interception does occur during precipitation, channels make up a small portion of the catchment area such that the overall contribution to stormflow during flood generating events is low.

The relative importance of the most common runoff generation mechanisms varies, but each requires saturation of at least a portion of the soil profile (hereafter referred to as partial soil saturation) [*Buttle*, 1994; *Buttle et al.*, 2004; *McGlynn et al.*, 1999; *Sidle et al.*, 2000; *Sklash and Farvolden*, 1979]. Because partial soil saturation is required to generate rapid lateral flux, the spatio-temporal distribution of runoff generation mechanisms is highly dependent on the patterns of water inputs coupled with the distributions of vegetation and geomorphic properties including soil properties (e.g. hydraulic conductivity, texture, porosity, pore size distribution), soil depth, slope gradient, slope position, and topographic curvature (surface and bedrock), among other factors. These runoff generation mechanisms can occur during both rainfall and snowmelt runoff processes, but the spatio-temporal patterns of specific mechanisms are expected to vary greatly between rainfall and snowmelt conditions due to large differences in the distribution of water inputs and antecedent soil wetness.

1.1.3 Hillslope hydrologic connectivity

The most important factor controlling how runoff generation translates into rapid streamflow response is the extent of connectivity between runoff source areas and the stream network [*Bonell*, 1993; *Dunne*, 1983; *Sidle et al.*, 2000]. Studies have illustrated that the extent, duration, and sequencing of hydrologic connectivity established throughout the catchment are directly responsible for controlling the non-linear response of runoff magnitude to water inputs under varying levels of catchment wetness [*Detty and McGuire*, 2010a; *James and Roulet*, 2007; *Jencso et al.*, 2010; *Jencso et al.*, 2009; *Penna et al.*, 2011]. Hydrologic connectivity thus forms a second-order control (behind water input patterns) on runoff source area dynamics and is important for both rainfall runoff and snowmelt runoff.

Hydrologic connectivity requires continuity of lateral flow between the runoff source areas and the stream channel, which can be disrupted by areas with high soil water storage deficits [*Jencso et al.*, 2009; *Kuras et al.*, 2008; *McNamara et al.*, 2005]. Hydrologic connectivity between streams and near-stream areas is strongly influenced by expansion and contraction of surface saturated areas and associated saturation-excess overland flow [*Freeze*, 1972; *Hewlett and Hibbert*, 1963; 1967; *Sidle et al.*, 2000; *Tsukamoto*, 1963]; however, subsurface mechanisms are also important in connecting streams to near-stream areas [*McDonnell*, 1990; *McGlynn et al.*, 1999; *Sidle et al.*, 2000]. In both cases, stream connectivity to near-stream areas is positively related to soil wetness [*McDonnell et al.*, 1998; *McGlynn et al.*, 1999] and can exhibit threshold effects [*Detty and McGuire*, 2010b]. Connectivity between near-stream areas and upslope areas also depends on the continuity of lateral flow, either overland or subsurface, which, in turn, requires connectivity of zones of soil saturation [*Buttle et al.*, 2004; *Jencso et al.*, 2009; *Ocampo et al.*, 2006]. Some studies have highlighted the important role of near-stream areas in controlling and buffering the response of streamflow to upslope inputs [*Buttle et al.*, 2004; *Jencso et al.*, 2010], and that the capacity for riparian buffering is a function of the riparian/hillslope size ratio [*Jencso et al.*, 2010]. Thus, streams, near-stream areas, and upslope areas form a connectivity continuum controlling the delivery of

runoff from water input areas to streams that is strongly linked with catchment wetness [*Buttle et al.*, 2004; *Detty and McGuire*, 2010a; b; *Jencso et al.*, 2010; *Jencso et al.*, 2009; *Penna et al.*, 2011].

Under rainfall-dominated conditions, water inputs in small catchments are generally spatially homogeneous and runoff processes are activated within a short temporal resolution (e.g. sub-hourly to sub-daily) [*Burns et al.*, 2001; *McDonnell*, 1990; *Sidle et al.*, 1995]. Under snowmelt-dominated conditions, hillslope hydrologic connectivity is more complex, as the distribution of catchment water inputs is spatially and temporally quite variable. Greater spatio-temporal variability of water inputs causes greater variability in the patterns of hillslope hydrologic connectivity and increases the opportunity for disconnection between source areas and the stream network [*Deng et al.*, 1994; *Jencso et al.*, 2009; *Kuras et al.*, 2008; *McNamara et al.*, 2005]. Moreover, it is conceivable that, as patterns of soil water content are dependent on water inputs and on geomorphology, adjacent areas may receive water inputs at the same time, but may contribute to runoff at different rates and times depending on local patterns of hillslope hydrologic connectivity.

1.2 Conceptualizing runoff

Construction of process-based numerical runoff models starts with a conceptualization of the hydrologic processes. As every model is a simplification of reality, the conceptualization determines how to represent the hydrologic system within the model in terms of the important processes that control hydrologic response at the scales of interest. For some processes, a detailed representation may be necessary, whereas other processes may be highly simplified or entirely ignored.

An important issue that has been recently investigated for rainfall-runoff modelling is the spatial scale of representation for various processes that are necessary in order to adequately predict the spatio-temporal variability of runoff response. This issue directly relates to the extent to which representation can be spatially aggregated. Many spatially

explicit runoff models have relied on fully distributed discretizations of catchments for representing spatial variability of runoff processes [*Graham and Butts*, 2005; *Wigmosta et al.*, 1994; *Wigmosta et al.*, 2002]; however, fully distributed models are difficult to parameterize and computationally intense. To address these limitations, hydrologic response unit (HRU) approaches [*Bongartz*, 2003; *Flügel*, 1997] aim to discretize catchments into functionally homogeneous elements where process variability at scales smaller than the element size are inconsequential to predicting hydrologic response. The advantage is that the HRU approach can reduce the number of model elements and subsequent effort required to parameterize the model, and may improve overall performance due to better functional representation. A comprehensive understanding of process variability and associated scales is paramount to successful HRU modelling.

Regardless of the process representation approach used, model conceptualization is refined through collection and analysis of process-based data. The following sections review developments in conceptual models of source area dynamics related to rainfall runoff and snowmelt runoff processes.

1.2.1 Rainfall runoff

One of the most referred to rainfall runoff conceptual models from earlier studies is the variable source area (VSA) concept. Credit for conceptualizing the model is often given to Hewlett and Hibbert [1963; 1967], but developments were also made by Tsukamoto [1963] and others. The VSA concept essentially treats saturated near-stream areas as extensions of the stream network that are fed by direct precipitation and by subsurface translatory flow from upslope areas. Runoff from saturated areas dominates source area contributions to rapid streamflow response and the extent of saturated area varies with wetting and drying of the catchment. As the catchment wets up and the extent of saturated area grows, the volume of water rapidly delivered to the stream network from saturated overland flow increases resulting in higher flows and more efficient catchment response.

Shortly after development of the VSA concept, the partial source area (PSA) concept was developed by Dunne and Black [1970a; b] and by Freeze [1972]. The PSA model is similar to the VSA model in that rapid catchment response is derived from expanding and contracting areas generating saturated overland flow; however, fluctuations of the PSA contribution to streamflow depend on topographic position and localized soil and water input conditions. In this respect, source area contributions to rapid streamflow response are not restricted to near-stream areas, but can come from upslope topographic positions of predictable recurring surface saturation. This concept led to modelling studies of the topographic wetness index concept [*Beven and Kirkby*, 1979; *Kirkby*, 1975] where soil wetness is predicted based on upslope contributing area and localized slope gradient. Topographic indices have been found to be effective for predicting the spatial patterns of soil saturation, hydrologic connectivity, and runoff generation [*Beven and Kirkby*, 1979; *Thompson and Moore*, 1996].

The VSA and PSA concepts were considered important models for conceptualizing spatial catchment response for many years, yet several studies from the same period demonstrated that subsurface flow mechanisms can be as important for generating rapid catchment response [*Beasley*, 1976; *Harr*, 1977; *Kirkby*, 1969; *Mosley*, 1979; *Whipkey*, 1965]. In addition to refuting saturated overland flow as the primary mechanism of rapid catchment response, the findings of several, mostly recent, studies suggest important subsurface linkages between upslope source areas and the stream network, with the extent of hillslope hydrologic connectivity varying greatly in both space and time [*Burns et al.*, 2001; *Detty and McGuire*, 2010b; *Sidle et al.*, 2000; *Tsuboyama et al.*, 2000]. In many forested catchments, soils are relatively shallow, highly permeable, and are underlain by relatively impermeable bedrock or glacial till [*Freer et al.*, 2002; *Kim et al.*, 2004; *McGlynn et al.*, 1999; *Sidle et al.*, 2000]. Under these conditions, highly conductive saturated zones can form above the confining basal layer and exert significant control on catchment response.

Building upon the findings of numerous hillslope process studies, Sidle *et al.* [2000] articulated a more holistic model (compared to the VSA and PSA concepts) to

conceptualize the source area dynamics of catchment response in rainfall runoff systems and called it the hydrogeomorphic concept. According to this model, as antecedent wetness increases in rainfall-dominated headwater catchments, the extent of hydrologically active areas progresses from narrow riparian corridors into linear hillslope segments and eventually into geomorphic hollows or zero-order catchments, with the role of subsurface flow increasing relative to saturated overland flow. They noted that soil moisture related threshold effects appear to control the timing of hydrologic connectivity between upslope areas and the stream network. The hydrogeomorphic concept thereby implies that catchments can be explicitly represented as three distinct hydrologic response unit types (riparian zones, linear hillslope segments, and geomorphic hollows) based on their geomorphic attributes with the function and dominance of each unit changing with variation in catchment wetness. Other studies, including McGlynn *et al.* [2004], have described similar concepts without using the hydrogeomorphic name.

The hydrogeomorphic concept is a useful framework for investigating the spatio-temporal dynamics of runoff generation processes and response through examining connectivity between distinct hydrogeomorphic units. Although the applicability of the hydrogeomorphic concept to rainfall runoff systems is widely supported by the findings of numerous studies, it is unlikely that the conceptual framework can be applied directly to snowmelt runoff systems without further development. The hydrogeomorphic concept does not account for large spatial variation in water inputs and the associated spatial distribution of resulting runoff processes, as occurs during snowmelt conditions. The contribution to streamflow from riparian areas, linear hillslopes, and geomorphic hollows under snowmelt conditions would not likely follow a sequential progression as articulated for rainfall conditions, and may contribute independently or in a much different sequence.

1.2.2 Snowmelt runoff

Several researchers have demonstrated that snowmelt runoff processes occur differently than rainfall runoff processes in terms of process variability across a hillslope or catchment scale [*Boyer et al.*, 1995; 1997; 2000; *Deng et al.*, 1994; *Kuras et al.*, 2008];

however, a holistic hydrogeomorphic-type conceptualization of snowmelt runoff response has not been well developed. Characterization of runoff generation is especially difficult in snowmelt-dominated catchments with complex terrain due to variable topography, soils, and vegetation, and their influences on water input timing and intensity, and antecedent wetness [*Grant et al.*, 2004; *Harms and Chanasyk*, 1998]. However, individual sites tend to exhibit similar seasonal dynamics and spatial variability can be described in terms of temporally stable relationships with transitions between seasonal patterns driven by changes in the water balance between rain, snow, snowmelt, and evapotranspiration [*Grant et al.*, 2004; *McNamara et al.*, 2005]. Grant *et al.* [2004], for instance, reported that streamflow response can be highly sensitive to inputs in late winter and early spring while the catchment is in a state of high soil water storage conditions. In contrast, streamflow response to water inputs can be minimal in summer and early fall during low soil water storage conditions.

Some studies have shown that early spring snowmelt runoff response is largely generated by outflow from riparian zones [*Kendall et al.*, 1999; *Kuras et al.*, 2008; *Price and Hendrie*, 1983]. Areas of unsaturated soil can persist on a hillslope through the winter, forming a hydrologic disconnect between upslope groundwater responses, generated by isolated snowmelt inputs, and the riparian zone [*Jencso et al.*, 2009; *Kuras et al.*, 2008; *McNamara et al.*, 2005]. As snowmelt progresses and the hillslope water table expands sufficiently to breach any hydrologic disconnect, the catchment becomes more responsive to upslope inputs, shallow flowpaths become increasingly important via transmissivity feedback, and upslope melt contributes substantial delayed flow [*Dunne and Black*, 1971; *Kendall et al.*, 1999; *Laudon et al.*, 2004]. The timing and amount of contribution from a particular hillslope location is controlled by topographic position, snowpack depth, and storage and transmission of water in the soil. Moreover, pressure pulses from upslope water inputs can result in rapid outflow of stored old water. In fact, isolated water inputs from late-lying upslope snow can maintain high groundwater levels at lower slope and riparian areas, even without the occurrence of downslope water inputs, and can control downslope response patterns throughout snowmelt recession [*Deng et al.*, 1994; *Kendall et al.*, 1999; *Kuras et al.*, 2008]. McGlynn *et al.* [1999] found that the snowmelt water

itself did not appear at depth in the riparian zone during the spring melt, despite correlation between the timing of upslope groundwater response and streamflow.

Understanding these snowmelt runoff processes provides a starting point for further development of a snowmelt runoff based hydrogeomorphic conceptualization to account for spatial variation in water inputs and the spatial distribution of resulting runoff response. In fact, studies by McNamara *et al.* [2005] and Kuras *et al.* [2008] address the temporal progression of catchment response and account for issues of spatial disconnection. Dunne and Black [1971] suggested that the PSA concept of runoff generation may be a useful conceptual framework within which to view snowmelt runoff source area dynamics; however, the small areas (0.3-2 ha) and elevation ranges (20-35 m) studied by Dunne and Black and McNamara *et al.* would have precluded observation of some of the added spatial complexities inherent in snowmelt runoff processes. This would limit the potential for observation of hydrologic response phenomena related to spatio-temporal variability in snow accumulation and melt processes. In addition, the spatial dynamics of runoff generation processes associated with distinct landscape geomorphic characteristics were not investigated in the McNamara *et al.* study.

1.3 Overview of the dissertation

The previous sections have highlighted several key points that are important for framing the direction and scope of this dissertation, as follows:

- The spatial variability of snowmelt is much greater than that of rainfall and has the potential to generate asynchronous water input patterns.
- Saturation of at least a portion of the soil profile is required to generate rapid lateral flux in montane catchments; thus, the space-time distribution of runoff generation in montane catchments is dependent on the interactions between water input patterns and the distributions of vegetation, soils, and topography.

- Upslope areas can be as important in controlling streamflow response as near-stream areas, and connectivity between runoff generation areas forms a second-order control (behind water input patterns) on runoff source area dynamics.
- Upslope snowmelt inputs can contribute substantial delayed streamflow response controlled by topography, snowpack conditions, and soil wetness, and any spatial organization in these factors could influence hydrologic connectivity and catchment response patterns.

This dissertation investigates interactions between the spatio-temporal variability of water inputs and the soil processes governing hydrologic response on the hillslope, and how these interactions might control the space-time patterns of runoff generation, primarily groundwater dynamics, in a snowmelt-dominated montane catchment. It addresses both vertical and lateral process controls and how these controls vary through space and time. The study employs a hillslope monitoring approach that was based on a stratified random distribution of points to ensure that statistical inferences could be reliably extrapolated to the entire study catchment.

The remainder of the dissertation comprises five chapters. Chapter 2 provides descriptions of the study catchment and the field methods. Chapter 3 addresses controls on the spatio-temporal variability of midwinter snowmelt and implications for the spatial organization of hydrologic connectivity at the start of active snowmelt in the spring. Chapter 4 investigates the interplay between water input dynamics and various hydraulic conductivity profiles as controls on the development of transient perched shallow groundwater via percolation-excess runoff generation. It addresses how this interplay might influence the spatial distribution of rapid runoff response versus delayed runoff response sites. Chapter 5 examines temporal variability in the spatial controls on catchment-scale groundwater dynamics. More specifically, it addresses the relative importance of vegetation, soil, and topographic characteristics in controlling if, where, and when groundwater response occurs within the context of temporally varying water input patterns and streamflow levels. The final chapter (chapter 6) provides a summary of important findings, integrates the study findings in a conceptual model for runoff

source area dynamics in snowmelt-dominated montane catchments, and outlines opportunities for future research.

2 Study area and data collection

2.1 Study catchment

The study was conducted within the 3.5 km^2 Upper Elk Creek (UEC) sub-catchment (49°21'28"N and 115°46'11"W) of the Cotton Creek Experimental Watershed (CCEW) near Cranbrook, British Columbia, Canada, approximately 540 km east of Vancouver (Figure 2.1). This study is part of the CCEW project, which focuses on the effects of forest harvesting and natural disturbance on snow accumulation and melt, runoff generation, and sediment transport [*Jost et al.*, 2007; *Jost et al.*, 2009; *Szeftel*, 2010; *Szeftel et al.*, 2011]. The UEC catchment is suitable for studying the influences of spatially variable water inputs on synchronization and de-synchronization of runoff generation processes, as it is snowmelt-dominated and incorporates large variations in elevation, slope gradient, aspect, forest cover, and topographic curvature.

The UEC is a second-order stream with two first-order tributaries (Elk south and Elk North sub-catchments). The UEC catchment is 72.0% forested with stands dominated by subalpine fir (*Abies lasiocarpa*) and Engelmann spruce (*Picea engelmannii*), and stands dominated by lodgepole pine (*Pinus contorta*) and western larch (*Larix occidentalis*) (Figures 2.2 to 2.4). Clearcuts in early stages of regeneration and two bedrock outcrops comprise 27.5% and 0.5% of the catchment, respectively. Hillslope gradients within the UEC catchment average 27%, ranging between nearly flat and 100%, and elevations range between 1438 and 1938 m. Mean annual precipitation is approximately 780 mm at the Upper Cotton (UC) climate station, which is at 1780 m elevation and approximately 750 m south of the UEC catchment boundary. Annual evapotranspiration within forested areas of the catchment is 450-550 mm based on modelling conducted in chapter 4. Annual, January, and July air temperatures at the UC climate station average 2.3, -7.6, and 16.8 °C, respectively. Spring snowmelt dominates the hydrologic regime. Snowpacks usually persist from October or November through April, May, or June. Maximum snowpack depths throughout the catchment vary between approximately 150 mm and 600 mm SWE during an average snowpack year.

Soils throughout the UEC catchment are dominated by sands and silts with abundant coarse fragments (Figure 2.5). They developed primarily on deep (in excess of 2-8 m) morainal tills with some isolated areas of colluvium (BC Geological Survey). Except at a limited number of isolated ridge top outcrops, bedrock is not observed throughout most of the catchment including along most road cuts (Figure 2.6), some of which exceed a depth of 8 m. Based on visual observations, the majority of vegetation roots reside within the upper 30 cm of soil with a lower root density between 30 cm and 50 cm below the surface. Although soil physical properties (particularly soil texture, coarse fragment content, and porosity) vary considerably across the catchment, vertical variations are, for the most part, gradual with little distinct soil layering. Generally, soils vary gradually from low density and high permeability at the surface to higher density and lower permeability at depth; however, some sites show negligible change (both visible and measured) in structure, texture, or permeability with depth to at least 1.5 m. By volume, soils (sampled at 45-55 cm depth; see sampling details in section 2.3) across the catchment average 42% porosity, 3% organics, 17% sand, 19% silt, 2% clay, and 17% coarse fragments, based on the USDA soil classification system. Riparian soils have a higher content of organic material than hillslope soils. Generally, little evidence of large soil macropores or cracks was observed, likely due to the limited amount of vegetation roots below 30 cm depth, the absence or limited abundance (based on visual observations) of burrowing animals (e.g. small mammals, earthworms) in the catchment, and the low clay content of the soils. The only exceptions were at the heads of ephemeral streams where large macropores were observed that had likely developed via subsurface erosional processes.

2.2 Study design

Fifty hillslope monitoring sites were established (33 in October 2005 and 17 in July 2006) at stratified random locations throughout the UEC catchment (Figure 2.1). Stratified random sampling was used to minimize the potential for investigator bias in site selection, and also to ensure that statistical inferences could be reliably extrapolated to the entire study catchment. The sample size was selected to maximize statistical

power while ensuring that the infrastructure could be maintained by only one person, particularly during installation and snow sampling. Strata were defined based on elevation (50% of the sites were established at locations above and 50% below the mean catchment elevation), insolation (50% of the sites at locations greater than and 50% less than the mean annual potential solar radiation within the catchment), forest cover (25% of the sites in clearcuts or regenerating stands and 75% in forested areas), and hydrogeomorphic position (20% of the sites in each of the following classes: riparian, concave-wet, concave-dry, convex-wet, and convex-dry). For the hydrogeomorphic classes, riparian was defined as being located within 10 m of the catchment or sub-basin mainstem channels. Concave versus convex was defined as positive and negative values, respectively, of the laplacian from a 3x3 neighborhood of cells surrounding each cell of interest in a 25 m resolution digital elevation model (DEM) (Terrain Resource Information Management data, BC Ministry of Forests and Range) for the catchment. Wet versus dry was defined as positive and negative values, respectively, of the topographic wetness index using a mass flux grid applied to the DEM. Elevation, insolation, and forest cover were selected for catchment stratification because they strongly influence snow depth, timing and intensity of melt, amount of evapotranspiration, and soil wetness. Hydrogeomorphic position was selected because of its association with subsurface runoff processes via flowpath convergence and divergence. The term hillslope hollow is used hereafter to refer to areas of pronounced surface concavity. The DEM analyses were conducted using Rivertools 3.0 (Rivix LLC). Potential solar radiation was modelled using Solar Analyst in ArcGIS 9.3.1 (ESRI).

At each site, groundwater wells were installed to the greatest depth possible with manual methods. Wells were selected rather than piezometers in order to capture the timing of groundwater initiation and subsequent water table dynamics rather than capturing only hydraulic head at a specific depth in the soil. For the initial installation, PVC wells with a 3.8 cm inside diameter were installed in soil pits that were dug by hand using augers, shovels, picks, and pry-bars (Figure 2.7). They were screened by cutting narrow slits in the sidewalls with 2 to 3 cm spacing and wrapping the pipes with geotextile to prevent the potential influx of sediments. The soil pits were back-filled with native soil. At sites

with limited or no groundwater responses, up to two additional attempts were made to increase the depths of the wells to improve the chances of observing groundwater responses, including installation of steel pointed wells using a hand-held sledgehammer. The steel wells were screened with narrow slits at 2 mm spacing. Driving the steel wells into the soil inhibited wrapping them with geotextile; however, sedimentation never became an issue. After the final installations were complete, the minimum, mean, and maximum well depths were 0.50 m, 1.09 m, and 1.64 m, respectively, and the wells were screened from the well bottom up to an average depth below the soil surface of 8 cm. Water table depth at each well was recorded every 30 minutes using Odyssey capacitance water level recorders (0.8 mm resolution). Odyssey recorders utilize a built-in data logger and are inexpensive; thus, they are suitable for a highly distributed groundwater monitoring network. A PVC pipe was installed within the steel wells to insulate the Odyssey sensors from potential interference.

Between October 2005 and September 2008, field campaigns were conducted in early February; early April; every 2 to 4 weeks through April, May, and early June; early summer; late summer; and mid-fall. Soil saturation, snowpack water equivalent (SWE), snow depth, and snow temperature were measured manually during site visits throughout winter and spring. Soil saturation was measured manually also throughout the summer and fall. Soil saturation measurements involved manually inserting a AquaPro capacitance probe to the desired depth in an epoxy access tube that had been installed in the soil during the snow-free season (Figure 2.7). An AquaPro probe was used because it allowed measurements to be made at any depth interval within the soil profile to a maximum depth of 1 m. Moreover, since only an epoxy tube was required to be installed at each site, the marginal cost for each site was low. PVC extension tubes were added to the epoxy access tubes for the winter period to facilitate soil saturation measurements below the snowpack (Figure 2.8). Snowpack water equivalent was measured using a Federal snow sampler. At each site, five snow samples were spaced at 4 m intervals on a contour across the hillslope centered at 5 m upslope from the groundwater well. With a total of 250 snow samples distributed among 50 sites, the snow surveys required one week to complete during midwinter with progressively less time required as the

catchment melted out. Snow temperature was measured at 20 cm depth intervals starting at the soil surface and also at a depth of 1 to 2 cm below the snow surface. During each field visit throughout the snowmelt season, snowcover extent and locations of overland flow were manually mapped (i.e. sketched) on a topographic map. Additional details of the data collection infrastructure at the hillslope sites are provided in Table 2.1.

At six of the 50 hillslope sites, additional automated infrastructure was established in October 2006 to capture additional information regarding hydrologic response at a sub-daily frequency. These measurements included volumetric soil water content, soil temperature, air temperature, and water input (i.e. snowmelt/rainfall) depth using snowmelt lysimeters. The 0 °C values were calibrated for the temperature sensors. Decagon loggers and ECH_20 sensors were used due to their small size, good performance, and low cost. These six sites are referred to as *lysimeter sites*, whereas all 50 sites that monitor hillslope runoff processes (including the six lysimeter sites) are referred to as *hillslope sites*. Each lysimeter consisted of a 2 m by 2 m (4 m^2) water collection surface constructed with a 10 mil polyethylene liner and 1.8 cm by 14 cm wooden sidewalls (Figure 2.9). The thin plastic liner was used to minimize potential impacts of the lysimeter on heat flux between the snowpack and the soil. Angled metal strips (2.1 cm per side) were installed edge-up on the sidewalls for isolation of the snow column above the lysimeter. The poorly decomposed litter layer was removed from the soil surface during installation to minimize perforation of the liner. The drain for the lysimeter was placed approximately 30-50 cm upslope from the lower edge of the lysimeter frame and consisted of a 3.8 cm wide thru hull (flange style) plastic fitting and a 3.8 cm inside diameter PVC pipe. From a dished lysimeter surface, the drain was oriented vertically downward into the soil and then sloped downslope approximately 10 cm below the soil surface (i.e. lysimeter surface) to a tipping bucket installed within an insulated cooler box that was buried in the soil (Figure 2.10). The upper approximately 5 cm of the cooler extended above the soil surface to enable access to the measurement system. The drain narrowed to 1.3 cm inside diameter for about 5 cm of length before entering the side of the cooler box. The drain and the tipping bucket mechanism were installed below the soil surface to prevent freezing of the drainage and measurement

systems. A 15-20 cm wide drainage trench extended downslope from the cooler box to prevent flooding of the measurement system. The tipping buckets were accessed during each field visit to confirm proper function, and the lysimeter calibrations of approximately 0.06 mm of water outflow per tip were confirmed before and after each snowcover season. Additional details of the data collection infrastructure at the lysimeter sites are provided in Table 2.1 and physiographic details of the lysimeter sites are provided in Table 2.2.

A stream gauge was established at the catchment outlet using a naturally constricted cross-section and six nested sub-catchment stream gauges were established upstream using 90° v-notch weirs (Figures 2.1 and 2.11). The weirs were designed to maximize the storage volume of the weir ponds in order to minimize the outflow approach velocity while being small enough to enable manual transport of the construction materials as far as 1 km from the nearest road access point. The weir plates were constructed with 2 cm plywood reinforced with 4 cm x 9 cm dimension lumber. Angled aluminum strips were installed edge-up on the v-notches to ensure a sharp and narrow outflow surface. The weir plates and ponds were lined with 10 mil polyethylene and back-filled with native soil. The sidewalls of the weir ponds were stabilized with soil-filled canvass bags. A steel drive-point stilling well was installed in each weir pond with a PVC encased Odyssey logger recording at a 30 minute interval. Streamflow was measured using slug injection of NaCl over the range of flows experienced during the study period (maximum of 439 l/s) to develop stage-discharge rating curves [*Moore*, 2005]. Salt dilution gauging is a suitable method for flows of this magnitude. Additional details of the data collection infrastructure at the streamflow sites are provided in Table 2.1.

Climate data including precipitation, air temperature, incoming short-wave radiation, relative humidity, wind speed, and snow depth were obtained from two automated climate stations that were previously established in regenerating clearcuts within CCEW: the UC climate station (1780 m elevation, 750 m south of the UEC catchment) and the Lower Cotton (LC) climate station (1390 m elevation, 1500 m southwest of the UEC catchment). Continuous SWE data are utilized from the Moyie Mountain snow pillow

(British Columbia Ministry of Environment station ID# 2C10P) located at 1930 m elevation and approximately 12 km south of the UEC catchment.

2.3 Site characterization

Soil properties, vegetation, and topography were characterized at each of the 50 hillslope sites. Soil samples were obtained from each site to quantify sand, silt, clay, coarse fragment, and organic contents as well as porosity. At two sites, multiple samples were gathered from a range of depths up to 1.1 m to assess vertical variations in soil properties. Samples were collected by digging a 45-50 cm deep soil pit, leveling the soil surface at the bottom of the pit, and removing a small sample of soil (approximately 500 g dry mass) at the center of the pit using a spork. The sample volume was determined by lining the sample hole with thin plastic sheeting, backfilling the hole with dry sand to the original soil surface at the bottom of the pit, and measuring the sand volume using a graduated cylinder. This method was used due to its ease of application in coarse, friable soils. After burning the soil samples to remove organic matter, soil grain size distribution analysis was conducted using wet sieve methods for particles larger than 0.05 mm and using a sedigraph for smaller particles. Organic matter content was computed from the loss in mass during ignition. Due to the relatively small size of the soil samples, the coarse fragment results from the soil grain size distribution analysis are not representative of particles larger than approximately 1 cm in diameter. Vertical variation in soil properties at each site was also noted from field-based observations (including manual soil texture tests) made during installation of groundwater wells and soil moisture instruments. The surface area of exposed bedrock was visually estimated for a 25 m by 25 m area centered over the groundwater well for each site. To characterize the local forest cover at each hillslope site, stand surveys were conducted using a 7.5 m radius plot around each groundwater well. This plot size allowed sampling of trees over an area covering at least two canopy openings and, thus, was considered to account for most of the trees strongly influencing the amount of insolation experienced at a site during mid-day when insolation is high. Height, diameter at breast height (DBH), and species for all trees greater than 2 m height were recorded. The total number of trees less than 2 m

height was noted. Clear-sky fraction was determined for each site based on photos taken horizontally over the groundwater well using a fish eye lense (Nikon fisheye converted FC-E8 lens) mounted to a digital camera (Nikon Coolpix 4500 4.0 megapixel), and analyzed using Hemiview (Delta-T Devices). Field measurements for characterization of the topography involved elevation (via a global positioning system, GPS), slope gradients in the upslope and downslope directions to a distance of approximately 10 m, and aspect along the downslope fall line, all taken from the location of the respective groundwater well.

Field saturated hydraulic conductivity (K_s) was measured using a Guelph Permeameter at approximately 0.25 m (49 sites), 0.50 m (47 sites), 0.75 m (39 sites), 1.00 m (10 sites), 1.25 m (3 sites), and 1.50 m (1 site) soil depths (Figure 2.12). The Guelph Permeameter was used because samples for standard laboratory tests could not be easily obtained due to the coarseness of the soil and because it is an in situ method that is capable of capturing the influences of soil macrostructure on hydraulic conductivity. Bedrock within 10 cm of the soil surface prohibited K_s measurement at one site. At two sites, the presence of persistently high groundwater prohibited K_s measurement below 30 cm depth since the Guelph Permeameter can only be applied in unsaturated soil. The resulting K_s values were averages of vertical and horizontal conductivities since depth and width dimensions of the water-filled portion of the bore-hole were approximately equal; however, hydraulic conductivity is likely roughly isotropic throughout the catchment since the soils are dominated by sand, silt, and gravel with minimal amounts of clay and since the soils are not stratified [*Mitchell*, 1993]. For each measurement, a 7 cm diameter hole was augered to the desired soil depth (Figure 2.13) and two K_s tests were conducted—one with 5 cm of hydraulic head and the other with 10 cm of head. K_s was calculated for each test using methods described in the Guelph Permeameter operating instructions [*Soil Moisture Equipment Corp*, 1991] and the arithmetic mean (the geometic mean resulted in a negligible difference) of both tests was used as the final K_s value.

2.4 Soil moisture data processing

The continuous volumetric soil water content data were re-scaled to percent saturation by fitting regression equations between the ECH_20 data (one equation for each ECH_20 sensor) and the soil saturation data acquired manually using the AquaPro soil moisture sensor. Both sensor types utilize capacitance measurements to determine soil wetness, but the ECH_20 sensor measures capacitance over a smaller volume of soil than the AquaPro sensor; thus, the ECH_20 measurements were more sensitive to spatial variation in pore structure, making spatial comparisons more problematic. The AquaPro data were calibrated to the local soils using a combination of wetting/drying bucket samples in the laboratory and measurements of fully saturated soils in the field. After re-scaling the ECH_20 data, the 20 cm and 40 cm data were averaged for each site to reduce the effects of individual sensor variability.

2.5 DEM development

After establishment of the hillslope sites, it became clear that the topographic variability across the hillslope (i.e. on contour) was not adequately represented by the 25 m resolution of the original DEM. Therefore, a 5 m resolution DEM was developed using photo interpretation methods applied to 1:15:000 scale aerial photos (LIDAR was cost prohibitive). However, the density of points around several hillslope sites was insufficient to capture the local topographic variability, so the raw photo interpretation points were supplemented with GPS points. GPS data (Trimble ProXT GPS and Ranger data logger) were gathered over a minimum area of 100 m by 100 m centered over each hillslope site. Base-station corrected GPS data were filtered to remove low quality (i.e. low satellite reception) points, and merged with the raw photo interpretation dataset. Points with apparent spurious errors were removed from the combined dataset and the final dataset was then grid-averaged. The final DEM was interpolated to a 5 m resolution using triangulation and was smoothed using a Gaussian filter. The final DEM was identified based on visual inspection of the topographic variability represented by the DEM compared to perceived topographic variability developed during field

investigations, and based on correlations for the 50 hillslope sites between the following DEM-based and field-based topographic indices: (1) DEM-based plan curvature and field-based lateral roughness height (i.e. elevation range between the highest point and the lowest point on contour along a 25 m x 25 m hypothetical plane parallel to the hillslope gradient); (2) DEM-based and field-based slope gradient; and (3) DEM-based and field-based aspect. R statistical software [*R Development Core Team*, 2010] was used for merging and filtering the raw point data. SAGA GIS (System for Automated Geoscientific Analyses) was used for grid averaging the point data and for interpolating and filtering the DEM. Rivertools 3.0 (Rivix LLC) was used for calculating plan curvature, slope gradient, and aspect from the DEM.

Table 2.1. Data collection infrastructure in the UEC catchment.

Site type	Number of sites	Data type	[a]Data frequency	Equipment	Additional details
Hillslope	50	Soil wetness (manual)	Weekly to bi-monthly	AquaPro capacitance soil moisture sensor	10 cm depth intervals
		SWE and snow depth	Weekly to bi-monthly	Federal snow sampler	5 samples at 4 m intervals on contour centered 5 m upslope from groundwater well
		Water table elevation	30 minutes	Groundwater well & Odyssey capacitance water level recorder	Screened to ~8 cm below soil surface
Lysimeter (infrastructure added to hillslope sites)	6	Water input rate	Hourly	Snowmelt lysimeter with tipping bucket gauge	See study design section of main text
		Air temperature	Hourly	ECH$_2$0 ECT temperature sensor	2 m above soil surface
		Soil temperature	Hourly	ECH$_2$0 ECT temperature sensor	10 cm below soil surface
		Soil wetness (automated)	Hourly	ECH$_2$0 EC-5 capacitance soil moisture sensor	20 cm and 40 cm below soil surface
Streamflow	7	Stream discharge	30 minutes	90° v-notch weir, stand pipe, & Odyssey capacitance water level recorder	Main outlet uses a naturally constricted cross-section instead of a v-notch weir

a. Weekly to bi-weekly measurements during the snowmelt season. Monthly to bi-monthly measurements during the snow-free and snow accumulation seasons.

Table 2.2. Characteristics of the lysimeter sites.

Site	Elevation (m)	Slope (%)	Aspect (°)	Forest cover	Soil texture
24	1641	55	209	Mature, lodgepole pine	Sandy loam
2006	1481	13	290	Mature, lodgepole pine	Silty loam
2013	1832	23	313	Mature, lodgepole pine, Engelmann spruce	Sandy loam
4004	1470	28	170	Clearcut, 0 m mean height	Sandy loam
6003	1652	20	305	Regeneration, 4 m mean height, lodgepole pine	Sand
6501	1753	19	169	Mature, lodgepole pine	Loamy Sand

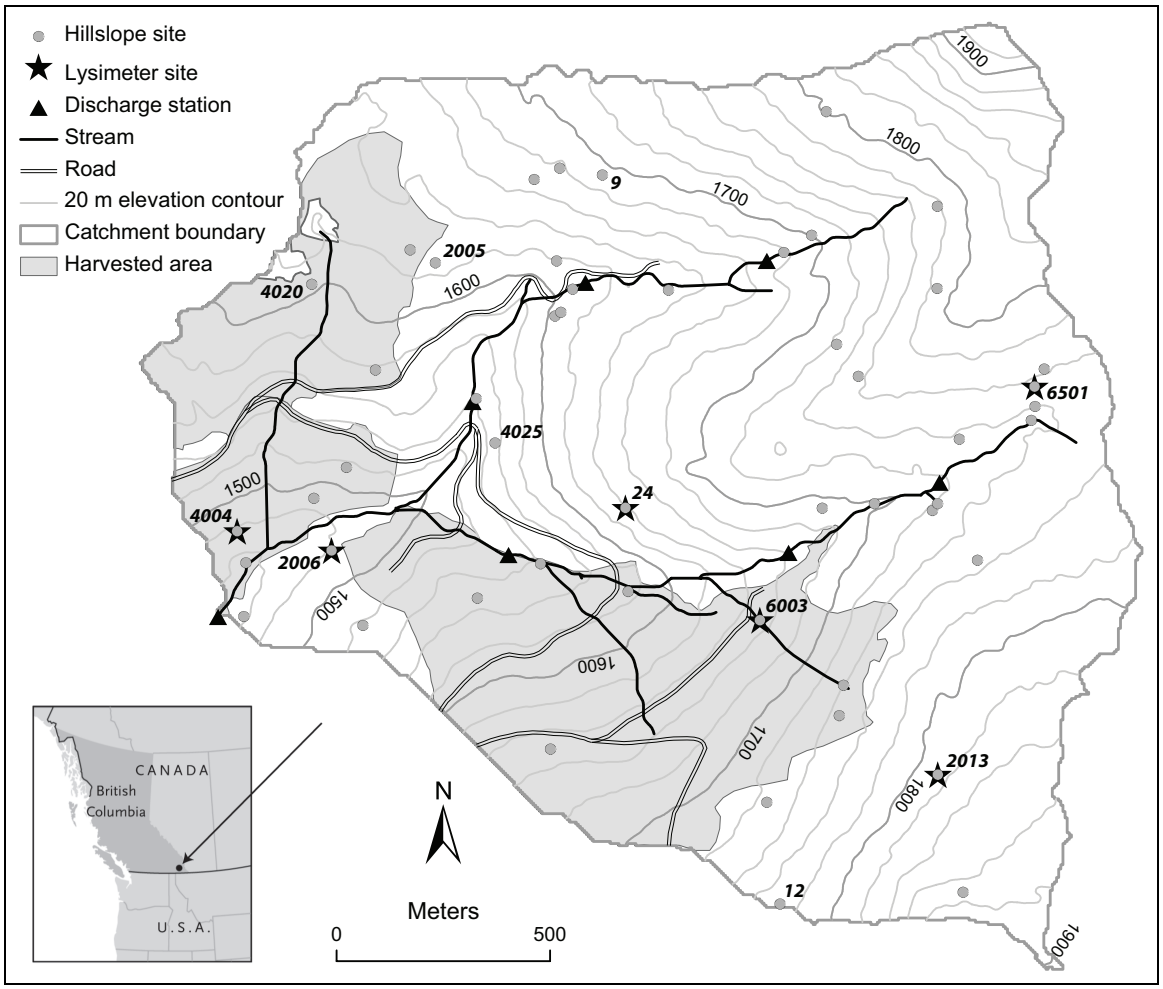

Figure 2.1. Location and study sites of the UEC catchment. Sites referenced in chapters 3 and 4 are labeled.

Figure 2.2. Overview of the UEC catchment looking north.

Figure 2.3. Overview of the UEC catchment looking northwest.

Figure 2.4. Overview of the UEC catchment looking southeast.

Figure 2.5. Soil profile (4-5 m deep) along a 1 month old road cut in the UEC catchment.

Figure 2.6. Approximately 100 m section of the road cut shown in Figure 2.5.

Figure 2.7. Hillslope site showing a PVC groundwater well (lower) and an epoxy access tube for manually measuring soil saturation using an AquaPro capacitance soil moisture sensor (upper).

Figure 2.8. Groundwater well and epoxy access tube from Figure 2.7 with a PVC extension added to the access tube to allow measurement of soil saturation while snow-covered.

Figure 2.9. Snowmelt lysimeter lined with 10 mil polyethylene, an outlet drain (surrounded by rocks to help keep a mesh debris filter in place), and a cooler box containing a tipping bucket mechanism for measuring lysimeter outflow.

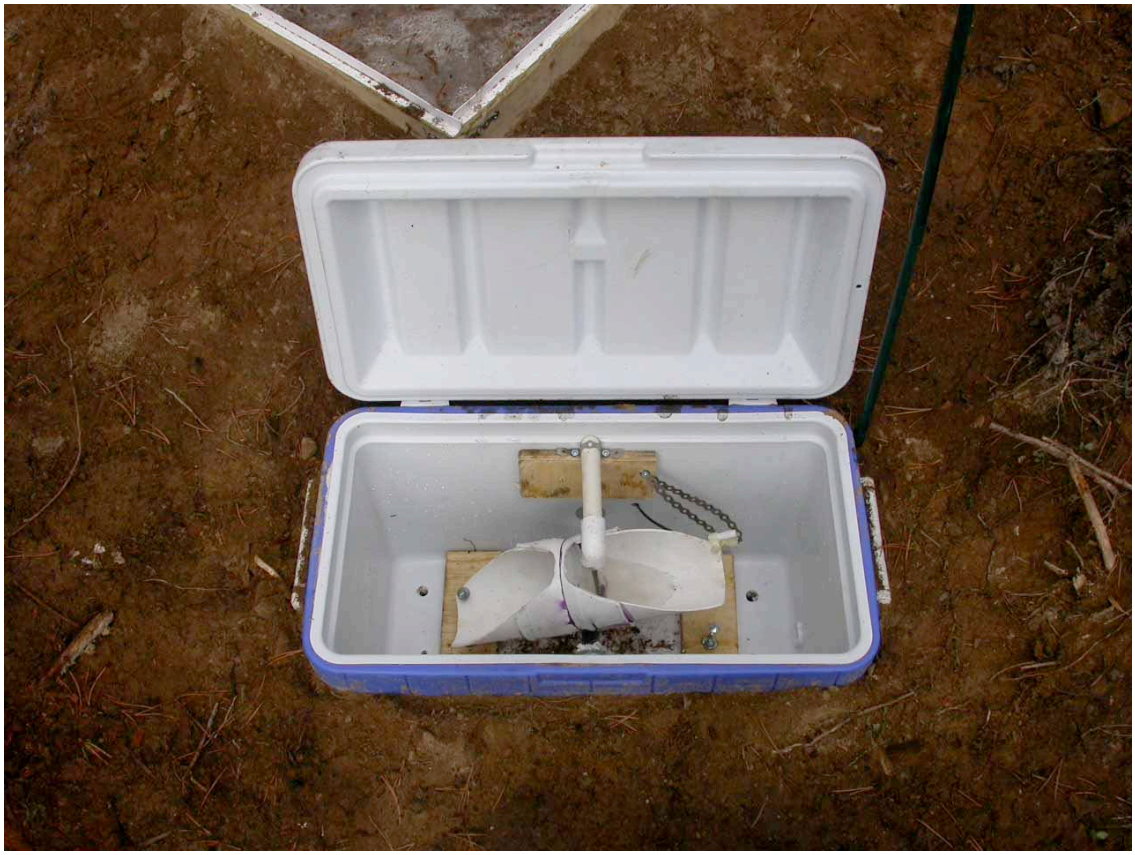

Figure 2.10. Tipping bucket mechanism for the snowmelt lysimeter shown in Figure 2.9.

Figure 2.11. Streamflow site with a 90° v-notch wier and a stilling well.

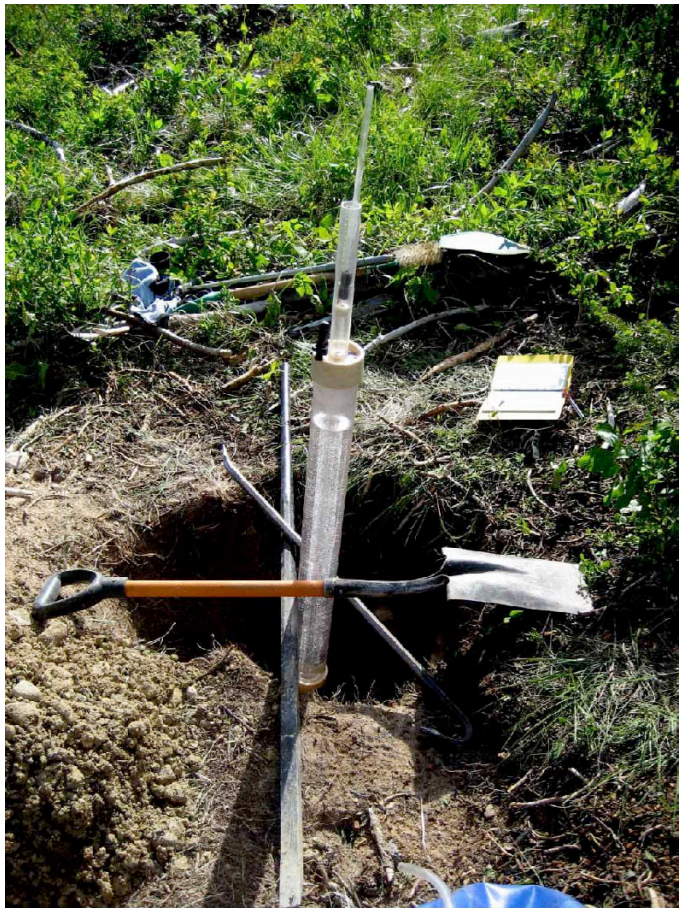

Figure 2.12. Hydraulic conductivity test in operation using a Guelph Permeameter.

Figure 2.13. Bore-hole prepared for a hydraulic conductivity test using a Guelph Permeameter.

3 Midwinter snowmelt: process controls and implications for catchment hydrology

3.1 Introduction

Soil heat flux is largely ignored or assumed constant in modelling of snowmelt processes [*Hock*, 2003; *Metcalfe and Buttle*, 1998; *Walter et al.*, 2005], particularly among spatially distributed models [*Bergstrom*, 1995; *Brubaker et al.*, 1996; *Daly et al.*, 2000; *Motoya et al.*, 2001; *Wigmosta et al.*, 2002]. Even in distributed models that account for soil heat flux, variability in the processes is highly simplified with the spatio-temporal variability of soil structure, composition, and wetness, and the associated variability of soil thermal properties, often ignored or simplified [*Anderton et al.*, 2002; *Marks et al.*, 1999; *Pohl et al.*, 2005]. The rationale for these simplifications is that snowmelt generation is normally dominated by net radiation and the turbulent heat fluxes. However, at locations where soils freeze irregularly or for limited durations and where deep insulating snowpacks persist, snowmelt generated by soil heat flux (i.e. ground melt) may occur and may result in substantial snowpack loss over a winter period of several months [*Kattelmann*, 1989; *Whitaker and Sugiyama*, 2005]. Not accounting for snow loss due to ground melt could lead to an overemphasis of the importance of other energy sources and could limit the accuracy of snowcover modelling and associated runoff response modelling.

Few empirical studies have reported the occurrence of ground melt. In part, this lack of observation may reflect the difficulty of isolating ground melt as a distinct process. For example, snow pillows and rigid snowmelt lysimeter designs (e.g. fiberglass, plywood) could decrease conductive heat transfer between the soil and the snowpack by creating an insulating barrier and by reducing contact with the soil surface, which would reduce the potential for ground melt. With manual snow sampling, snow pillows, and snow depth sensors (the latter requiring snow density in order to estimate SWE), snowmelt cannot be detected while snow is accumulating, and snowmelt generated by soil heat flux cannot be distinguished from other sources of snowmelt while snowpack loss is occurring. Manual snow sampling is also subject to substantial sampling variability and does not identify the

timing of ablation between surveys. Additionally, it can be even more difficult to separate melt generated by soil heat flux from melt generated by other energy sources accurately in locations with frequent midwinter snowmelt events generated by surface energy inputs.

This study monitored snow accumulation and melt processes through the winters of 2006/07 (2007) and 2007/08 (2008) for the purpose of investigating seasonal variation of runoff source area dynamics for a montane snowmelt-dominated catchment. Snowmelt lysimeters were installed within the catchment to monitor spring snowmelt for the purpose of calibrating a snowmelt runoff model. Melt was recorded at all sites throughout the midwinter season of 2007 with nearly continuous subzero air temperatures, and averaged over 1 mm/d at one site. Given the persistence of lysimeter runoff, even during extended periods of subzero air temperatures, it appears that soil heat flux was the most likely source of melt energy. The intention of the overall project was not to study ground melt processes. The midwinter melt observations were unanticipated, but suggest that soil heat flux should not be automatically discounted as an important source of energy for snowpack loss and soil wetting.

The objectives of this chapter are (1) to analyze the midwinter snowmelt patterns, (2) to examine the dominant processes controlling the spatio-temporal variability of the midwinter melt, particularly the potential role of soil heat flux, and (3) to explore the implications of the midwinter melt for catchment hydrology. The analysis is based on the hypothesis that much of the midwinter melt was driven by soil heat flux and, thus, can be considered ground melt. Hence, the occurrence and rate of midwinter melt should be controlled by soil temperature, air temperature, soil wetness, and snow depth: soil temperature influences the amount of stored energy available for upward soil heat flux; soil wetness influences the thermal conductivity of the soil, which influences the rate of upward soil heat flux; and air temperature, together with snow depth, influences the snowpack temperature gradient, which influences the rate of upward heat flux within the snowpack and, thus, the amount of soil heat flux available to melt snow.

3.2 Data analysis

3.2.1 Midwinter periods

Commencement of each midwinter period was defined as the first day of subzero air temperatures following the last occurrence of water input resulting from a surface melt event in the October-December period. For this study, the term surface melt includes both melt at the upper surface of the snowpack and melt of snow suspended in the forest canopy. Termination of each midwinter period was defined as the last day of consecutive subzero air temperatures prior to the first occurrence of a multi-day surface melt event that resulted in water input at most lysimeter sites. The resulting 2007 and 2008 midwinter periods extended from November 22, 2006, to March 3, 2007 (102 days), and December 10, 2007, to April 1, 2008 (114 days), respectively. Hourly data were aggregated to daily intervals for analysis, as the frequency of lysimeter tipping bucket tips was too low during the midwinter periods to permit analysis of hourly data. Any exceptions to the use of daily data are noted.

3.2.2 Soil heat flux modelling

The soil heat flux modelling outlined in this section was conducted by Mike Novak as noted in the preface. I provided the data to run the model, analyzed the model output, and prepared the results for presentation.

A finite element numerical solution of the one-dimensional soil heat flow equation was used to verify whether or not conduction of heat from the soil to the snow could supply sufficient energy to account for the melt measured by the lysimeters during the midwinter period of 2007. The heat flow equation was expressed as follows:

$$C\frac{\partial T}{\partial t} = \frac{\partial}{\partial z}\left(k\frac{\partial T}{\partial z}\right) \qquad (3.1)$$

where C is the volumetric heat capacity of the soil (J m^{-3} K^{-1}), T is the soil temperature (K) at time t (s) and at depth z (m), k is the soil thermal conductivity (W m^{-1} K^{-1}). The heat flux modelling assumed a 15 m deep vertical solution domain that used hourly soil temperature measured at 10 cm soil depth as a surface boundary condition for a semi-infinite profile below that depth. A zero flux plane was assumed as a lower boundary condition. Soil thermal properties were defined for each lysimeter site based on formulations developed by Campbell [1974], incorporating soil physical properties (bulk density, organic matter fraction, and clay fraction) and soil wetness (based on volumetric water content at 20 cm and 40 cm depths and depth to the water table), which were measured at each site. The soil matric potential above the water table was assumed to be a linear function of depth with the slope determined by fitting an assumed soil water retention curve for sandy soil based on Yamanaka *et al*. [1998] to an average of the 20 cm and 40 cm water contents (assumed to apply at the 30 cm soil depth). Hydrostatic equilibrium was assumed for soil depths below the water table. When the groundwater level was above the 30 cm depth, a hydrostatic profile was assumed for all soil depths.

The model simulation spanned the period of October 26, 2006, through July 8, 2008. To "warm-up" the soil temperature profile, a preliminary model run with the boundary conditions described above was executed assuming a uniform initial soil temperature profile of 5 °C and the model was subsequently re-run assuming an initial soil temperature profile equal to that for t = 1 year from the preliminary model run. The solution predicted soil temperature and soil heat flux on an hourly basis for all depths in the solution domain; however, the soil heat flux of greatest interest was that at the actual soil surface (i.e. 10 cm above the surface of the solution domain), so a first-order estimation of heat storage changes in the upper 10 cm of the field soil was calculated by assuming that values of C and $\partial T / \partial t$ in that layer were given by the solution values at the surface of the solution domain (i.e. which corresponds to the 10 cm depth in the field soil). This change in heat storage term was then added to the soil heat flux determined for the surface of the solution domain (i.e. at the 10 cm depth in the field soil).

3.2.3 Statistical analysis

Time series regression models were developed for each of the lysimeter sites to investigate the dominant processes controlling midwinter melt variability. The influences of weather conditions on snowpack processes are well established for snowpack metamorphosis and for surface melt events, but little is known regarding the influences of weather and soil conditions on melt generated during cold midwinter periods, particularly in relation to interactions with soil heat flux. Potential predictor variables considered included air temperature, soil temperature, and soil saturation at each site. Snow depth, solar radiation, wind speed, and vapor density recorded at the UC climate station were also considered as proxy variables related to surface energy exchange. It is acknowledged that the proxy data, which were collected at a single climate station, might represent the conditions at some sites better than other sites, but they were incorporated in the absence of similar data from each site to approximate relative changes in overall catchment conditions from day to day.

Autocorrelation and partial autocorrelation functions (ACF and PACF, respectively) were calculated for melt at each site to evaluate the strength and persistence of memory in the melt time series. Cross-correlation functions (CCF) of melt with the potential predictor variables were calculated to identify variables that might be most suited to predict melt and at what time lags the correlations were strongest. Further cross-correlation analysis of air temperature with melt was completed using a 30 day moving window to investigate whether the delay in melt response varied through the winter.

Using the ACF, PACF, and CCF results as guidance, predictor variables were sequentially added to a regression model for each site to predict melt. After adding each variable, the Akaike information criterion (AIC) [*Akaike*, 1987] was used for model evaluation and for selecting the final model. The presence of serial correlation in the model residuals was investigated by calculating the ACF, the PACF, and the Durbin-Watson test statistic [*Durbin and Watson*, 1950; 1951] from the model residuals, as well as by examining a plot of residuals against time. The Mann-Kendall test statistic

[*Kendall*, 1938], the Shapiro-Wilk test statistic [*Shapiro and Wilk*, 1965], a normal probability plot, and a plot of residuals versus predicted values were used to evaluate the residuals for trends, normality, linearity, and homoscedasticity. Statistical significance for all tests was evaluated using a 0.05 significance level. R statistical software [*R Development Core Team*, 2010] was used for all statistical analyses.

For each site, model development began by including melt with lag terms of 1, 2 and 3 days as predictors. AIC was used to determine which lags to retain. Next, air temperature terms with lags of 0 through 4 days were added and retained based on AIC. The square of air temperature was also included in the model selection due to non-linearity in the residuals. After including air temperature, predictors were added in order based on the maximum cross correlation. Because melt could decrease soil temperature and increase soil saturation, same-day terms (i.e. lag-0, same-day responses) were excluded from the model selection to isolate the influences of soil temperature and soil saturation on melt rates. For sites 24, 2006, and 4004 (Figure 2.1), the time series were restricted to the periods November 22 - January 12, November 22 - January 1, and November 22 - February 4, respectively, for model development due to missing data (sites 24 and 4004) and due to difficulties with fitting statistical melt models to two short periods dominated by surface melt at sites 2006 and 4004 (refer to section 3.3.1 and Figure 3.7 for more details).

Additional regression models were developed to predict daily changes in soil temperature and soil saturation in response to daily melt inputs through the 2007 midwinter period. For both model types, potential predictor variables were limited to necessary autocorrelation lag terms and to melt input terms (same-day and lagged). Data were limited to December 7 and later for the soil saturation models to remove the immediate effects of soil drainage following the November 19-20 surface melt water input event. Otherwise, data were subset similarly and model selection followed a similar procedure as for the melt prediction models. Same-day melt was included for consideration in the model development since it is believed that soil temperature and wetness responded more rapidly to melt than vice versa.

3.3 Results

3.3.1 Winter weather and snowpack conditions

Figure 3.1 summarizes water input to the soil, air and soil temperatures, and soil wetness as means of all six lysimeter sites, along with snow accumulation (SWE) at the Moyie Mountain snow pillow, for the 2007 and 2008 winters. The maximum SWE was slightly lower in 2007 than in 2008 (540 mm on April 7, 2007, and 555 mm on April 28, 2008, respectively). For the midwinter periods only, the mean air temperature was slightly lower in 2007 than in 2008 (-7.5 °C and -7.0 °C, respectively) with slightly lower accumulated precipitation (297 mm and 312 mm of water equivalent measured at the UC climate station, respectively). Through both midwinter periods, air temperatures cycled between multi-day periods of extreme cold weather and multi-day periods of only slightly subzero weather. In both years, the weather remained only slightly subzero after early February until the onset of active surface melt, which began in early March in 2007 and in early April in 2008.

Although the midwinter conditions were similar between the two years, the early-winter conditions were sufficiently different to establish contrasting antecedent soil hydrothermal conditions. The 2007 early-winter period (i.e. November 2006) experienced early snowpack development while air temperatures remained around freezing for most of the period (Figure 3.1). Several rainstorm/snowmelt events increased soil wetness, but failed to eliminate the established snowpack. The early development of a deep insulating snowpack preserved the wet and unfrozen soil conditions for the remaining winter. In contrast, the 2008 early-winter period (i.e. November and early December 2007) experienced delayed snowpack development and an approximately two-week period of cold weather with temperatures dropping below -10 °C (Figure 3.1). The cold weather was followed by a brief warming event and a sudden return to cold weather. More rapid snowpack development began after the return to cold weather. The cold, dry weather and delayed snowpack development led to extensive soil freezing and drier soils than in early-winter 2007, which persisted through

the remaining winter due to the insulating effects of the subsequent snowpack development.

3.3.2 Midwinter snowmelt

Snowmelt was recorded throughout most of the 102 day midwinter period of 2007 (Figure 3.2a) and at all six lysimeter sites (Table 3.1; Figure 2.1). Snowmelt occurred at sites 4004 and 6003 through all weather conditions including extended periods of extreme cold conditions (e.g. late November and mid-January). Using a 0 °C air temperature threshold, the positive and negative degree-day heat sums from the start of the 2007 and 2008 midwinter periods show that positive air temperatures were negligible throughout both periods, particularly compared to the severity of the negative air temperatures (Figure 3.2c). Midwinter mean melt rates at the six sites averaged 0.46 mm/d and ranged between 0.11 mm/d (site 2013) and 1.06 mm/d (site 6003). The maximum SWE measured manually at the six sites in 2007 averaged 266 mm and ranged between 180 mm and 394 mm (Table 3.1). The ratio of the accumulated midwinter melt to the maximum SWE for each site averaged 0.18 and ranged between 0.03 and 0.37. At site 2013, the accumulated midwinter melt was 11 mm and the maximum SWE was 394 mm, which suggests that approximately 3% of the total snowfall (405 mm) was lost to melt, not accounting for evaporation/sublimation losses, comprising approximately 1% of the mean annual precipitation. At site 6003, the accumulated midwinter melt was 108 mm and the maximum SWE was 294 mm suggesting that approximately 27% of the total snowfall (402 mm) was lost to melt. Moreover, 108 mm of snow water loss comprises approximately 14% of the mean annual precipitation, and, thus, represents a substantial portion of the water budget on both seasonal and annual bases. In contrast, the midwinter mean melt rates at the six sites averaged only 0.06 mm/d throughout the 114 day midwinter period of 2008, and the melt occurred during the latter relatively warm portion of the midwinter period (Figure 3.2b) and primarily at one location (site 4004) (Table 3.1).

The soil heat flux modelling results show that sufficient upward heat flux was generated at the soil surface over the 2007 midwinter period to account for the measured midwinter melt (assuming that all soil heat flux is used to generate melt) at all sites except site 6003, and that similar amounts of soil heat flux were generated in 2008 (Figure 3.3a). The heat flux resulted from a positive temperature gradient within the upper 4-5 m of soil (Figure 3.3b) that was generated from heat stored during the respective previous snow-free season, particularly the summer period. Soil heat flux density on any particular day of the year was similar between the two midwinter periods despite the differences in the amounts of measured midwinter melt. During both midwinter periods, the heat flux density was highest at the start of the midwinter period and decreased steadily throughout the winter (Figure 3.3c), which is consistent with a loss of stored soil heat and corresponding decrease in the strength of the soil temperature gradient throughout the winter (Figure 3.3b). Predicted midwinter mean snowmelt rates ranged between 0.61 mm/d and 0.91 mm/d and between 0.53 mm/d and 0.68 mm/d among all sites in 2007 and 2008 (Figure 3.3a), respectively, showing the sensitivity of the predicted soil heat flux rates to varying soil conditions, as the heat flux model was parameterized specific to the composition (Table 2.2), wetness, and temperature of the soil at each site and at each hourly time-step, and the conditions varied extensively from site to site (wetness and temperature conditions are discussed further in section 3.2.3).

The patterns in Figure 3.4 show that snowmelt rates reached minimum values and began increasing at sites 4004 and 6003 on at least two occasions during midwinter 2007 while air temperatures increased from synoptic lows of approximately -20 °C to -25 °C up to approximately -10 °C to -15 °C. Similar patterns occurred at the other fours sites, but with more delayed responses. Moreover, during field investigations on February 11, 2007, the lower portion of the 94 cm deep snowpack at site 6003 was wet and water was observed dripping from the base of the snowpack in a melted air pocket located approximately 1.5 m from the lysimeter. This melt was observed in the early afternoon while the air temperature was -2.5 °C after rising from a nightly low of -7.7 °C, and while the snowpack internal and surface temperatures were -4.3 °C and -2.5 °C, respectively. The positive and negative degree-day heat sums (based on hourly data) accumulated over

the prior 14 day period were 1.5 °C D and -95.5 °C D, respectively, with a maximum hourly air temperature during the prior 14 day period of 2.2 °C.

3.3.3 Melt in relation to measured soil temperature and wetness

The mean soil temperature at 10 cm depth among all sites was 1.7 °C at the start of the 2007 midwinter period (i.e. November 22, 2006) and varied between 1.1 °C and 2.1 °C (Table 3.1). The mean among all sites was 0.2 °C at the start of the 2008 midwinter period (i.e. December 10, 2007) and varied between -0.5 °C and 0.7 °C. As the 2007 midwinter period progressed, the soil cooled at five of six sites (Figure 3.5a) and functioned as a heat source with vertical heat loss to the overlying snowpack. In contrast, the soil warmed through the midwinter period of 2008 (Figure 3.5b) and functioned as a heat sink while gaining heat from deeper soils and, potentially, the snowpack, depending on the direction of the snow/soil interface temperature gradient. In 2007, melt varied positively with soil temperature at the start of the midwinter period, whereas cold soils at the start of midwinter 2008 appeared to inhibit subsequent melt (Figure 3.6a).

The mean soil saturation among all sites was 78.9% at the start of the 2007 midwinter period and varied between 70.8% and 84.5% (Table 3.1). The mean among all sites was 61.1% at the start of the 2008 midwinter period and varied between 42.2% and 79.5%. Midwinter mean melt in 2007 varied positively with the level of soil saturation at the start of the midwinter period, but a similar relation did not exist in 2008 (Figure 3.6b).

These soil temperature and wetness patterns were likely representative of the widespread conditions in each year based on field observations at the 50 hillslope monitoring sites. Soil plugs at most sites were unfrozen and wet during snowpack surveys in February 2007, whereas soil freezing was present at most sites during snowpack surveys in February 2008. Manual soil wetness surveys showed that soils were generally wetter in October and February of 2007 than in October and February of 2008, respectively.

3.3.4 Melt in relation to air temperature

The midwinter mean air temperature among all sites was -7.5 °C in 2007 and varied between -6.2 °C and -8.4 °C (Table 3.1). The mean among all sites was -7.0 °C in 2008 and varied between -3.5 °C and -7.8 °C. Midwinter mean snowmelt for the six sites in 2007 increased linearly with increasing midwinter mean air temperature, with the exception of site 6003, but a similar relation did not exist in 2008 (Figure 3.6c). The outlier in the 2007 data likely resulted from the combination of high soil temperature and high soil wetness (both discussed in section 3.2.3).

Through midwinter 2007, melt rates varied with air temperature through the entire range of subzero temperatures at all sites (Figure 3.7). At the site with the greatest melt (site 6003), melt varied between 0.48 mm/d and 1.74 mm/d, including periods when the daily mean air temperature was less than -20 °C (Figure 3.8a). Other sites with less snowmelt (e.g. site 2013) also experienced melt during extreme cold conditions, but four sites did experience short breaks in melt during and shortly after periods when daily mean air temperatures dropped below approximately -15 °C to -20 °C, depending on the site. At the site with the lowest melt (site 2013), melt varied between 0 mm/d and 0.48 mm/d (Figure 3.8a). In contrast, site 4004 (a southwest aspect, lower elevation, clearcut site, and the only site with substantial melt in 2008) experienced melt in 2008 only on days when the daily mean air temperature exceeded approximately -6 °C (Figure 3.8b).

Cross-correlation analysis of daily melt and daily air temperature for the midwinter period of 2007 showed that the greatest correlations for individual sites ranged between 0.38 (site 2006) and 0.72 (site 6501), and melt lagged air temperature by 1 day and 4 days, respectively. A plot of daily melt (lagged 3 days) against daily air temperature for sites 6003 and 2013 clearly illustrates a delayed meteorological control on melt for both high melt and low melt sites (Figure 3.8c). The plot also suggests that a minimum air temperature threshold of approximately -14 °C controlled the occurrence of melt at site 2013. At similarly low air temperatures, however, melt continued at site 6003,

suggesting that other processes were also responsible for controlling the overall melt rates.

The relation between melt and air temperature at site 6003 shows marked hysteresis (Figure 3.9). Melt was comparatively greater (given equal air temperatures) through cooling phases than through warming phases. Cross-correlation analysis using a 30 day moving window shows that the lag between melt and air temperature associated with maximum correlation was greater through the middle portion of the midwinter and varied negatively with air temperature (Figure 3.10). The same was true for all other sites.

3.3.5 Statistical modelling of daily melt for the 2007 midwinter period

From the ACF/PACF analysis of daily melt for the midwinter period of 2007, lag-1 memory was highly significant at all sites and lag-2 or lag-3 memory was slightly significant at sites with lower air temperatures. From the CCF analysis, air temperature and vapor density were strongly correlated with melt at all sites and lags varied from 1 to 4 days. Variables that were slightly to moderately correlated with melt included soil temperature, soil saturation, snow depth, and wind speed; however, correlations were not significant at all sites. Lags of 1 to 3 days were apparent at some sites also for snow depth and wind speed.

All of the final regression models are statistically significant (Table 3.2). The amount of variance explained by the models ranges from 82% to 97%, and no significant serial correlation or trends remain in the model residuals. Moreover, normality, linearity, and homoscedasticity of the residuals are acceptable for all sites. All of the models include lagged melt and air temperature terms. Generally, models for forested sites and sites with lower midwinter melt rates include melt and air temperature terms with greater time lags compared to clearcut sites and sites with higher melt rates. The sites with greater lags and lower melt rates also had relatively cold soils at the start of the midwinter period (e.g. sites 2013 and 6501). Models for all sites except 4004 and 6501 include same-day snow depth terms. The model for site 6003 includes lag-1 and lag-2 soil temperature terms.

Models for sites 4004 and 6003 include same-day vapor density. Soil saturation and other meteorological variables were not significant at predicting melt variability on a daily basis.

3.3.6 Soil temperature and wetness responses to melt

At several sites, occurrences of relatively high melt rates during the 2007 midwinter period were accompanied immediately or shortly after by more rapid decreases in soil temperature and more rapid increases or less rapid decreases in soil saturation (Figure 3.7). These patterns are particularly noticeable for the surface melt events that occurred at site 2006 on January 2 and at site 4004 in early February, but are also noticeable for melt variability during the other periods. To investigate the potential responses of soil wetness and soil temperature to melt inputs, regression models were developed to predict daily changes in both soil wetness and soil temperature using daily melt inputs from the 2007 midwinter period. As outlined in the methods section, data were additionally stratified to remove the effects of the surface melt input events.

For three sites (24, 2013, and 4004), 55-72% of the variance in daily change in soil saturation is accounted for by daily melt inputs (same-day and/or 1 day lag) (Table 3.3). For four sites (24, 4004, 6003, and 6501), 31-43% of the variance in daily change in soil temperature is accounted for by daily melt inputs (same-day and/or a 1 day lag) (Table 3.4). The model results suggest that, at some sites, soil wetness responded positively and soil temperature responded negatively to melt inputs; however, the low to moderate amounts of variance accounted for by several of the models suggest that other processes were also responsible for controlling daily changes in soil temperature and wetness.

Based on the model coefficients, mean melt rates of approximately 0.49, 0.09, and 0.64 mm/d would have been sufficient to offset soil drainage at sites 24, 2013, and 4004, respectively. The actual mean melt rates for the respective subset periods were 0.35, 0.11, and 0.62 mm/d, respectively. Interestingly, soil wetness through the respective subset periods was approximately maintained at sites 2013 and 4004, but not at site 24

(Figure 3.7). Similar calculations with soil wetness for sites 2006, 6003, and 6501, and with soil temperature for all sites would be meaningless due to the combination of low amounts of variance accounted for by the models and model intercepts that were not significant.

3.3.7 Was the midwinter melt in 2007 unusual?

The difference in melt occurrence between the 2007 and 2008 midwinter seasons appears to have been controlled by the weather conditions, particularly air temperature, leading up to and during the early stages of winter snowpack development in relation to its influence on the depth of frozen soil (i.e. the depth where soil heat flux generated ice-melt occurs). Specifically, the 2007 season was characterized by warm weather followed by rapid development of the snowpack, which served to retain heat in the shallow soil and, thus, ensure that any soil heat flux generated ice-melt occurred at the soil surface. To help assess whether or not the weather and snowpack conditions in 2007 were unusual in this regard, Figure 3.11 illustrates the covariance of air temperature averaged over the preceding 7 days (i.e. a 7 day moving window) and SWE measured at the Moyie Mountain snow pillow for the two study seasons (indicated by lines) and over the 1998-2008 period of record (indicated by dots). Over the period while the first approximately 75 mm of SWE accumulated, air temperatures for 2007 were within the range of background variability. In 2008, however, air temperatures were within background variability for the first approximately 25 mm of accumulation, but then dropped and remained below the background range for the subsequent 50 mm of accumulation. These results suggest that the warm air temperatures during the early stages of winter snowpack development in 2007 (which resulted in warm shallow soils being insulated by the snowpack) were likely typical, and that the cold air temperatures during the early stages of winter snowpack development in 2008 (which resulted in cold shallow soils being insulated by the snowpack) were likely atypical.

3.4 Discussion

3.4.1 Was the midwinter melt caused by soil heat flux?

Multiple lines of circumstantial evidence suggest that much of the midwinter melt recorded in 2007 resulted from soil heat flux and, thus, can be considered ground melt. Specifically, the persistence of lysimeter runoff throughout the midwinter period with little or no positive air temperatures at six independent sites incorporating large contrasts in elevation, slope gradient, slope aspect, forest cover, and soil wetness is difficult to explain based on only surface melt (Figure 3.7), particularly when the cumulative negative air temperature degree-day heat sum is contrasted with the cumulative positive heat sum for 2007 (Figure 3.2c). While the winters of 2007 and 2008 had similar air temperatures, substantial melt occurred only during 2007, which had higher shallow soil temperatures at the start of the midwinter period. The importance of ground melt is also supported by the fact that synoptically varying melt rates re-started or began increasing on multiple occasions during 2007 in response to warming weather conditions while air temperatures were as low as -15 °C (Figure 3.4). Two of these sites (2006 and 2013) are located on northwest aspect forested hillslopes where the potential for melt during subzero air temperatures to be generated by solar radiation inputs would have been negligible. The observation of basal melt at site 6003 on February 11, 2007, while the upper and middle portions of the snowpack were sub-freezing and after several weeks with air temperatures persisting primarily between -5 °C and -25 °C with minimal positive air temperatures further supports the importance of ground melt. Finally, the heat flux modelling indicates that there was sufficient heat stored in the soil to support the midwinter melt rates in 2007, except at site 6003 (Figure 3.3a). An additional source of melt energy could have been heat advection from upslope areas via groundwater flow, as site 6003 is located in the trough of a hillslope hollow and experienced a high water table that gradually declined from a soil depth of 0.47 m to 0.87 m throughout midwinter 2007. Similar heat advection processes may have occurred at site 2006.

Two notable exceptions occurred when midwinter melt was unlikely to have been caused by only soil heat flux. Relatively warm, overcast, and humid weather accompanied by high wind speeds occurred on January 1-2 when approximately 7 mm of melt was recorded at site 2006, likely generated by turbulent heat fluxes causing melt in the forest canopy at lower elevations. On February 5-8, warm, sunny weather was associated with 3 mm of melt at site 4004 that was likely generated by radiation fluxes. The data logger at site 4004 was removed for maintenance February 6-11, so data were not recorded on those days at that site.

3.4.2 Controls on the spatio-temporal variability of ground melt

The most fundamental condition required for ground melt to occur is that the temperature at the snow-soil interface must be 0 °C; otherwise, snow in contact with the soil cannot be warmed to the melting point and, thus, will not melt. The importance of this control is highlighted by the fact that modeled soil heat flux rates were similar between the midwinter periods of 2007 and 2008, but melt did not occur in 2008 due to frozen shallow soils. It is possible for soils to warm after snowpack development resulting in a gradual rise in the lower boundary of frozen soil and eventual contribution of soil heat flux to snowmelt when the soil is no longer frozen, but the soil warming process is slow and could take longer than the duration of the midwinter period. If the snow-soil interface temperature is 0 °C, then the rate of upward heat flux to the soil surface must exceed the rate of upward heat flux from the base of the snowpack for ground melt to occur. Otherwise, all soil heat flux is partitioned to upward heat flux in the snowpack and eventually lost to the atmosphere

The rate of heat conduction in any material depends on the temperature gradient through it and its thermal conductivity. As the snow-soil interface temperature will be 0 °C during snowmelt, the temperature gradient in the soil is controlled only by the temperature profile below the soil surface. The soil thermal conductivity varies with soil structure, composition, and wetness. Water has greater thermal conductivity than air (0.58 vs. 0.024 W m^{-1} K^{-1}, respectively); thus, as soil saturation increases and water

replaces air in pore space, the thermal conductivity of the soil increases. Hence, soil temperature, wetness, structure, and composition can all control the spatial variability of soil heat flux. The influences of soil temperature and wetness on the spatial variability of ground melt are highlighted by the 2007 results in Figures 3.6a and 3.6b. Greater soil temperature and wetness at the start of the 2007 midwinter period resulted in greater amounts of soil heat storage and higher rates of release for ground melt throughout the remaining winter. Soil temperature and wetness are the only controls on soil heat flux that can vary rapidly enough to influence its within-season temporal variability. However, relations between these two variables and ground melt were either weak or not evident in the statistical melt models, likely due to their limited temporal variability during the midwinter period of 2007 and the potentially overwhelming effect of the relatively rapid changes in the conditions governing upward heat flux in the snowpack.

Given that the soil heat flux rates vary relatively slowly in time and given that the snow-soil interface temperature will be 0 °C during snowmelt, temporal variability in ground melt would be controlled primarily by changes in the basal snowpack temperature gradient, which would, in turn, be influenced by the propagation of surface temperature variations into the snowpack. Low internal snowpack temperatures generate stronger basal snowpack temperature gradients and promote greater upward heat flux leaving less heat available for ground melt, whereas high internal snowpack temperatures suppress upward heat flux at the base of the snowpack, thus, allowing more soil heat flux to be partitioned into melt. The influence of air temperature and snowpack heat flux on the spatial pattern of ground melt rates in 2007 is illustrated in Figure 3.6c. The influence of air temperature on temporal variations is illustrated in Figures 3.7 and 3.8 and in the importance of air temperature as a predictor variable in the ground melt models (Table 3.2).

The rapid response of midwinter melt to synoptic air temperature variation (i.e. 2-4 day lags with snowpacks up to 1.3 m in depth) that was observed during midwinter 2007 (Figures 3.2, 3.4, and 3.7) indicates that surface temperature changes must have propagated into the snowpack relatively rapidly in order to influence basal snowpack

temperature gradients and, thus, the partitioning of soil heat flux between upward conduction and melt. The thermal diffusivity of snow is too low ($0.1 \cdot 10^{-6} – 0.4 \cdot 10^{-6}$ m^2/s [*Oke*, 1987]) for conduction alone to account for the response; however, forced air convection through the snowpack due to wind pumping and/or atmospheric pressure changes can enhance the rate of propagation of temperature variations in snow [*Albert and McGilvary*, 1992; *Sturm and Johnson*, 1991]. There is some empirical evidence at mid-latitude sites that synoptic-scale surface temperature variations can propagate relatively deeply into a snowpack. Watson *et al.* [2006] documented synoptic-scale variability in snowpack temperatures at a site in Wyoming where the snowpack depth peaked at approximately 1.3 m (similar to snowpack depths at UEC). Fluctuations of several degrees were recorded at 75 cm above the soil surface, even as the snowpack approached its maximum depth. Synoptic-scale fluctuations occurred, but were weaker, at 10 cm above the soil surface. The magnitude of variation decreased as the snowpack depth increased. Deems *et al.* [2002] reported synoptic-scale variations in the vertical temperature gradient within a snowpack, averaged between 10 cm above the soil and 30 cm below the snow surface, at a site in Montana where the snowpack depth peaked at 1.6 m. The temperature gradients varied roughly in phase with snow surface temperature, indicating rapid propagation through at least the top 30 cm of snow.

Midwinter melt responded more rapidly to air temperature changes at clearcut sites and at sites where overall air temperatures and soil heat flux inputs were greater, and also more rapidly at any particular site when air temperatures were greater at the site. The conditions favoring a greater lag in melt response to air temperature were, thus, associated with forest cover, lower snowpack temperatures, and stronger snowpack temperature gradients. The thermal conductivity of snow varies positively with snow temperature and with temperature-induced metamorphism; thus, the observed lags in response and their spatial and temporal variability are consistent with the physics associated with conductive heat transfer and storage, and with reduced rates of forced convection (i.e. wind-pumping) at forested sites due to lower wind speeds. It should be noted, however, that delays in melt response that were apparent in the data were likely

partially generated by delays associated with the time required for water to drain along the base of the snowpack and through the lysimeter drainage system.

In the melt regression models, lagged melt and air temperature account for snowpack water and heat storage effects, respectively. Same-day snow depth accounts for the influence of snow depth on the strength of the snowpack temperature gradient and the extent to which convective forces can influence snow temperatures near the base of the snowpack. The mean of the two lagged soil temperatures accounts for the influence of long-term variability of soil heat flux on ground melt and the difference between the two lagged soil temperatures accounts for the influence of short-term variability of soil heat flux on ground melt. Same-day vapor density could account for influences on the snowpack temperature gradient via increased rates of latent heat transfer from the atmosphere to the snowpack during periods of high atmospheric vapor content. It could also relate to increased rates of incoming long-wave radiation, as atmospheric emissivity varies with vapor pressure.

3.4.3 Hierarchy of spatio-temporal controls

The stark contrast in the occurrence of ground melt between 2007 and 2008, despite having similar soil heat flux rates, illustrates that the occurrence of widespread shallow soil freezing upon the establishment of a deep insulating snowpack forms a first-order (i.e. inter-annual temporal) control on the occurrence of ground melt. Provided that the early-winter soil temperature does not inhibit ground melt, spatial variability in the seasonal accumulation of ground melt is controlled by spatial variability in early-winter soil temperature, early-winter soil wetness, and midwinter air temperature. In 2007, the range in mean ground melt rates among sites was greater than the range through time at most sites, suggesting that these three variables form second-order (i.e. intra-seasonal spatial) controls on ground melt. The roughly similar range of variance in the patterns for 2007 in Figure 3.6 suggest that each of these three variables is of roughly similar importance as spatial controls, although the outlier in Figure 3.6c suggests that the importance of soil saturation, soil temperature, and heat advection via groundwater flow

might dominate air temperature where soil temperature and soil saturation are both high (e.g. above approximately 2 °C and 80%, respectively).

Within a season with ground melt occurring, small-scale (e.g. daily to weekly) temporal variability of melt is controlled by small-scale variability in air temperature, as illustrated by the patterns in Figure 3.8c and by the melt models (Table 3.2); hence, air temperature forms a third-order (i.e. intra-seasonal temporal) control on ground melt. Small-scale temporal variability of snow depth, soil temperature, and vapor density may also exert some control, but to a lesser extent than air temperature. There is a physical basis for expecting that small-scale temporal variability of soil wetness should also be important, but the results do not corroborate this notion.

3.4.4 Implications for catchment hydrology

Notwithstanding the fact that no soil wetness terms were found to be significant in the modelling of daily melt, soil heat flux and ground melt might be capable of forming a positive feedback response loop through the influence of soil wetness on soil thermal conductivity. This notion is supported by the positive response of soil saturation to ground melt inputs at some sites (e.g. sites 24, 2013, 4004), as illustrated by the soil saturation models (Table 3.3). In contrast, a negative feedback response loop might be capable of forming between soil heat flux and ground melt through the influence of soil temperature on the amount of heat available for upward flux. Soil temperature responded negatively to ground melt inputs at several sites (e.g. sites 24, 4004, 6003, 6501), as illustrated, albeit weakly, by the soil temperature models (Table 3.4). The responses of soil temperature and soil wetness counteract each other in their potential to influence ground melt rates. It is uncertain whether either response could be sufficient to significantly impact ground melt patterns, and it is uncertain which of the two opposing feedback responses might dominate.

During the midwinter period of 2007, the greatest amount of melt occurred at the site with the highest early-winter soil wetness and soil temperature, and resulted in soil

wetness being maintained or enhanced through the midwinter period. In contrast, the lowest amount of melt occurred at the site with the lowest early-winter soil wetness and midwinter mean air temperature, and nearly the lowest early-winter soil temperature, and resulted in static soil wetness. Sites with intermediate melt inputs experienced soil drying through the winter. Even if the hypothesized feedback response loops between ground melt and soil wetness are insignificant, midwinter ground melt may still influence catchment-scale hydrologic response. If the relation between midwinter ground melt and soil wetness at the start of the midwinter period (Figure 3.6b) is more broadly representative, then locations that start the midwinter period with greater soil wetness receive more ground melt inputs, which leads to a reinforcement of any pre-existing spatial soil wetness patterns. If soil wetness and ground melt inputs are spatially organized, then hillslope hydrologic connectivity would likely be enhanced via ground melt, which would enhance catchment hydrologic responsiveness at the start of the active melt period and during spring runoff. Moreover, if heat advection via groundwater flow is an important contribution to the amount of soil heat available for upward flux at hillslope hollow locations, then the spatial organization of subsurface flow patterns would contribute to an additional self-reinforcing process controlling the spatial organization of ground melt, soil wetness, and hillslope hydrologic connectivity.

If soil heat flux and ground melt are capable of forming a positive feedback response loop (via soil wetness response) that would dominate any negative feedback response loop formed (via soil temperature response), then the feedback response process would further enhance the overall level and spatial organization of spring soil wetness. Detailed physical modelling of the ground melt processes is necessary to further understand this issue.

3.4.5 Challenges with using lysimeters to measure ground melt

Snowmelt lysimeters are often susceptible to freezing, leakage, and blockage of the drain pipes, liners, and tipping buckets. None of the lysimeters at any of the sites experienced problems with the drain pipes, but data are missing for January 13 through February 11,

2007, at site 24 due to water freezing in the tipping bucket. Additionally, data are missing for February 6 through February 11, 2007, at site 4004 and for December 10, 2007, through February 20, 2008, at site 24 due to data recorder malfunctions. The lysimeter liners were susceptible to perforation from the snow pressing the relatively thin polyethylene sheeting against coarse fragments or debris; however, perforations were found to be negligible during inspections of the liners following spring melt-out.

A problem with using lysimeters of any construction for measuring ground melt is that they eliminate upward vapor flux and the associated latent heat flux, and can decrease upward heat conduction from the soil to the snowpack during the snowcover season. The liners used in this study might have caused excess soil heat retention from the warm snow-free period persisting into the snowcover period due to having a slightly lower thermal conductivity than that of soil, which could have increased the amount of ground melt. Excess retention of soil heat from the snow-free period was not a concern for the high ground melt midwinter period of 2007 because the liners were installed in October 2007 immediately prior to the commencement of snowfall; however, elimination of latent heat flux and reduction of soil heat conduction might have been concerns for both years. These effects would have caused the lysimeters to underestimate the magnitude of ground melt, in which case ground melt would have been even greater than was measured. Nevertheless, detailed physically based modelling of surface and subsurface heat and water fluxes at multiple sites is necessary to understand better any influences of the lysimeter liners on ground melt. Detailed physically based modelling is also necessary to understand better the processes controlling ground melt, any interactions and feedback responses between the processes, and any potential influences on catchment hydrology. For instance, since forest cover removal alters soil temperature, soil wetness, snow accumulation, and meteorology, it should also influence soil heat flux dynamics and the occurrence and rate of ground melt.

This study is one of only a few that have measured ground melt inputs directly using lysimeters. Kattelmann [1989] measured a consistent basal melt rate of 0.5 mm/d with lysimeters (unspecified liner material) that was generated by soil heat flux under a

seasonal snowpack at a 2100 m elevation site in Sierra Nevada, California. Whitaker and Sugiyama [2005] observed background melt rates of 0.8-1.0 mm/d under seasonal snowpacks at three low elevation sites in maritime Japan. The background melt continued through periods of prolonged subzero air temperatures. They presumed that the melt was generated by soil heat flux and suggested that it could accumulate to as much as 120 mm over a 4 month period. It is likely that the use of thin, flexible polyethylene sheeting for the lysimeter liners in this study instead of thick, rigid materials (e.g. fiberglass, plywood), along with the study location being conducive to ground melt via unfrozen soils and deep snowpacks, was a large factor in facilitating the observation of ground melt. Soil thermal conductivities vary between 0.25 and 2.2 W m^{-1} K^{-1} depending on the soil texture and wetness. The thermal conductivities of snow, polyethylene, plywood, and fiberglass are 0.05-0.25, 0.42-0.51, 0.13, and 0.04 W m^{-1} K^{-1}, respectively. Since the thermal conductivity of polyethylene is closer to that of soil than are the thermal conductivities of plywood and fiberglass, and since the polyethylene liners used in this study were much thinner than plywood and fiberglass, the impact of the lysimeter liners on reducing soil heat conduction to the snowpack was likely minimal compared to the impacts of lysimeter liners used in other studies [*Prevost et al.*, 1991; *Sensoy et al.*, 2006; *Thyer et al.*, 2004; *Winkler et al.*, 2005].

3.5 Conclusions

Continuous and widespread snowmelt was observed throughout periods of extreme cold weather conditions during midwinter 2007. Multiple lines of circumstantial evidence suggest that much of the melt resulted from soil heat flux and, thus, can be considered ground melt. Negligible midwinter melt was observed in 2008, which appeared to result from the presence of frozen soil upon the development of a deep insulating snowpack. Among six sites, accumulated snowpack losses throughout midwinter 2007 comprised between 3% and 27% of the winter snowfall and between 1% and 14% of the annual water budget. Midwinter melt increased with increasing early-winter soil temperature and wetness, and increasing midwinter air temperature, which formed important controls on the spatial variability of melt. Synoptic air temperature patterns formed an important

control on the temporal variability. Lateral advection of soil heat via groundwater flow might have also increased midwinter melt. Though the rates of melt varied considerably between sites, the positive influence of early-winter soil temperature and wetness on midwinter melt might enhance early-spring hillslope hydrologic connectivity and associated spring runoff response. The weather and snowpack conditions leading to high rates of melt during midwinter 2007 do not appear unusual for the study region.

Table 3.1. Summary of snowpack, soil, and air temperature conditions. Midwinter snowmelt (minimum, mean, maximum), accumulated snowmelt, maximum SWE (measured manually), ratio of accumulated melt over maximum SWE, mean air temperature, and soil temperature and saturation at the start of the midwinter period.

Year	Site	[a]Melt (mm/d)			[a]Accum melt (mm)	Max SWE (mm)	Accum melt / Max SWE	Mean air temp (°C)	Initial soil temp (°C)	Initial soil sat (%)
		Min	Mean	Max						
2007	24	0.00	0.29	0.78	21	180	0.12	-6.90	1.74	81.6
	2006	0.00	0.42	4.72	43	188	0.23	-7.02	1.92	78.5
	2013	0.00	0.11	0.48	11	394	0.03	-8.41	1.31	70.8
	4004	0.12	0.67	4.13	64	232	0.28	-6.20	1.82	81.0
	6003	0.48	1.06	1.74	108	294	0.37	-8.15	2.13	84.5
	6501	0.00	0.22	0.66	22	308	0.07	-7.86	1.05	77.1
2008	24	0.00	0.00	0.00	0	182	0.00	-3.46	NA	NA
	2006	0.00	0.00	0.06	0	206	0.00	-6.01	0.47	79.5
	2013	0.00	0.00	0.00	0	402	0.00	-7.83	-0.46	54.6
	4004	0.00	0.37	3.09	42	224	0.19	-5.18	-0.14	42.2
	6003	0.00	0.01	0.18	1	420	0.00	-7.09	0.23	71.8
	6501	0.00	0.00	0.00	0	304	0.00	-7.12	0.73	57.5

a. Data are missing for site 24 on January 13 - February 11, 2007, and on December 10 - February 20, 2008, and for site 4004 on February 6-11, 2007. After excluding surface melt, the mean 2007 ground melt for sites 2006 and 4004 was 0.33 and 0.63 mm/d, and the maximum was 0.96 and 1.14 mm/d, respectively.

Table 3.2. Regression models for ground melt on day "t" (M_t). Predictor variables are snowmelt memory (M_{t-i}; i is number of days lag), air temperature (Ta), soil temperature (Ts), snow depth (SD), and vapor density (ρ_v) for the midwinter period of 2007. Data for sites 24, 2006, and 4004 were subset to November 22 - January 12, November 22 - January 1, and November 22 - February 4, respectively.

Site	Model	SE_{res}	R^2	p-value
24	$M_t = 0.387 + 0.400 \cdot M_{t-1} + 0.001 \cdot Ta_{t-1}^2 + 0.034 \cdot Ta_{t-1} + 0.002 \cdot Ta_{t-2}^2 + 0.055 \cdot Ta_{t-2} + 0.215 \cdot SD$	0.074	0.907	< 0.001
2006	$M_t = 0.471 + 0.391 \cdot M_{t-1} + 0.003 \cdot Ta_{t-1}^2 + 0.091 \cdot Ta_{t-1} + 0.280 \cdot SD$	0.054	0.966	< 0.001
2013	$M_t = 0.094 + 0.325 \cdot M_{t-1} + 0.314 \cdot M_{t-2} + 0.005 \cdot Ta_{t-2} + 0.001 \cdot Ta_{t-3}^2 + 0.015 \cdot Ta_{t-3} + 0.048 \cdot SD$	0.041	0.820	< 0.001
4004	$M_t = 0.062 + 0.648 \cdot M_{t-1} + 0.001 \cdot Ta^2 - 0.001 \cdot Ta_{t-1}^2 + 0.001 \cdot Ta_{t-2}^2 + 0.024 \cdot Ta_{t-2} + 0.094 \cdot \rho_v$	0.098	0.883	< 0.001
6003	$M_t = -0.361 + 0.650 \cdot M_{t-1} + 0.001 \cdot Ta^2 + 0.023 \cdot Ta_{t-1} - 1.901 \cdot Ts_{t-1} + 2.188 \cdot Ts_{t-2} + 0.268 \cdot SD + 0.054 \cdot \rho_v$	0.080	0.913	< 0.001
6501	$M_t = 0.170 + 0.514 \cdot M_{t-1} + 0.226 \cdot M_{t-2} + 0.0005 \cdot Ta_{t-1}^2 + 0.012 \cdot Ta_{t-1} + 0.008 \cdot Ta_{t-2}$	0.049	0.883	< 0.001

Table 3.3. Regression models of daily change in soil saturation on day "t"(ΔS_t). The predictor variable is snowmelt (M_{t-i}; i is number of days lag) for the midwinter period of 2007. Data were limited to December 7 and later, and were otherwise subset similarly to that outlined in Table 3.2.

Site	Model	SE_{res}	R^2	p-value
24	$\Delta S_t = -0.163 + 0.336 \cdot M_t$	0.049	0.633	< 0.001
2006	$\Delta S_t = 0.003 - 0.165 \cdot M_t + 0.113 \cdot M_{t-1}$	0.059	0.134	0.24
2013	$\Delta S_t = -0.025 + 0.282 \cdot M_t$	0.023	0.545	< 0.001
4004	$\Delta S_t = -0.413 + 1.338 \cdot M_t - 0.700 \cdot M_{t-1}$	0.128	0.722	< 0.001
6003	$\Delta S_t = -0.060 + 0.066 \cdot M_{t-1}$	0.032	0.228	< 0.001
6501	$\Delta S_t = -0.044 + 0.128 \cdot M_t$	0.047	0.109	0.002

Table 3.4. Regression models of daily change in soil temperature on day "t" (ΔTs_t). Predictor variables are memory of daily soil temperature changes (ΔTs_{t-i}; i is number of days lag) and snowmelt (M_{t-i}) for the midwinter period of 2007. Data were subset similarly to that outlined in Table 3.2.

Site	Model	SE_{res}	R^2	p-value
24	$\Delta Ts_t = -0.005 - 0.061 \cdot M_t + 0.055 \cdot M_{t-1}$	0.010	0.346	0.005
2006	$\Delta Ts_t = -0.001 - 0.027 \cdot M_{t-1}$	0.009	0.237	0.056
2013	$\Delta Ts_t = -0.006 + 0.003 \cdot M_{t-1}$	0.009	0.001	0.820
4004	$\Delta Ts_t = 0.004 - 0.074 \cdot M_t + 0.058 \cdot M_{t-1}$	0.009	0.429	< 0.001
6003	$\Delta Ts_t = 0.007 - 0.052 \cdot M_t + 0.039 \cdot M_{t-1}$	0.008	0.350	< 0.001
6501	$\Delta Ts_t = 0.004 + 0.447 \cdot \Delta Ts_{t-1} - 0.092 \cdot M_t + 0.081 \cdot M_{t-1}$	0.015	0.306	< 0.001

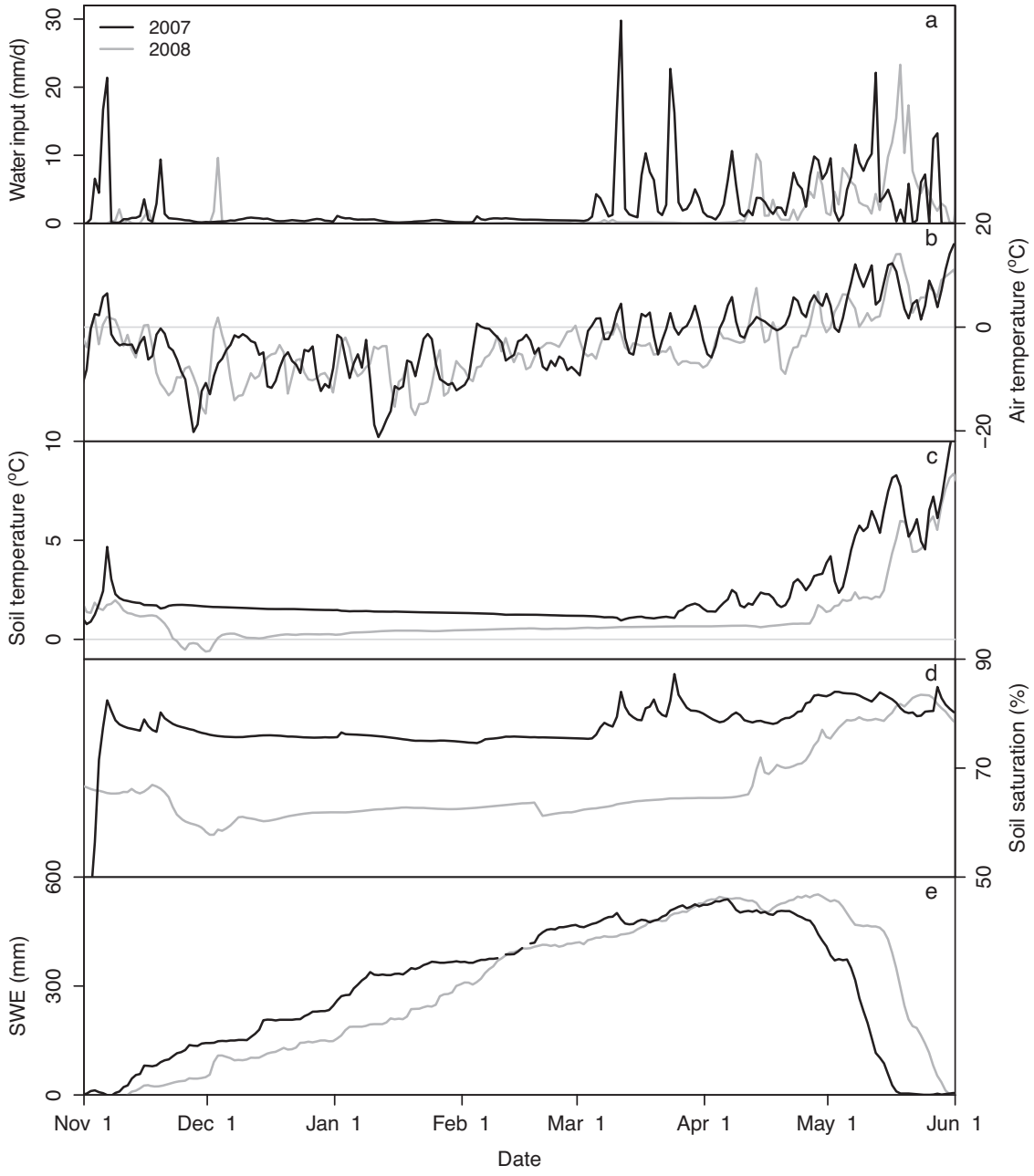

Figure 3.1. Water input to the soil, air temperature, soil temperature (10 cm depth), and soil saturation (mean of 20 and 40 cm depths) for UEC catchment (mean of all sites) and SWE for Moyie Mountain snow pillow during the winters of 2007 and 2008 (daily data).

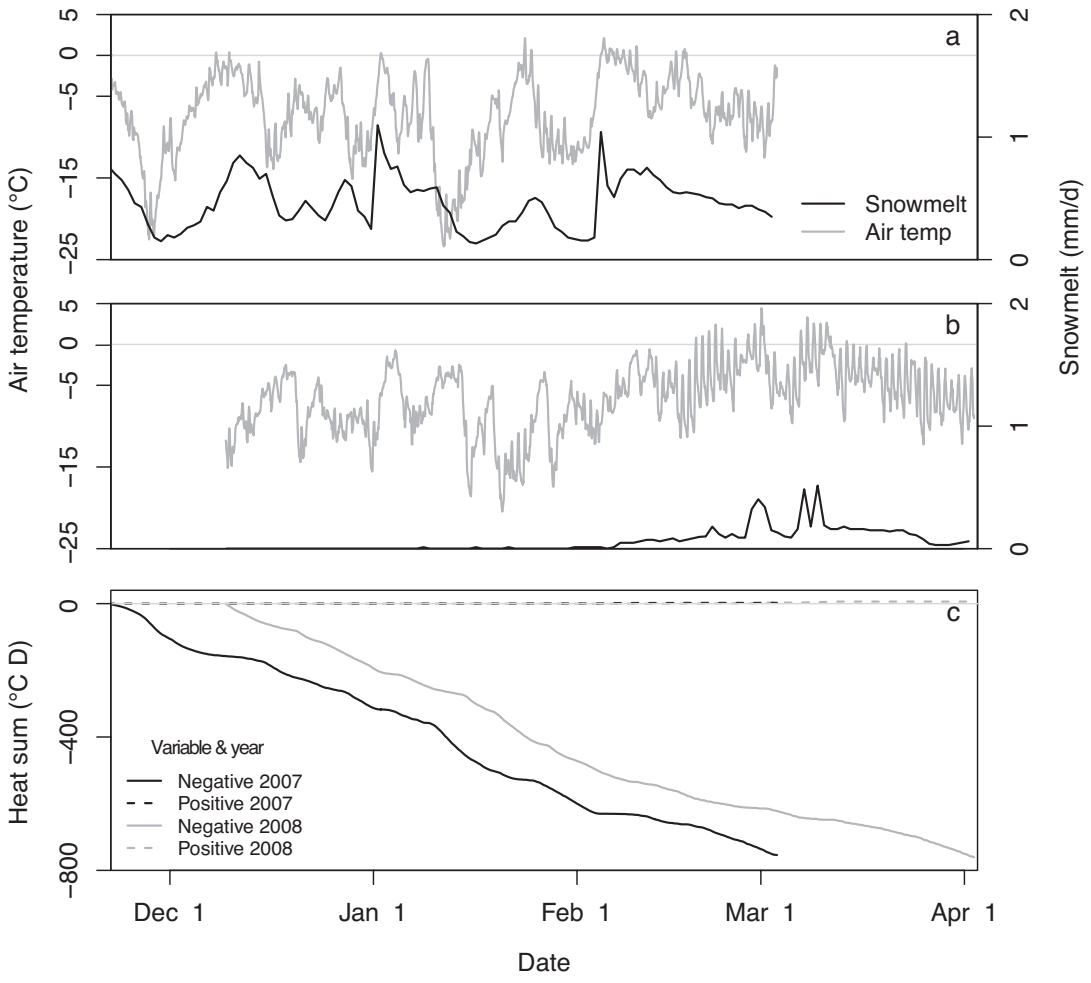

Figure 3.2. Hourly air temperature and daily snowmelt (mean of all sites) for the midwinter periods of (a) 2007 and (b) 2008, and (c) cumulative negative and positive air temperature degree-day heat sums (mean of all sites) from the start of the midwinter periods of 2007 and 2008 based on hourly data and assuming a 0 °C threshold.

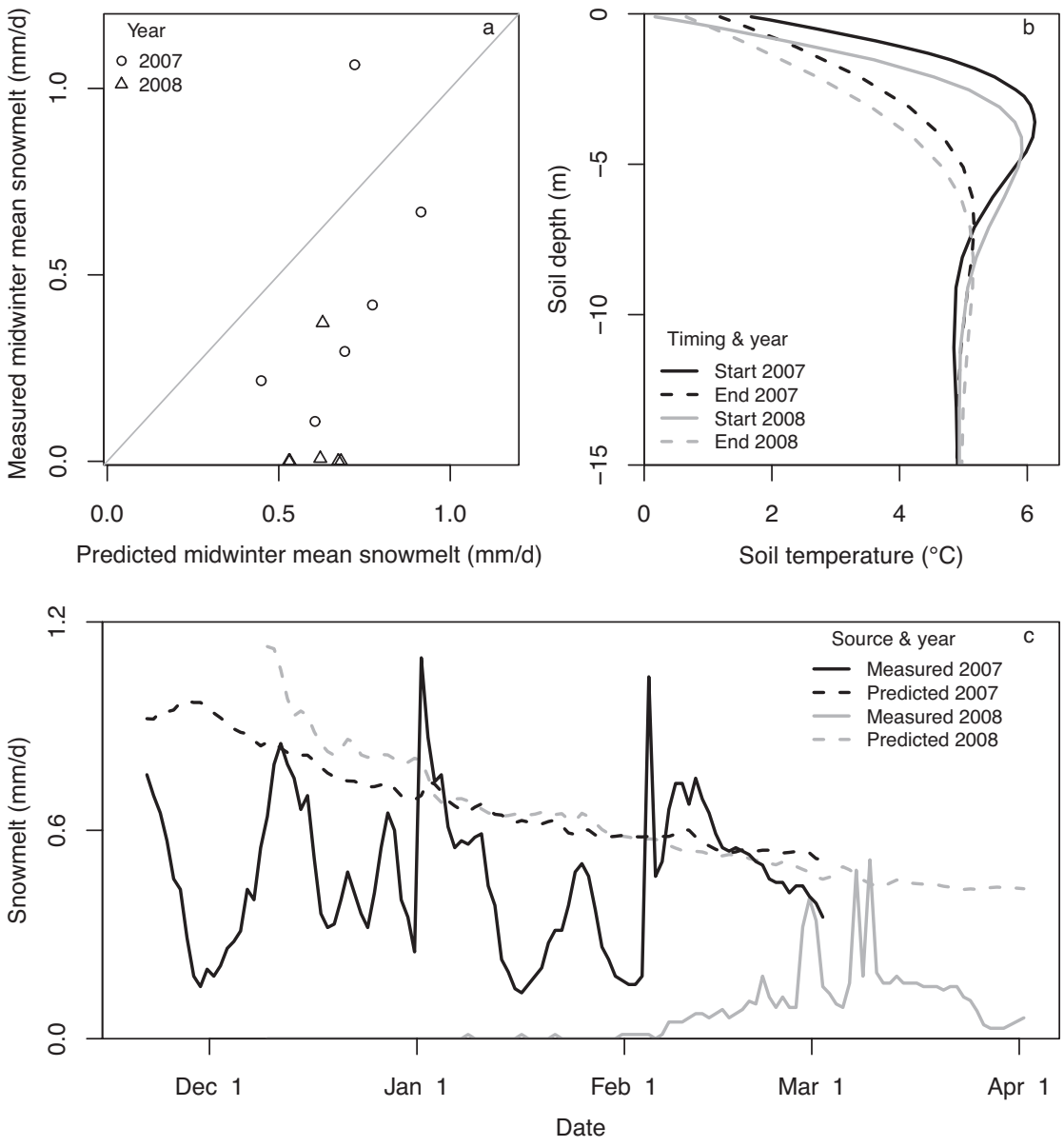

Figure 3.3. Predicted versus measured midwinter mean snowmelt (a), predicted soil temperature profiles for the start and end of both midwinter periods (mean of all sites) (b), and measured and predicted snowmelt (mean of all sites) (c). The predicted melt rate calculations assume that all soil heat flux from the heat flux modelling is used for melting snow.

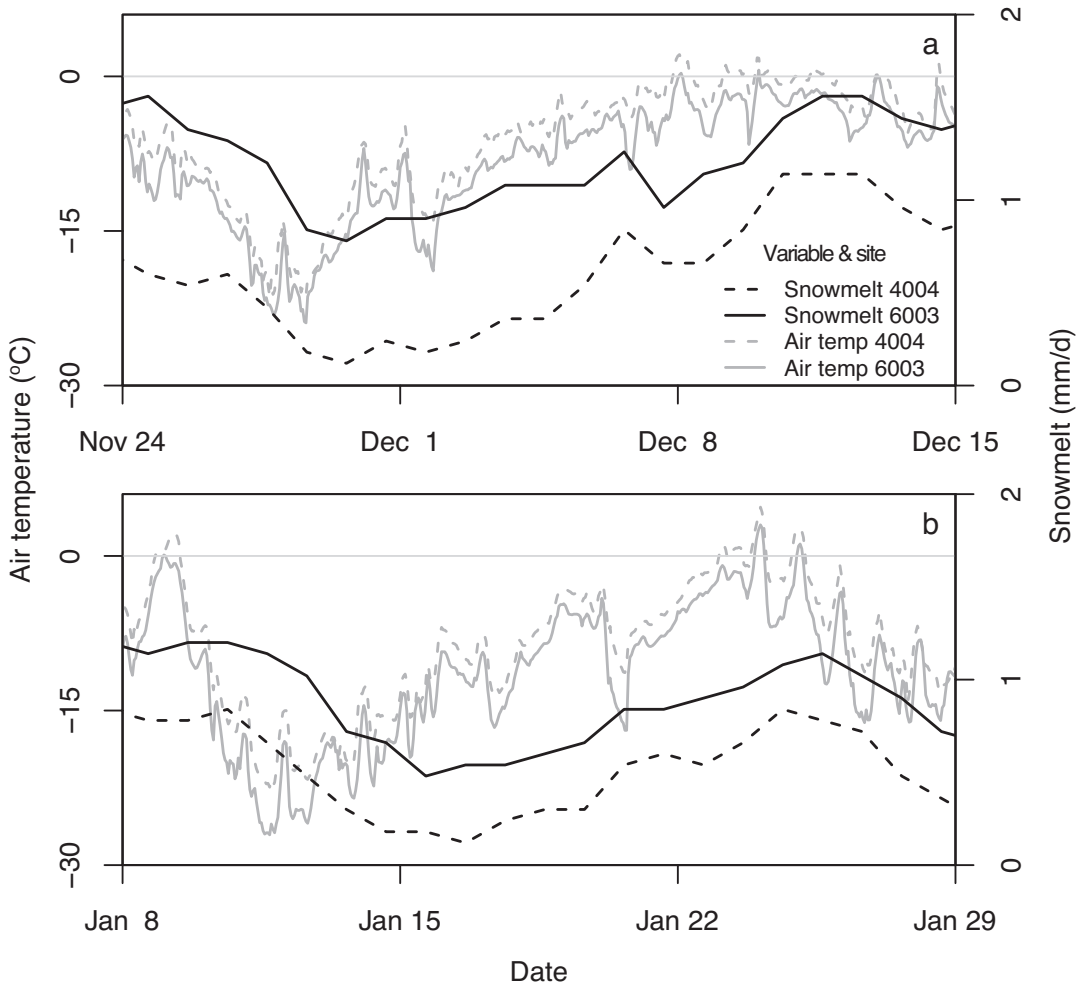

Figure 3.4. Hourly air temperature and daily snowmelt at sites 4004 and 6003 for two subsets of the 2007 midwinter period.

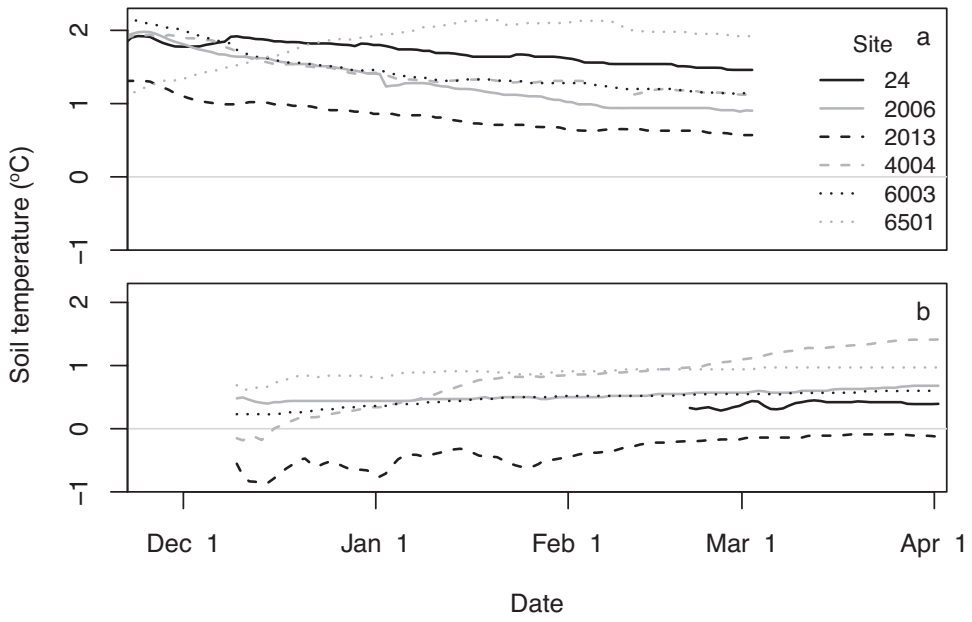

Figure 3.5. Daily soil temperature (10 cm depth) for the midwinter periods of (a) 2007 and (b) 2008.

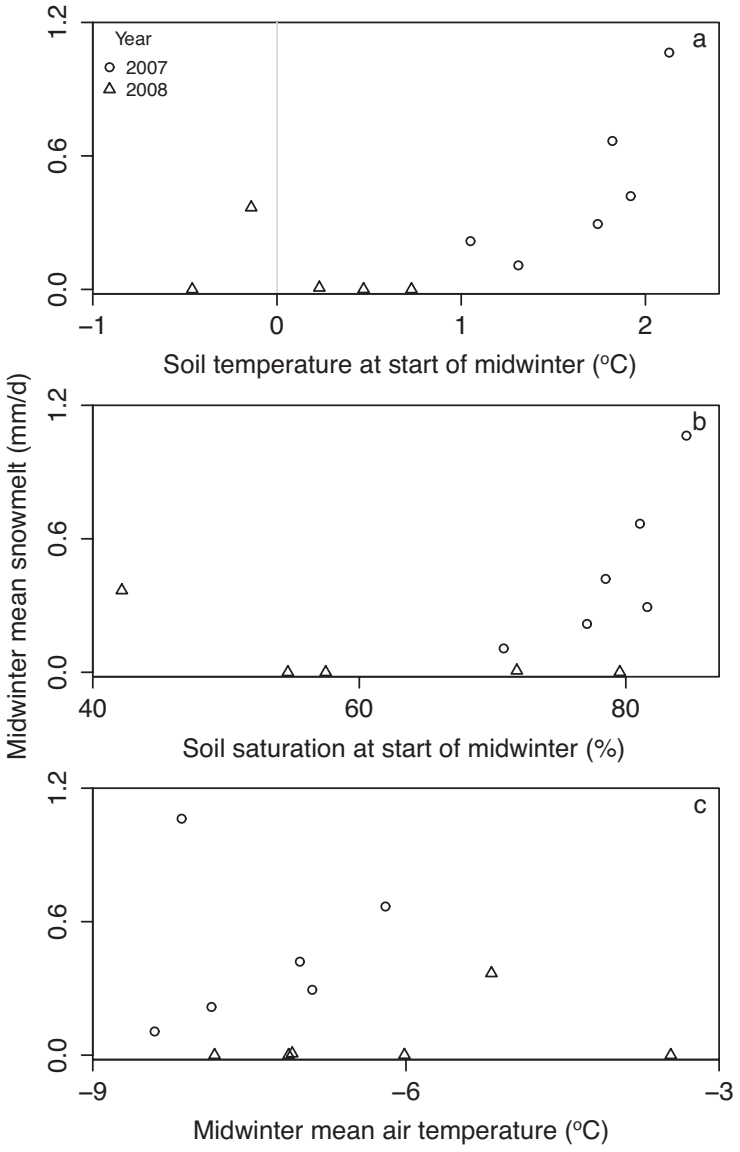

Figure 3.6. Midwinter mean snowmelt and (a) soil temperature (10 cm depth) at the start of the midwinter period, (b) soil saturation (mean of 20 and 40 cm depths) at the start of the midwinter period, and (c) midwinter mean air temperature. The 2007 outlier in panel c is site 6003. The 2008 outlier in all panels is site 4004.

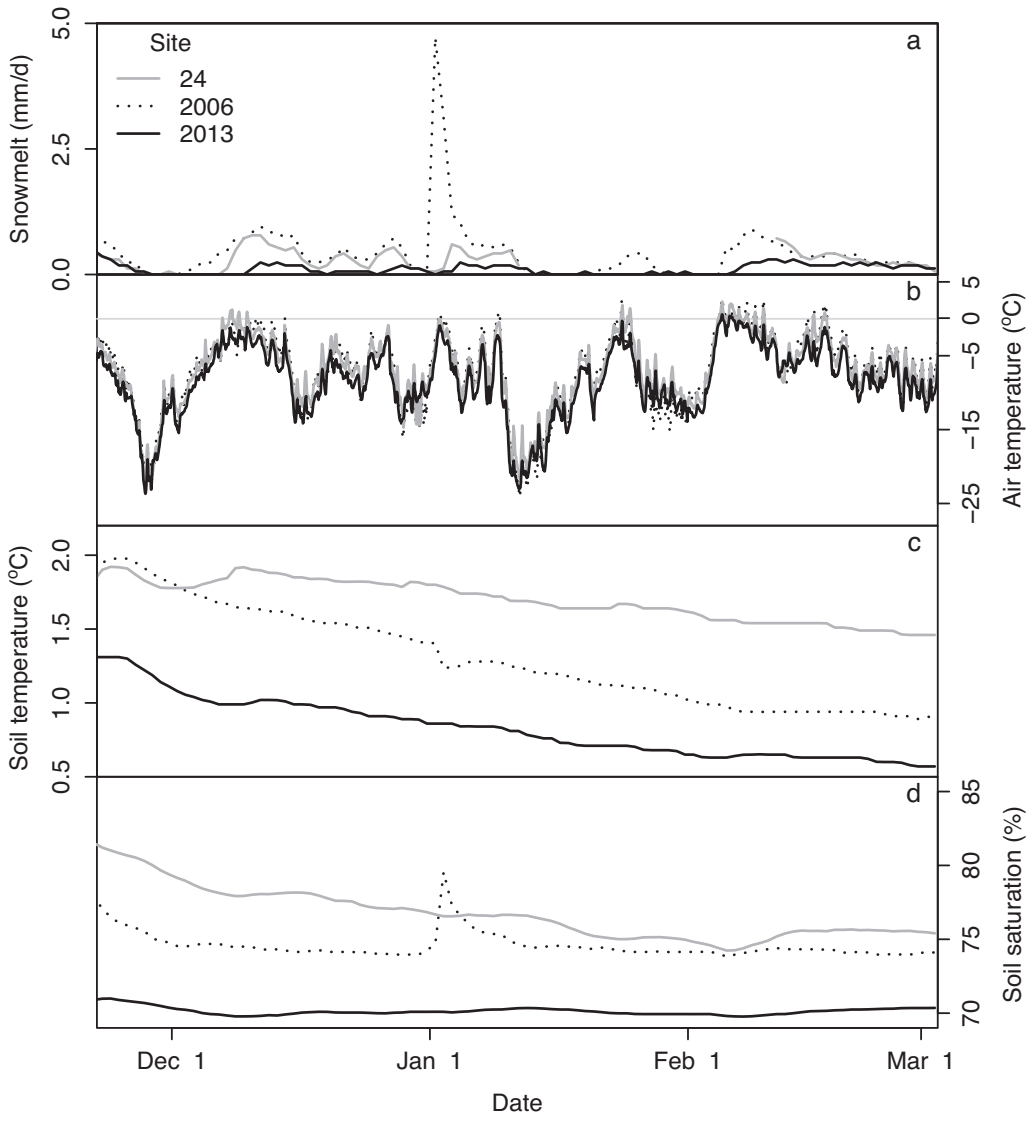

Figure 3.7. Snowmelt, air temperature, soil temperature (10 cm depth), and soil saturation (mean of 20 and 40 cm depths) at the lysimeter sites (panels a through h), and snow depth, solar radiation, wind speed, and vapor density at the Upper Cotton climate station (panels i through l) for the midwinter period of 2007. Note the canopy melt event on January 2-3 at site 2006 (panel a) and the radiation generated melt event on February 5 at site 4004 (panel e). Data are missing for melt on January 13 - February 11 at site 24 and for all variables on February 6-11 at site 4004.

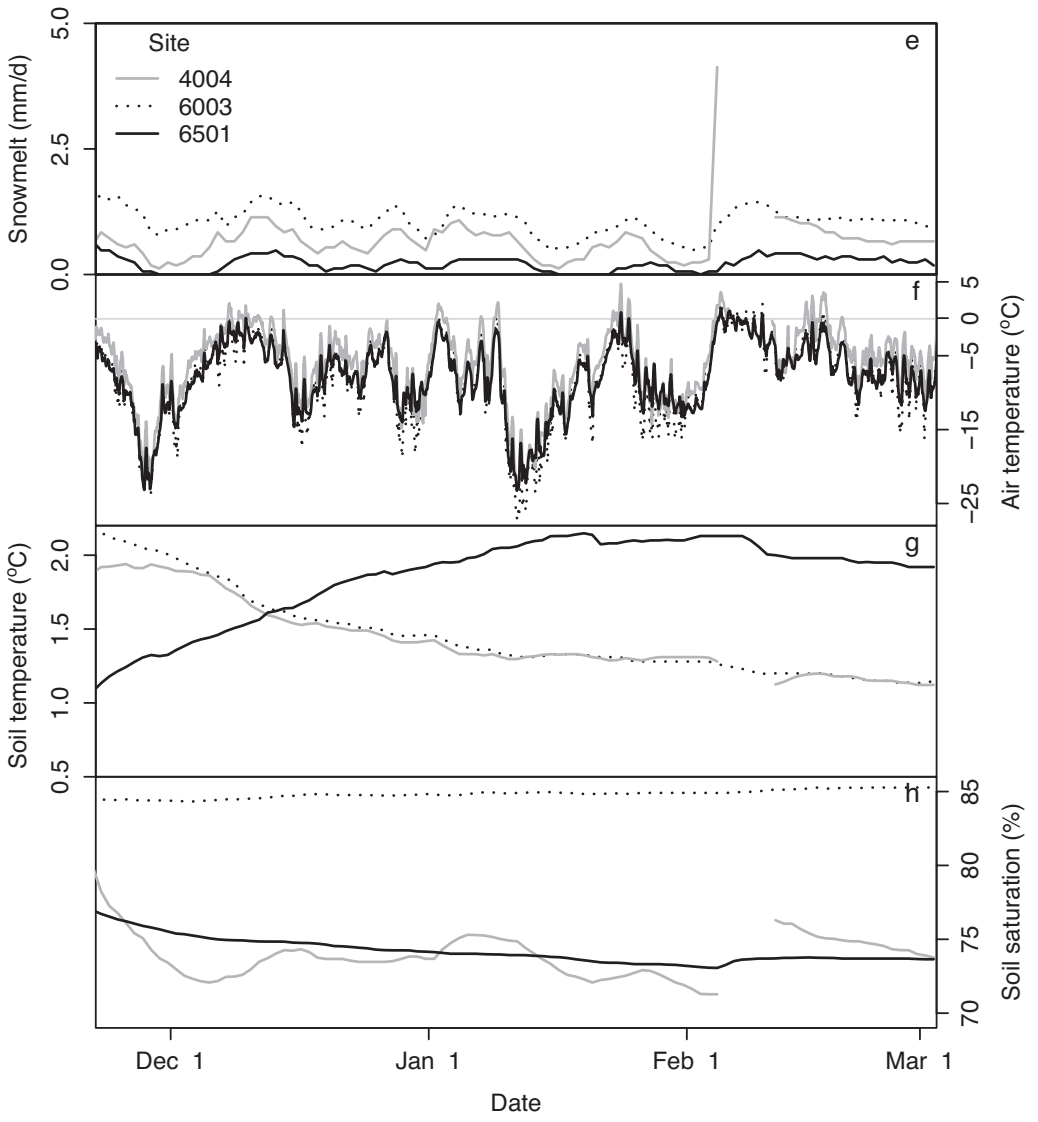

Figure 3.7 continued.

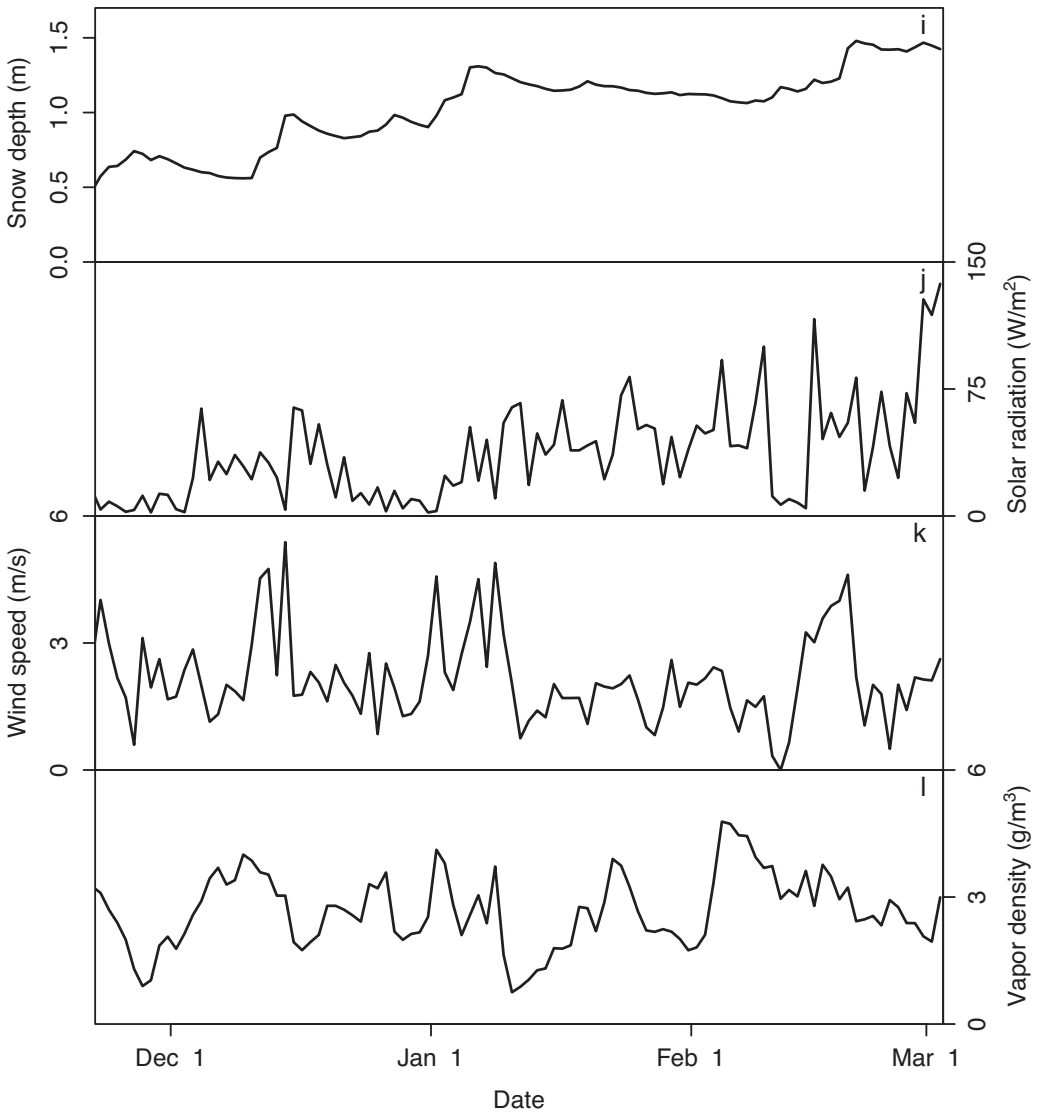

Figure 3.7 continued.

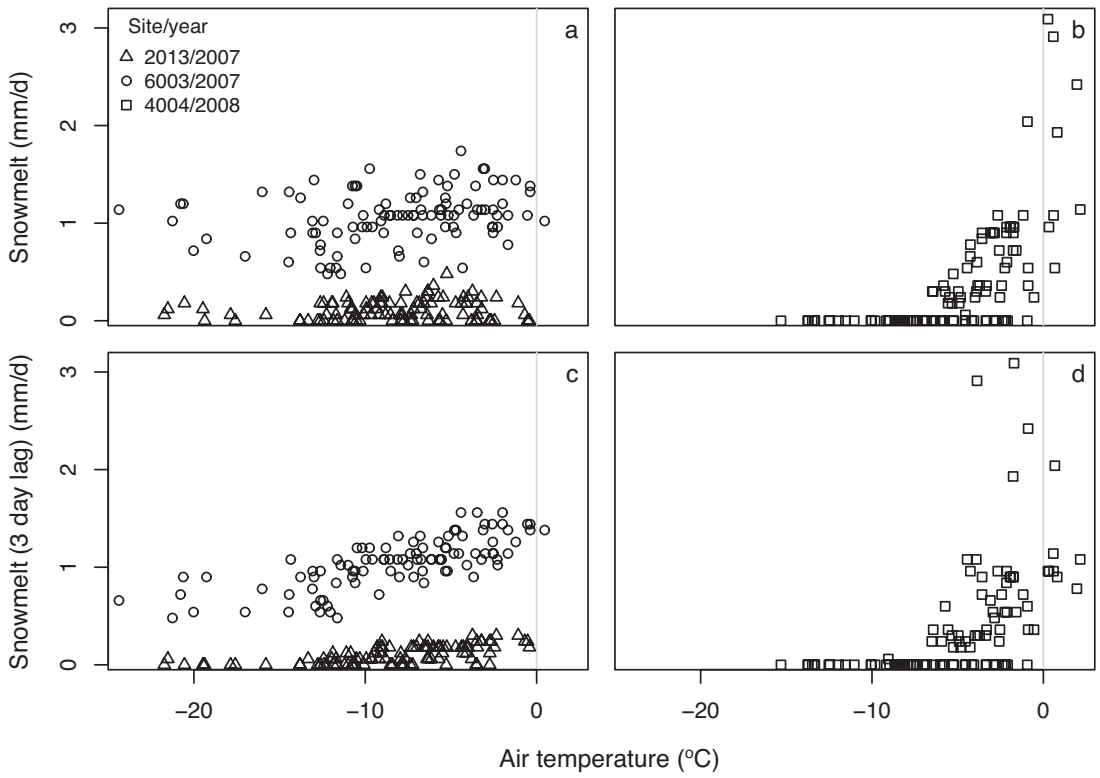

Figure 3.8. Relation between daily snowmelt and daily mean air temperature for the midwinter period without a 3 day lag for (a) 2007 and (b) 2008, and with a 3 day lag for (c) 2007 and (d) 2008.

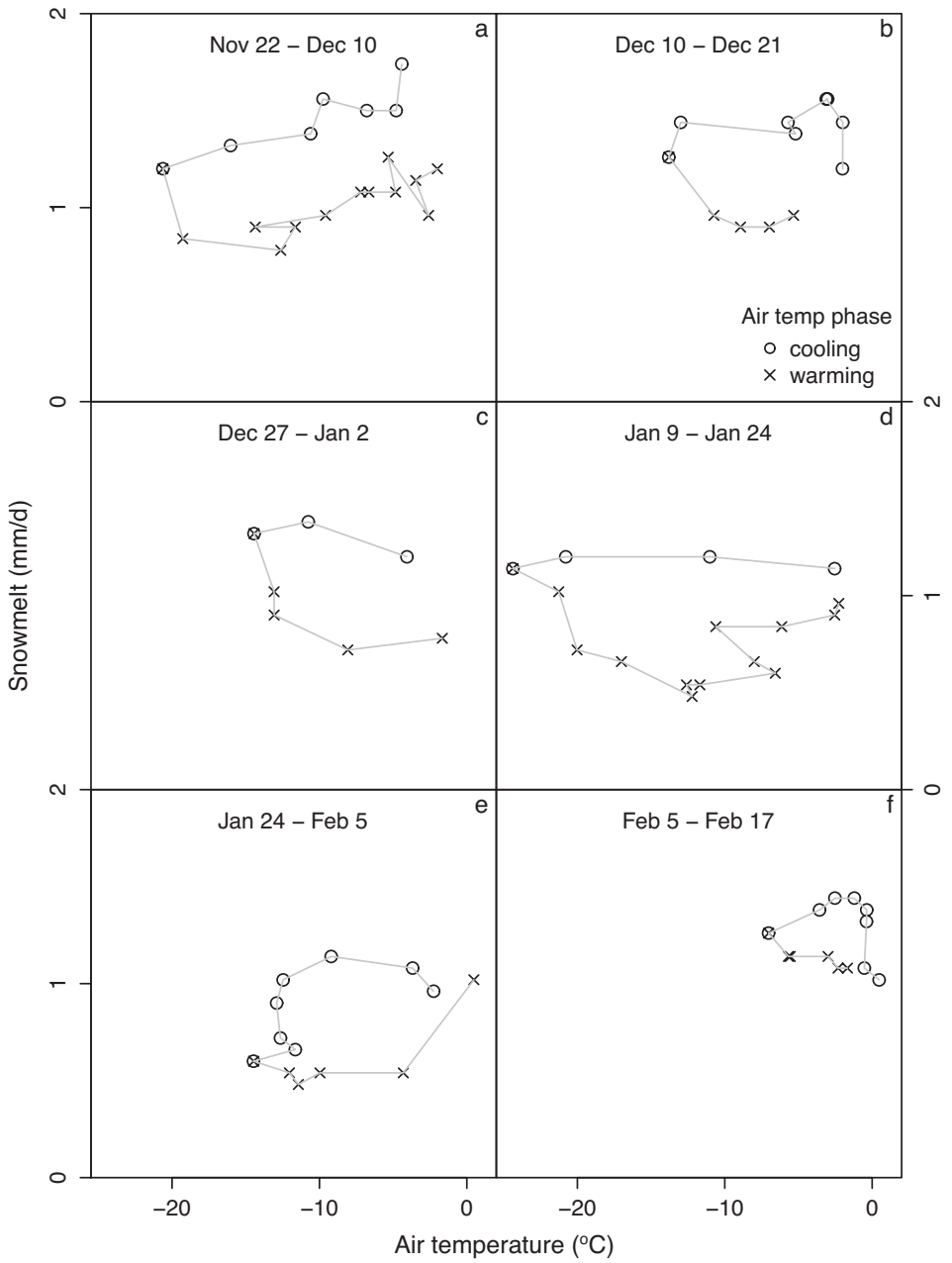

Figure 3.9. Daily snowmelt and daily air temperature at site 6003 for the midwinter period of 2007 showing cooling/warming hysteresis.

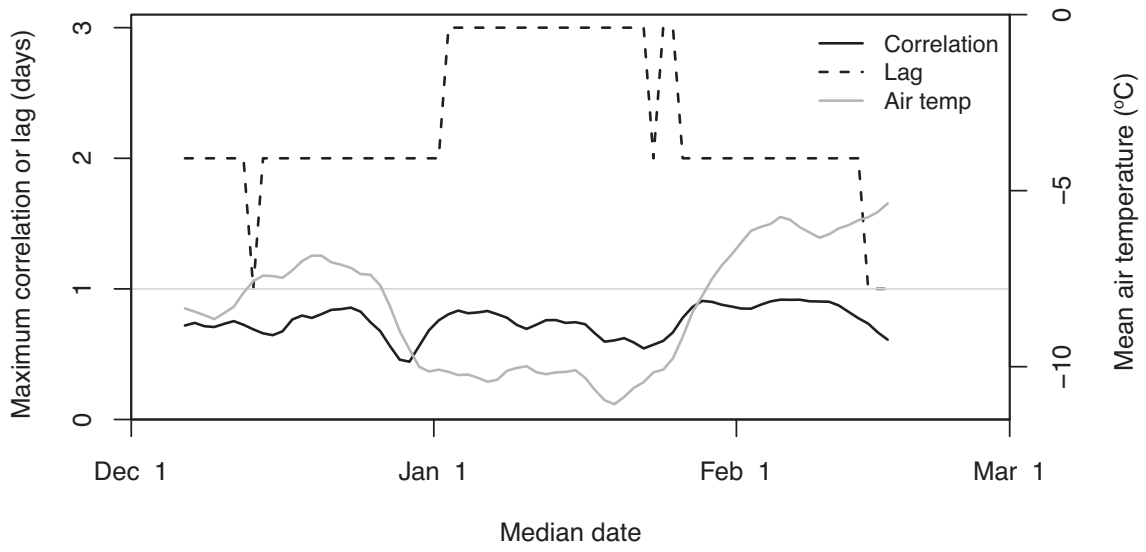

Figure 3.10. Maximum correlations between air temperature and snowmelt, and associated snowmelt lags from CCF analysis using a 30 day moving window, along with 30 day mean air temperature for site 6003 during the midwinter period of 2007.

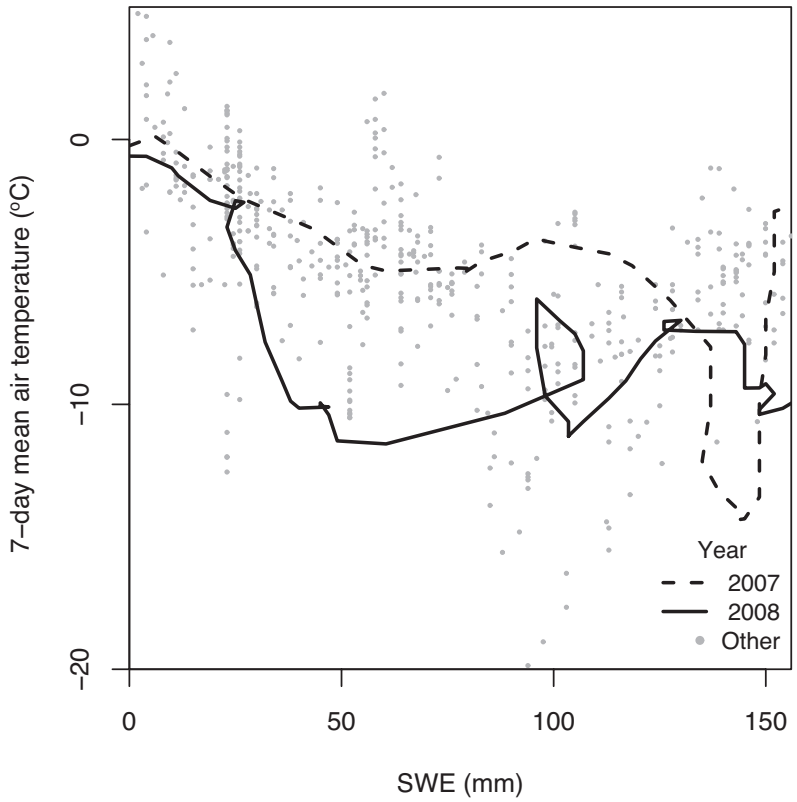

Figure 3.11. 7 day mean air temperature and SWE on day 7 from a 7 day moving window for the Moyie Mountain snow pillow for 2007, 2008, and other years within the 1998-2008 period of record.

4 Water input dynamics and hydraulic conductivity controls on percolation-excess runoff generation

4.1 Introduction

Development of a shallow saturated layer within the soil (hereafter referred to as perched groundwater) is widely recognized as important for generation of lateral subsurface flow regardless of whether the lateral flux is dominated by matrix flow or by macropore flow [*Harr*, 1977; *Kendall et al.*, 1999; *Lehmann et al.*, 2007; *Noguchi et al.*, 2001; *Sidle et al.*, 1995; *Tromp-van Meerveld and McDonnell*, 2005; *Whipkey*, 1965; *Zaslavsky and Sinai*, 1981a; b]. In many studies focused on soil hydrology and hillslope runoff processes, investigations were conducted at sites with distinct soil layering and associated permeability contrasts at some depth below the surface, particularly where a permeable soil overlies bedrock or compacted glacial till, such that soil saturation developed from the bottom up [*Anderson and Burt*, 1978; *Detty and McGuire*, 2010a; *Kendall et al.*, 1999; *Kirkby*, 1969; *Monteith et al.*, 2006a; *Ocampo et al.*, 2006; *Whipkey*, 1965]. As a result, bottom-up saturation has come to dominate the way many hydrologists perceive runoff generation in permeable soils, which has strongly influenced the development of runoff models. For example, the models DHSVM [*Wigmosta et al.*, 1994], TOPMODEL [*Beven et al.*, 1995], Hillvi [*Weiler and McDonnell*, 2004], and MIKE SHE [*Graham and Butts*, 2005] all assume, in principle, that runoff generation occurs via bottom-up saturation in soils where the infiltration rate exceeds the rate of water input at the surface.

Where soils are relatively deep (e.g., several meters) and saturated hydraulic conductivity (K_s) varies gradually with depth, saturated layers can develop at the depths where K_s limits downward percolation relative to the rate of percolation from above, promoting non-stationary soil water convergence in the vertical direction within the soil profile [*Buttle*, 1994; *Harr*, 1977; *Redding and Devito*, 2008; 2010]. Following Redding and Devito [2008; 2010], we refer to transient perched groundwater development by this process as *percolation-excess runoff generation*. It functions similarly to infiltration-excess runoff generation, but occurs below the soil surface. Under these conditions, an

interplay can form between the K_s profile and the water input intensity during an event that could strongly influence the depth of control for groundwater initiation [*Redding and Devito*, 2008; 2010]. This interplay could also influence runoff response dynamics via impacts on effective soil depth (i.e. depth to an effective restricting layer), unsaturated soil storage capacity, and the total time for percolation to the saturated layer.

Some authors have acknowledged the importance of water input intensity as a control on subsurface response in layered soils [*Kirkby*, 1969; *Lehmann et al.*, 2007; *Noguchi et al.*, 2001; *Redding and Devito*, 2008; 2010; *Sidle et al.*, 1995; *Tromp-van Meerveld and Weiler*, 2008]; however, the depth of groundwater initiation likely would be much more stationary in soils with distinct layering (due to the presence of a stationary restricting layer) than in soils with gradually changing K_s. Moreover, antecedent soil wetness and total water input have received more attention than input intensity within runoff generation studies, in general, and the influence of input intensity in soils with gradually changing K_s, in particular, has received little attention. One exception is Redding and Devito [2008; 2010] who found that an interplay between the K_s profile and water input intensity played an important role in partitioning vertical versus lateral fluxes while investigating runoff response in deep (20 to 240 m) glacial till soils with gradual changes in soil properties with depth and no clear restricting layer. Harr [1977] found that K_s decreased with depth due to changes in density and pore-size distribution and facilitated the development of perched groundwater, but he did not explore the potential interplay between groundwater initiation depth and water input intensity. Whipkey [1965] found that perched groundwater developed above a wetting front due to high pore tension and associated resistance to wetting, but he focused on the influence of total water input and input duration without relating the soil saturation dynamics to input intensity. While some of the earlier studies in hydrology formed a basis for conceptualizing percolation-excess runoff generation [*Buttle*, 1994; *Harr*, 1977; *Redding and Devito*, 2008; 2010; *Whipkey*, 1965], the process has not been explored in detail as a potentially important runoff generation mechanism (notwithstanding the work of Redding and Devito [2008; 2010]) and has not played an important role in the conceptualization of runoff models.

The objectives of this chapter are (1) to explore the plausibility and dynamics of the percolation-excess runoff generation mechanism using field measurements and (2) to use physically based modelling to verify and extend the analysis of the field data and generalize the environmental controls on percolation-excess runoff generation. The simulation exercises incorporate extreme conditions and focus on specific processes of interest for investigating the interplays between K_s, water input intensity, total water input, and antecedent wetness in controlling development of transient perched soil saturation. The analysis is based on the hypothesis that for a wet and freely draining soil where K_s decreases gradually with depth, the depth of control for initiation and development of a transient perched saturated layer during a water input event will be the soil depth where the water input intensity equals the vertical K_s. This hypothesis assumes a negligible loss of water to the atmosphere or unsaturated soil storage during infiltration and percolation, and that the percolation rate is constant with depth above the saturated zone. Moreover, it is hypothesized that upon initiation of soil saturation, the saturated zone will expand upwards and simultaneously continue to percolate downwards from the depth of initiation at a decreasing rate due to the decreasing K_s. It is further expected that decreasing antecedent wetness will delay the initiation of soil saturation and increase the depth of initiation below the soil surface due to losses to unsaturated storage. Extension of these hypotheses suggests that groundwater dynamics will be highly sensitive to spatial variability in the K_s profile and to spatial and temporal variability in the water input intensity, and that the dynamics of the water input intensity during an event could be more important in controlling groundwater response than will be the total water input. Moreover, perched groundwater will not develop in soils where the minimum vertical K_s within a profile substantially exceeds the maximum water input intensity, resulting in deep percolation and unsaturated storage.

4.2 Data analysis

4.2.1 Empirical analysis

Empirical analyses focused on evaluating groundwater responses generated by their corresponding water input events for several sites. Of the 50 hillslope monitoring sites, detailed analyses were applied to groundwater data from only seven sites where several discrete groundwater response events could be identified as responding to discrete water input events (i.e. groundwater responses were observed and it was not apparent that the responses were being influenced by lateral flux from upslope areas). Details of the site physiographies are provided in Table 4.1. At the remaining 43 sites, either little (seven sites) or no (13 sites) groundwater response was observed over the period of record (October 2006 through July 2008), or persistent groundwater (presumably due to lateral flux from upslope areas) obscured the discrete groundwater response signals associated with the local water inputs (20 sites). Three remaining sites exhibited groundwater dynamics that were suitable for this analysis, but were excluded from the analysis due to problems with obtaining accurate water input data. Among the seven sites that were utilized for analysis, two (sites 24 and 6501) were lysimeter sites with water input and soil wetness continuously measured. For the five other sites, high resolution water input and soil wetness data were simulated using the Simultaneous Heat and Water (SHAW) model [*Flerchinger*, 2000], as described in section 4.2.2.

For the sites that were utilized in the empirical analysis, individual water input events were defined as having input rates of at least 0.25 mm/h with any periods of input less than 0.25 mm/h lasting no longer than 1 hour. Consecutive events were separated by at least two hours with water inputs below 0.25 mm/h. Each event pair (i.e. water input event and associated groundwater response event) was included in the analysis only if the groundwater table was at or below a depth of 2 cm above the well bottom when the groundwater response event commenced. Otherwise, the particular groundwater response event was considered to be obscured by prior events or by lateral flux from upslope areas and was discarded from the analysis. For multi-peak input events and

associated multi-peak groundwater response events, the minimum water input intensity between consecutive peaks was used to separate individual input events provided the associated groundwater level returned to a depth within 2 cm of the well bottom before the subsequent groundwater response event commenced.

For each water input and groundwater response event pair, several measures were calculated including maximum 1 hour water input intensity, total water input, antecedent soil wetness (i.e. soil wetness at the start of the input event), maximum groundwater level, an estimation of total lateral flux, and lateral flux coefficient. For sites without continuous soil wetness data, antecedent soil wetness was obtained from the SHAW model results. The estimation of total lateral flux was computed as follows: first, an exponential function (Table 4.1) was fit to the hydraulic conductivity data for the site, which was then combined with the groundwater level time series to generate a soil transmissivity time series (assuming the soil was saturated between the water table depth and the well bottom). The groundwater table was assumed to be parallel to the soil surface and transmissivity was multiplied by a 1 m wide section of hillslope and the hillslope gradient. The estimated lateral flux was then summed over the duration of each response event. A lateral flux coefficient was calculated as the estimated total lateral flux divided by the volume of water input on a 1 m^2 area over the duration of the water input event. The estimated lateral flux does not account for any lateral flux below the well bottom; however, errors arising from this omission were minimized by the fact that hydraulic conductivity and, therefore, transmissivity decreases exponentially with depth at five of seven of the analyzed sites. At one of the two sites (site 6501) where this exponential pattern does not exist (out of seven analyzed sites in total), the bottom of the well was located on a low permeability rock surface, which would minimize this source of error. At the other site (site 4025), significant amounts of lateral flux might have occurred below the bottom of the well, as a low-permeability layer was not observed.

According to the hypothesized percolation-excess mechanism, groundwater formation should initiate at the soil depth where the K_s equals the water input intensity. For each site, the temporal variability of this depth was computed by combining the derived K_s

function (Table 4.1) with the water input time series, and the maximum level (i.e. minimum depth below the soil surface) for each groundwater response event was then selected as the predicted initiation depth of the perched groundwater.

Multiple linear regression was used to investigate the influences of antecedent soil wetness, input intensity, and total input on variability in groundwater response (maximum groundwater level and total lateral flux). The AIC [*Akaike*, 1987] and adjusted R^2 were used for model evaluation and for selecting the final model. A normal probability plot and a plot of residuals versus predicted values were used to evaluate the residuals for normality, linearity, and homoscedasticity. Statistical significance for all tests was evaluated using a 0.05 significance level. R statistical software [*R Development Core Team*, 2010] was used for all statistical analyses. The models were used to further evaluate the influence of each predictor variable on groundwater response.

4.2.2 Deterministic modelling

The SHAW model was used in this study for two purposes: (1) to generate high resolution water input and soil saturation data for non-lysimeter sites that were incorporated in the empirical analyses and (2) to further explore soil saturation dynamics and the hypotheses that perched groundwater can be generated via the percolation-excess runoff generation mechanism where K_s decreases gradually with soil depth and that the depth where soil saturation initiates can be highly sensitive to water input intensity. SHAW is a physically based 1-D model that can account for heat, mass, and solute fluxes within and between multiple vegetation, snow, residue, and soil nodes. It can represent all seasons and can account for snow accumulation, snowmelt, and evapotranspiration/sublimation processes. It was initially developed at the USDA Agricultural Research Service in Pullman, Washington [*Flerchinger and Saxton*, 1989a; b], and has undergone modification to its subroutines at the USDA ARS Northwest Watershed Research Center, Boise, Idaho since initial development [*Flerchinger*, 2000; *Flerchinger and Pierson*, 1991; *Flerchinger et al.*, 1996a; *Flerchinger et al.*, 1996b; *Link et al.*, 2004]. A hybrid version of the model modified by Link *et al.* [2004] was initially

used in this study, but it melted the snowpack too early at forested sites in the UEC catchment, as it does not consider the influence of forest cover on atmospheric stability at the snowpack surface. Thus, the following changes were incorporated in the model to improve its performance: (1) radiation transmission and scattering within canopies of varying leaf angle distribution from Flerchinger and Yu [2007], (2) the incoming longwave radiation algorithm from Flerchinger *et al.* [2009], (3) the within-canopy Lagrangian theory turbulent transfer algorithms with correction for atmospheric stability from Leuning [2000], and (4) the density algorithm for newly fallen snow from SHAW model version 2.3 [*Flerchinger*, 2000]. Mean R^2 for predicting SWE at the seven analyzed sites improved from 0.79 to 0.96 (mean sample size of 7.1) and mean error in the timing of melt-out for the two lysimeter sites that were analyzed improved from 17.8 days too early to 0.3 days too early.

As SHAW is a 1-D model, it does not explicitly account for lateral fluxes through a soil profile and all water losses occur via deep soil drainage through the lower boundary of the simulation domain. Conceptually, the model is consistent with a soil having no lateral flux or, alternatively, with a soil existing within an infinite slope where lateral outflow equals lateral inflow at all times. As a result, groundwater response dynamics simulated by the model are most representative of a soil within a linear hillslope where flow paths are neither convergent nor divergent.

For the purpose of generating high resolution water input and soil wetness data for the non-lysimeter sites, SHAW model results were manually fit to the lysimeter site data to find approximate parameter values for the UEC catchment that would generate reasonable water inputs in terms of both quantity and timing. Values for model parameters controlling vegetation (e.g. height, leaf area index, transpiration), soil (e.g. texture, density, surface roughness, soil water retention, K_s), and snow (e.g. surface roughness) properties were defined to reflect the respective site characteristics and to fit the SWE, melt-out timing, and soil saturation data for the site. These same parameters were then adjusted accordingly for modelling the non-lysimeter sites. For unsaturated conditions, SHAW model adjusts matric potential and hydraulic conductivity using the

saturation level (%), an air entry potential (m), and a pore size distribution parameter [*Brooks and Corey*, 1966; *Campbell*, 1977]. The latter two parameters were assumed to be vertically constant at each site, but variable between sites. Assumed values varied from -0.09 to -0.50 m for air entry potential (m) and from 4.5 to 5.0 for the pore size distribution parameter, depending on the soil texture at each site [*Clapp and Hornberger*, 1978]. Weather data for input to the model were generated as an elevation-based linear interpolation between the UC and LC climate stations for air temperature, wind speed, relative humidity, and precipitation. Solar radiation was taken as an average of the data from both climate stations. SHAW model adjusts solar radiation internally for local aspect and hillslope gradient. The assumed soil wetness and soil temperature profiles for the start of the model period (November 1, 2006) were adjusted to improve the fit of the model results to the measured SWE, water input, and soil wetness data.

For the purpose of exploring soil saturation dynamics and investigating the hypotheses, three water input scenarios were simulated for each of two soil properties scenarios. Water input series #1 involved nine values of water input intensity (0.2, 0.3, 0.4, 0.5, 1, 2, 3, 5, or 10 mm/h) while holding total water input (100 mm) and antecedent soil wetness (75% saturation throughout the soil profile) constant between runs. Water input series #2 involved 11 values of total input (3, 6, 9, 18, 27, 36, 45, 54, 72, 108, and 144 mm) while holding input intensity (3 mm/h) and antecedent wetness (75% saturation throughout the soil profile) constant between runs. Water input series #3 involved nine values of antecedent wetness (50, 55, 60, 65, 70, 75, 80, 85, and 90% saturation throughout the soil profile) while holding input intensity (3 mm/h) and total input (100 mm) constant between runs. The water input amounts and intensities for the three water input series were selected to fit within the range of variability observed for individual water input events in the catchment during the period of study. The antecedent wetness for water input series #1 and #2 was selected so that the soil was sufficiently wet to minimize attenuation caused by unsaturated soil storage, but sufficiently dry to minimize the formation of saturated zones caused by soil profile readjustment (i.e. without the addition of event water).

Parameterization of K_s for both soil properties scenarios is provided in Figure 4.1. Soil nodes were spaced every 0.05 m from the surface to 2 m depth, then every 0.1 m to 2.5 m, then at 2.75 m, 3 m, 3.5 m, and 4 m. Soil properties scenario #1 represented a high permeability soil layer over a low permeability layer with an abrupt permeability contrast at the interface between both layers at 2 m depth (i.e. a 2-layer K_s profile), whereas soil properties scenario #2 represented the typical site in the UEC catchment where K_s decreases exponentially with depth with no abrupt changes in K_s within the profile (i.e. a decreasing K_s profile). A high rate of change in K_s with depth in the upper 0.25 m of soil was established in both scenarios to reflect macroporosity that was observed in the shallow rooting zone in the catchment and to avoid development of infiltration-excess overland flow in the modelling results. Notwithstanding this fact, soil properties scenario #1 is referred to as a 2-layer profile to emphasize the permeability contrast at 2 m depth. For both soil properties scenarios, the air entry potential and the pore size distribution parameter varied gradually from -0.10 m and 1.0 at the surface to -0.59 m and 7.0 at 4.0 m depth, respectively, to represent changes in pore structure with depth.

Further to the conditions defined for the specified scenarios, air temperature, wind speed, relative humidity, solar radiation, and soil temperature (at all depths) were held constant at 2 ºC, 0.1 m/s, 99%, 0 W/m^2, and 2 ºC within the water input datasets, respectively, and both vegetation and soil residue were excluded from the site profiles. These conditions were defined to minimize or exclude several surface processes (e.g. evaporation and soil freezing) in order to ensure that the rate of infiltration is consistent with the rate of precipitation, as the focus of the modelling was on subsurface response to percolation processes. Soil density, porosity, and sand, silt, and clay contents were set equal to the catchment average values (1.54 g/cm^3, 0.42, 45.3%, 50.2%, and 4.5%, respectively). Soil organic content was assumed to be negligible.

4.3 Results

4.3.1 Analysis of water input – groundwater response event data

The K_s data and groundwater hydrographs for the analyzed sites are provided in Figures 4.1 and 4.2, respectively, for the seven sites that were selected for detailed analysis. No data were plotted in Figure 4.2 for periods lacking an observed groundwater response. Of the seven analyzed sites, sites 24 and 6501 are the only sites where water input was measured. K_s decreased approximately continuously (based on the point measurements) with soil depth at site 24, but not at site 6501 (Figure 4.1). In fact, site 6501 exemplifies the 2-layer soil profile, as the high conductivity surface soil is underlain by rock (either bedrock or a large boulder), although the K_s of the underlying rock is not shown in Figure 4.1 because its conductivity was not measured.

The maximum measured groundwater level (on an event basis) is strongly related to the predicted groundwater initiation depth under wet antecedent soil conditions at site 24 (Figure 4.3a) and the relation weakens with decreasing antecedent wetness. At site 24, the maximum measured groundwater level varies nonlinearly with the antecedent wetness (Figure 4.3f), and with the maximum water input intensity (Figure 4.3k) and the total water input (Figure 4.3p) under wet antecedent conditions. Event thresholds of approximately 75% soil saturation, 0.5 mm/h input intensity, and 2 mm total input appear to control the occurrence and/or magnitude of groundwater response.

The overall patterns observed for site 24 are corroborated by the data for the other sites with decreasing K_s profiles (i.e. sites 9, 12, 2005, and 4020), except the relations are not as strong because of scatter in the data, possibly due to error in the modeled water inputs (Figure 4.3). Furthermore, the maximum measured groundwater level is consistently under-predicted for sites 12 and 2005 (Figure 4.3c, 4.3d), also possibly due to error in the modeled water inputs or due to error in the K_s functions (Table 4.1) based on the measured K_s data (Figure 4.1). Antecedent wetness thresholds vary between 60% and 75%. Although the nonlinear shape of the relations for the antecedent wetness data

should be robust to measurement and modelling errors (Figure 4.3f-4.3j), the absolute values of the antecedent wetness thresholds should be interpreted with caution for the modeled sites (Figure 4.3g-4.3j) due to upward bias in the modeled soil wetness data at low and moderate values. The input intensity thresholds are relatively consistent between all five sites (Figure 4.3k-4.3o) despite the incorporation of modeled water inputs for four of the sites. Total water input thresholds vary between 2 mm and 10 mm (Figure 4.3p-4.3t).

In contrast to the results for the sites with decreasing K_s, a relation between the maximum measured groundwater level and the predicted groundwater initiation depth is not evident for site 6501 (Figure 4.4a), regardless of the antecedent wetness, and the maximum groundwater level varies irrespective of the antecedent wetness, water input intensity, or total input (Figure 4.4c, 4.4e, 4.4g). Although weak relations exist with antecedent wetness, input intensity, and total input for site 4025 (Figure 4.4d, 4.4f, and 4.4h), the data from site 4025 generally corroborate the overall patterns for site 6501, particularly in comparison with the strength of the relations for the decreasing K_s sites (Figure 4.3). Moreover, a 1.5 m to 4 m offset exists between the absolute values of the predicted initiation depth of the groundwater tables and the maximum measured groundwater level for site 4025.

The relations for total lateral flux and lateral flux coefficient with maximum water input intensity and total water input are similar to the corresponding relations for maximum groundwater level, but the threshold dependence on antecedent wetness is more obvious (Figures 4.5a and 4.6a) and the scatter about the relations is greater (Figures 4.5b-c and 4.6b-c). Total lateral flux and lateral flux coefficient data for the sites with modeled water inputs are not presented for conciseness; however, as in the case for the maximum groundwater level results (Figures 4.3 and 4.4), the data for the modeled sites corroborate the results for the empirical sites (sites 24 and 6501).

For sites with decreasing K_s profiles, a comparison of the overall maximum measured groundwater level (among all of the analyzed events) for each site against measured K_s at

a specific soil depth for the respective site shows a negative relation (plotting all sites together) for the 0.5 m and 0.75 m soil depths, whereas no relation is apparent for the 0.25 m depth (Figure 4.7). Moreover, data for the sites with non-decreasing K_s profiles lie outside the relation for the 0.5 m soil depth, but are generally consistent with the relation for the 0.75 m depth showing the importance of deep soil K_s in controlling groundwater response.

4.3.2 Regression analysis of the event data

Regression models were developed to predict the maximum measured groundwater rise above the well bottom and total lateral flux on an event basis for sites 24 (i.e. decreasing K_s profile) and 6501 (i.e. 2-layer K_s profile). The regression analysis focused on the sites with measured water inputs due to the potential for uncertainty in the simulated water input rates to influence the regression results, and it only incorporated events with a measured groundwater response since incorporating events with no groundwater response resulted in poor fits based on the residual plots. For site 24, all of the final regression models are statistically significant and normality, linearity, and homoscedasticity of the residuals are acceptable in all cases after applying necessary transformations. For site 6501, a model could not be found that was both physically meaningful and acceptable in terms of normality, linearity, and homoscedasticity of the residuals; therefore, none of the models for site 6501 is presented.

For site 24, 65% of the variance in the maximum groundwater rise was accounted for by input intensity, total input, and antecedent wetness (Table 4.2). A plot of partial responses for the model shows that, within the data ranges of the predictor variables, input intensity had the greatest influence on the maximum measured groundwater rise (Figure 4.8). The influences of total input and antecedent wetness were similarly lower in magnitude, but antecedent wetness shows a marked threshold effect at approximately 75% saturation. The model results suggest that maximum groundwater rise responded exponentially to increasing input intensity, but asymptotically to total input (Figure 4.8).

For total lateral flux at site 24, two final models were selected for comparison to explore the explanatory power of water input intensity: a full model incorporating all three predictor variables despite input intensity not being a significant variable in the model, and a reduced model incorporating only total input and antecedent wetness (Table 4.2). The two models explained 57% and 56% of the variance in total lateral flux, respectively. The partial plots show that antecedent wetness had the strongest influence and total input had the second strongest influence on total lateral flux regardless of which model (full or reduced) is considered; moreover, a threshold effect is apparent for antecedent wetness, as for maximum groundwater rise. Based on the partial plots and the minimal difference in explained variance between the full and reduced models, it is clear that input intensity is unimportant for explaining variability in total lateral flux among input events that generated measured groundwater responses at site 24, despite its strong influence on the maximum groundwater rise.

4.3.3 Modelling exploration of event response

Under both soil properties scenarios (i.e. 2-layer K_s and decreasing K_s) and under all three water input series (i.e. variable input intensity, variable total input, and variable antecedent wetness), a saturated zone initiates during an event and the groundwater table rises after initiation while the saturated zone percolates downward forming a wetting front, both at a decreasing rate following initiation (Figure 4.9). Moreover, the groundwater initiation depth and the timing of initiation vary substantially with the decreasing K_s profile, but vary minimally with the 2-layer K_s profile. With the 2-layer profile, groundwater initiation depth generally coincides with the permeability contrast depth of 2.0 m and occurs approximately 10 to 15 hours following the commencement of the event. The only exception is with variable antecedent wetness (Figure 4.9f) where the timing of initiation advances with increasing antecedent wetness and occurs slightly higher in the profile with the highest antecedent wetness (90%); however, the variation in initiation depth is less than that for variable antecedent wetness with the decreasing K_s profile (Figure 4.9e).

With the decreasing K_s profile, the depth of initiation moves upward in the soil profile with increasing water input intensity from a depth below the surface of 2.0 m with the 0.4 mm/h event to a depth of approximately 0.8 m with the 10 mm/h event (Figure 4.9a). Events with intensities less than 0.4 mm/h do not generate a groundwater response with either K_s profile, as the K_s for soils below 2 m depth was defined as 0.36 mm/h (i.e. $1x10^{-7}$ m/s) for both profiles (Figure 4.1). With the decreasing K_s profile, the timing of groundwater initiation advances from approximately 10 days to 7 hours with increasing input intensity (Figure 4.9a). Similarly, greater total input and greater antecedent wetness both cause groundwater initiation to occur earlier and closer to the soil surface (Figures 4.9c and 4.9e). Exceptions are the events with less than 36 mm of total input or less than 65% antecedent wetness, which do not generate a groundwater response. Furthermore, initiation does not continue to occur earlier or closer to the soil surface as total input increases beyond 72 mm. The timing and depth of initiation for the high total input events, which all have an input intensity of 3 mm/h, are consistent with those for the 3 mm/h input intensity event under the variable intensity input series; hence, input intensity constrains the depth and timing of initiation.

Despite the fact that the initiation depth is generally constant with the 2-layer profile, the maximum groundwater level reached during each event increases with increasing input intensity, total input, or antecedent wetness (Figure 4.10). At low total input or low antecedent wetness, soil saturation develops with the 2-layer K_s profile, but not with the decreasing K_s profile, presumably due to attenuation in the unsaturated zone with the decreasing K_s profile. At low intensity or moderate total input, the maximum groundwater level is closer to the soil surface with the 2-layer K_s profile than with the decreasing K_s profile. However, at moderate or high intensity, high total input, or moderate or high antecedent wetness, the decreasing K_s profile experiences higher maximum groundwater levels than the 2-layer K_s profile. Moreover, the spread between the maximum groundwater levels associated with the two different profiles increases with increasing intensity; hence, the rise in the groundwater initiation depth with increasing input intensity under the decreasing K_s profile augments the upward expansion of the saturated zone.

Equations for the K_s profiles for both soil properties scenarios were used to predict, analytically, the groundwater initiation depth for water input series #1 (i.e. variable water input intensity) as was done for the empirical analysis presented in Figures 4.3a-e and 4.4a-b. The results show that the K_s equations for the decreasing K_s profile slightly over-predict the groundwater initiation depth and slightly under-predict the maximum groundwater level compared to the SHAW model results (Figure 4.11). The latter results are consistent with the patterns observed for sites 9, 12, and 2005 (Figure 4.3). In contrast, the K_s equations for the 2-layer K_s profile are able to predict the groundwater initiation depth since it is static at approximately 2 m, but not the maximum groundwater level.

4.4 Discussion

4.4.1 Controls on groundwater response

Antecedent wetness forms a first-order threshold-type control on the occurrence and magnitude of groundwater response (Figures 4.3, 4.8, and 4.10), which is consistent with the findings of several other studies [*Noguchi et al.*, 2001; *Redding and Devito*, 2008; 2010; *Sidle et al.*, 1995]. However, water input intensity also exerts an important control on the depth of initiation during the development of transient perched shallow groundwater for soils with decreasing K_s profiles. This finding is supported by three points: (1) the ability to predict the maximum groundwater level by relating the K_s profile to the maximum 1 hour water input intensity during an event (Figure 4.3); (2) the regression analysis for site 24, which showed that maximum groundwater rise is more sensitive to water input intensity than to total water input (Figure 4.8); and (3) the SHAW model results for the decreasing K_s profile, which showed that the groundwater initiation depth reaches a maximum asymptotic value that is restricted by the input intensity (Figure 4.10). In contrast, soils with a 2-layer K_s profile have a stationary restricting layer and, therefore, the groundwater initiation depth does not vary with input intensity.

The SHAW modelling further suggests that input intensity, along with total input and antecedent wetness, can influence the maximum groundwater level (if not the groundwater initiation depth) regardless of the specific K_s profile (Figure 4.10), due to the interplay between the rate of percolation from above and the rate of water loss to deeper percolation. Other studies have also highlighted the importance of an interplay between input intensity and subsurface response [*Noguchi et al.*, 2001; *Sidle et al.*, 1995]. However, the maximum groundwater level is more sensitive to input intensity when K_s decreases with depth, as it experiences the added dynamic of variability in the depth of groundwater initiation. Moreover, it appears that maximum groundwater level is more predictable from input intensity for soils with gradually decreasing K_s compared to soils with abrupt permeability contrasts or no change in K_s with depth (Figures 4.3, 4.4, and 4.11).

The K_s decreases more-or-less exponentially with depth at approximately 75% of the UEC study sites suggesting that percolation-excess groundwater response could be a widespread phenomenon in the catchment. Redding and Devito [2008; 2010] also observed the process at Utikuma Lake in north-central Alberta, Canada. Spatial variation in K_s profiles throughout the catchment in combination with space-time variation in the water input intensity could, therefore, produce complex space-time variations in the initiation depth and the upper and lower boundaries of soil saturation. However, the distribution of percolation-excess groundwater response could be limited by the presence of deeply penetrating macropores causing bypass flow [*Detty and McGuire*, 2010b; *Weiler and Naef*, 2003] or by the distribution of sites lacking a percolation-limiting layer. Approximately 25% of the UEC study sites have non-decreasing K_s profiles and a groundwater response was never recorded at approximately 65% of these sites, even after up to three attempts to install the groundwater wells deeper. At some of these sites, the upper 1 to 1.5 m of soil have minimum conductivities that are an order of magnitude greater than the highest water input rate recorded during the study period (14 mm/h). These findings are consistent with those of Lehmann *et al*. [2007] and Redding and Devito [2010] that percolation does not generate a subsurface response until rainfall intensities exceed some threshold that is dictated by the permeability of the underlying

geology. The control of K_s on vertical versus lateral flux partitioning in the soil is further highlighted by the relations in Figures 4.7b and 4.7c.

The space-time distribution of percolation-excess groundwater response could also be limited by variables influencing lateral groundwater convergence (e.g. upslope drainage area and slope gradient). At least 40% of the UEC study sites appeared to receive lateral flux from upslope locations, as individual groundwater response events persisted through multiple consecutive input events. With persistent hillslope groundwater, localized water inputs might not generate percolation-excess groundwater response, even with a decreasing K_s profile, as percolating water could reach an established water table before being restricted by the vertical K_s of the soil. However, the localized inputs would still contribute to hillslope lateral flux and, therefore, increase the water table level.

Approximately 35% of the sites with non-decreasing K_s profiles experienced either limited or persistent groundwater response, indicating that a restricting layer (e.g. the rock surface observed at site 6501) must reside slightly below the lowest depth of the K_s measurements. Two of these responsive sites are located in hillslope hollows with persistently high groundwater levels and in close proximity to the upper extents of ephemeral streams. Field evidence indicated that subsurface erosional processes had generated the high conductivities of the shallow soils at both sites making them unique compared to all other sites with non-decreasing K_s profiles.

4.4.2 Implications for catchment response

The finding that antecedent wetness exerts a threshold effect on maximum groundwater level and total lateral flux (Figures 4.3, 4.5, and 4.8) suggests that antecedent wetness could form a first-order control on both maximum stormflow response and total stormflow response via its influence on the amount of water lost to storage in the unsaturated zone. Several other researchers have documented the important influence of antecedent wetness on runoff response [*Noguchi et al.*, 2001; *Redding and Devito*, 2008; 2010; *Sidle et al.*, 1995]. The results in Figure 4.8 suggest that total stormflow response

might also be influenced more by total input than by input intensity. However, maximum stormflow response might be influenced more by input intensity than by total input for soils where K_s decreases with depth, based on two points: (1) the finding that maximum groundwater level and, thus, maximum lateral flux are more sensitive to input intensity than to total input (Figure 4.8); and (2) the finding that input intensity strongly influences the timing of groundwater initiation (Figure 4.9a).

Transient perched groundwater that develops via a percolation-excess mechanism could potentially enhance rapid runoff response beyond that generated via the transmissivity feedback mechanism. The higher the groundwater initiates within the soil profile, the less distance the water table would need to rise to intersect higher conductivity soils [*Bishop*, 1991; *Buttle*, 1994], including lateral macropores. Moreover, less time would be required for water to percolate to the saturated zone, increasing the likelihood of saturation to the soil surface and, thus, generation of saturation overland flow [*Kirkby*, 1969; *Zaslavsky and Sinai*, 1981a]. However, downward percolation below the groundwater initiation depth, as illustrated in Figure 4.9, would act to attenuate rapid response mechanisms. The results in Figure 4.10a for maximum groundwater level suggest that attenuation might dominate the influence of percolation-excess processes on rapid runoff response for low input intensity events, whereas the rising groundwater initiation depth might dominate for high intensity events. Furthermore, it is likely that the dominant influence also depends on the specific soil profile characteristics. For instance, a high rate of change in K_s with depth might minimize attenuation of the rapid response mechanisms, and vice versa for a low rate of change in K_s.

Locations within a catchment with convergent lateral flow pathways might actually experience minimal or negligible lateral flux if vertical K_s profiles throughout most of the upslope drainage area are not conducive to the formation of perched shallow groundwater. For example, site 6501 and one downslope site (Figure 2.1) are located in the middle and lower portions of a well-defined hillslope hollow, yet only occasional short-duration, discrete groundwater response events were observed at each site. These findings suggest that K_s profiles throughout both local and upslope areas, and not just

topographic position, control the spatial distribution of runoff generation (e.g. bottom-up versus percolation-excess soil saturation, persistent versus infrequent or negligible saturation, rapid lateral flux versus deep percolation). Hence, the dynamics of catchment response might be highly sensitive to the spatial distribution of various K_s profiles, which would have important implications to the reliability of terrain indices as a basis for predicting runoff generation and hillslope hydrologic connectivity. Redding and Devito [2010] also suggested that prediction of the timing and magnitude of lateral flow and associated hillslope hydrologic connectivity would be complicated by spatial variability in the depth to an effective restricting layer. Similarly, Monteith *et al.* [2006a; b] found that topographic metrics had a limited relationship with spatial patterns of groundwater residence times and other groundwater properties, and suggested that K_s and soil thickness should be considered.

Since the annual precipitation in the UEC catchment exceeds the actual annual losses to evapotranspiration, it is inferred that sites with limited or negligible shallow groundwater response contribute to baseflow via deep percolation rather than to stormflow via rapid runoff response pathways. These findings suggest that sites with high values of K_s throughout the upper 1 or 2 m of soil might be particularly important for sustaining runoff during low flow periods in catchments where precipitation exceeds evapotranspiration. In contrast, sites having highly conductive shallow soils (e.g. due to subsurface erosional processes) coupled with persistent groundwater responses due to the presence of an underlying restricting layer and large upslope drainage area could be particularly important for establishing hillslope hydrologic connectivity and for generating high rates of runoff.

4.5 Conclusions

In-situ measurements show that soil K_s decreases gradually with depth at approximately 75% of the sites in the UEC catchment. Empirical and modeled groundwater response data suggest that, at locations where K_s decreases gradually with depth, transient perched shallow groundwater might form via a percolation-excess runoff generation mechanism,

and that the initiation depth and maximum level of the perched groundwater might vary according to an interplay between the K_s profile and the water input intensity dynamics during an event. Moreover, the data suggest that the groundwater initiation depth and the maximum groundwater level can be predicted by relating the K_s profile to the water input intensity during an event. Despite the important influence of input intensity on groundwater dynamics, antecedent wetness appears to exert a first-order control over the development of transient perched groundwater. Input intensity appears to exert less influence than total water input and antecedent wetness on total lateral flux, but influences maximum groundwater level more and, therefore, may also exert greater influence on maximum stormflow response. At sites where K_s does not decrease gradually with depth, water input intensity does not appear to influence the depth of groundwater initiation due to a stationary lower restricting layer, but may exert some control over the maximum groundwater level via an interplay between the rate of water input and the rate of water loss to deep percolation. The spatial distribution of various K_s profiles appears to influence the spatial distribution of runoff response within the UEC catchment, and may supersede the influence of topography on groundwater response at locations with deep, highly conductive soils.

Table 4.1. Site characteristics and regression models for saturated hydraulic conductivity (K_s; m/s) as a function of soil depth (z; m) based on the Guelph Permeameter data presented in Figure 4.1.

Site	Elevation (m)	Slope (%)	Aspect (°)	Forest cover	Soil texture	[c]Upslope area (ha)	Well depth (m)	K_s model
[a]9	1702	26	223	Mature, lodgepole pine	Silty loam	0.015	1.10	$K_s(z) = 0.12997 \cdot e^{-12.4972 \cdot z}$
12	1780	17	277	Mature, lodgepole pine	Sandy loam	0.003	0.66	$K_s(z) = 0.00012 \cdot e^{-6.0061 \cdot z}$
[a]24	1641	55	209	Mature, lodgepole pine	Sandy loam	0.005	1.35	$K_s(z) = 0.00245 \cdot e^{-7.7779 \cdot z}$
2005	1629	20	189	Mature, lodgepole pine	Sandy loam	0.018	0.68	$K_s(z) = 0.00014 \cdot e^{-7.8724 \cdot z}$
4020	1606	28	149	5 m regen, lodgepole pine	Sandy loam	0.018	0.93	$K_s(z) = 0.00007 \cdot e^{-6.7480 \cdot z}$
4025	1551	61	272	Mature, lodgepole pine	Silty loam	0.095	1.13	$K_s(z) = 0.00004 \cdot e^{-1.3988 \cdot z}$
[b]6501	1753	19	169	Mature, lodgepole pine	Loamy sand	0.370	1.35	$K_s(z) = 0.00001 \cdot e^{-0.0337 \cdot z}$

a. The 0.25 m soil depth K_s value was removed from the regression to improve the prediction of K_s over the range of observed groundwater levels.

b. The 0.25 m through 0.6 m soil depth K_s values were removed from the regression to improve the prediction of K_s over the range of observed groundwater levels.

c. Calculated using a 5 m DEM.

Table 4.2. Regression models for event based maximum measured groundwater rise above the well bottom (GW, m) and total lateral flux (LF, l/m) at site 24. Predictor variables are water input intensity (I, mm/d), total water input (T, mm), and antecedent soil wetness (θ, %). Only events with measured groundwater responses were included in the regressions.

Variable	Model	SE_{res}	R^2	p-value
GW	$\log(GW) = -7.98 + 0.41 \cdot I + 0.57 \cdot \log(T) - 0.47 \cdot \theta^{9}$	0.65	0.65	< 0.001
LF—full	$\log(LF) = -9.00 + 0.13 \cdot I + 0.76 \cdot \log(T) - 0.66 \cdot \theta^{13}$	0.89	0.57	< 0.001
LF—reduced	$\log(LF) = -8.64 + 0.83 \cdot \log(T) - 0.62 \cdot \theta^{13}$	0.88	0.56	< 0.001

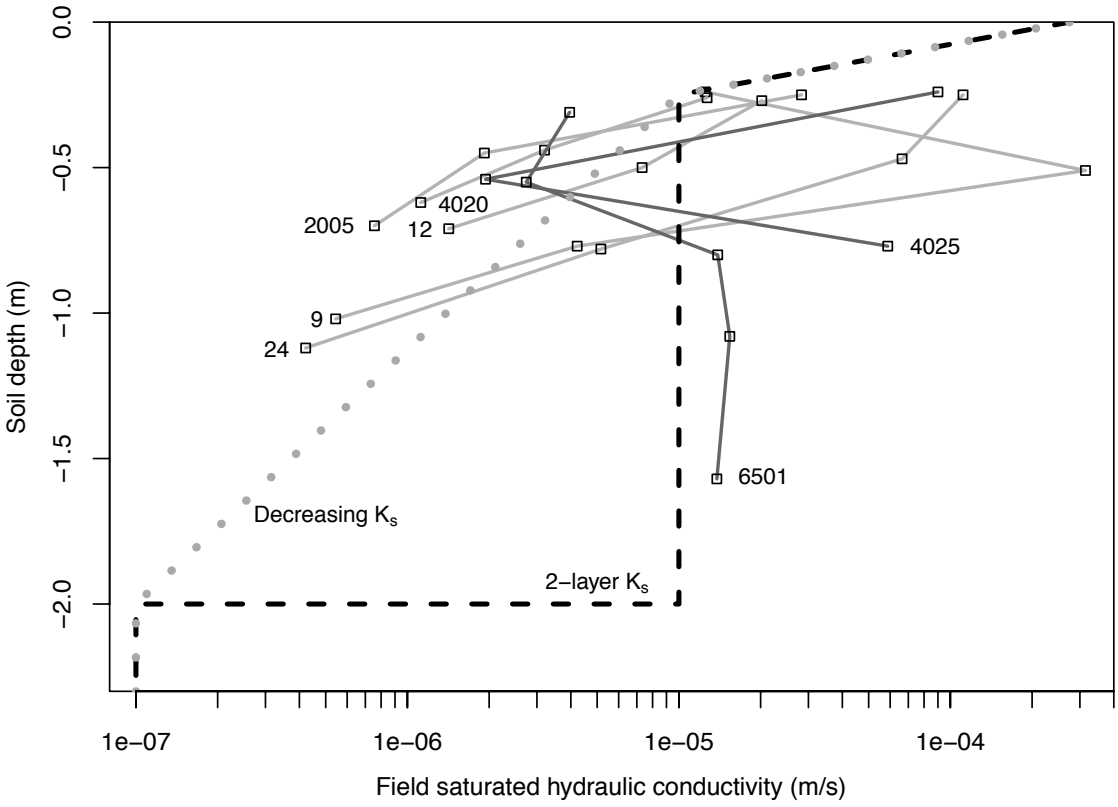

Figure 4.1. Field saturated hydraulic conductivity (K_s) data from Guelph Permeameter tests showing sites (site number indicated in the figure) having exponentially decreasing K_s with soil depth (light grey solid line) and sites having non-decreasing K_s with soil depth (dark grey solid line). These data form part of the analysis dataset. Hypothetical decreasing K_s (dotted line) and 2-layer K_s (dashed line) profiles are also defined for the SHAW modelling analysis.

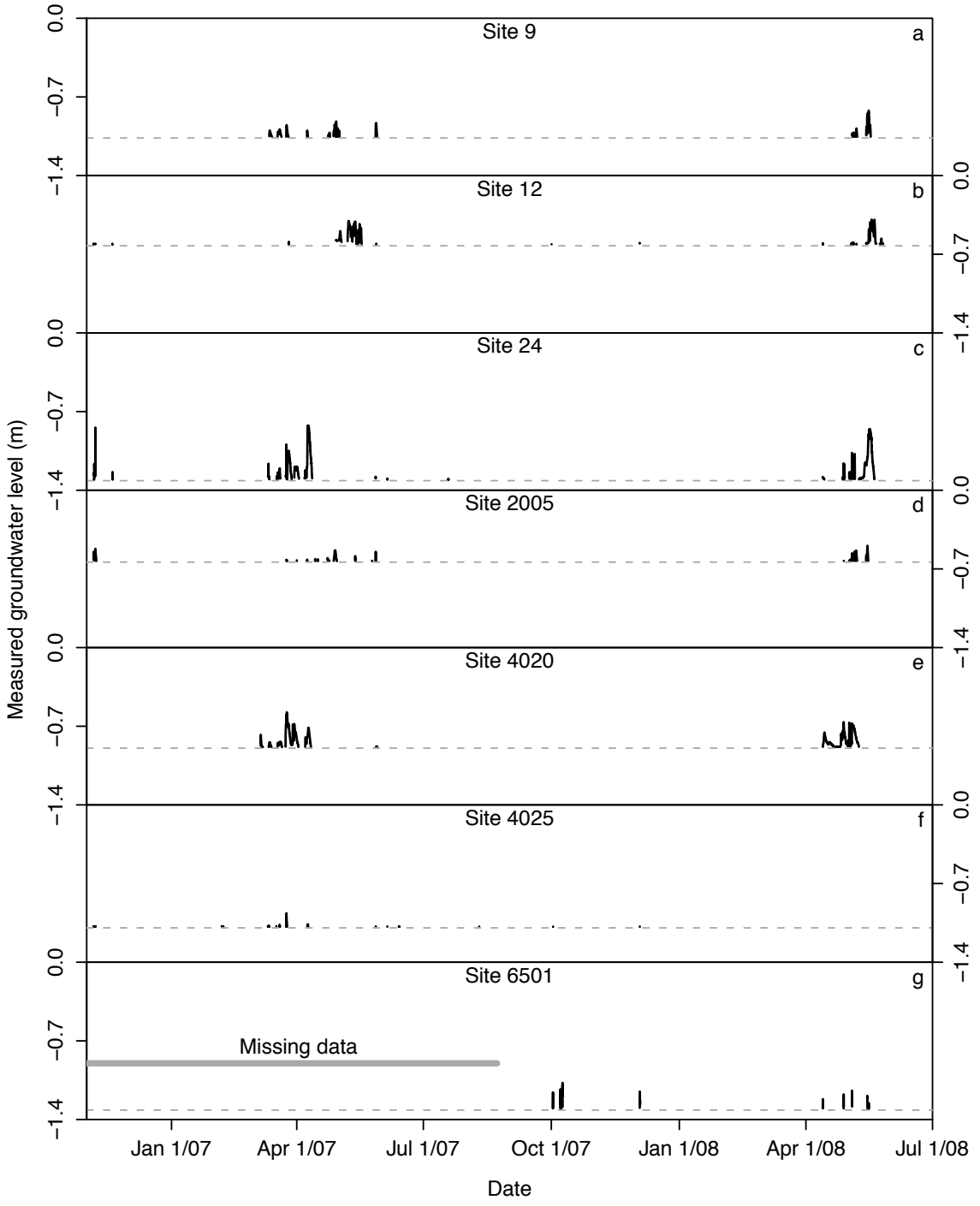

Figure 4.2. Measured groundwater level for each site within the analysis dataset. No data are plotted for periods lacking an observed groundwater response. Well bottoms are indicated by dashed lines.

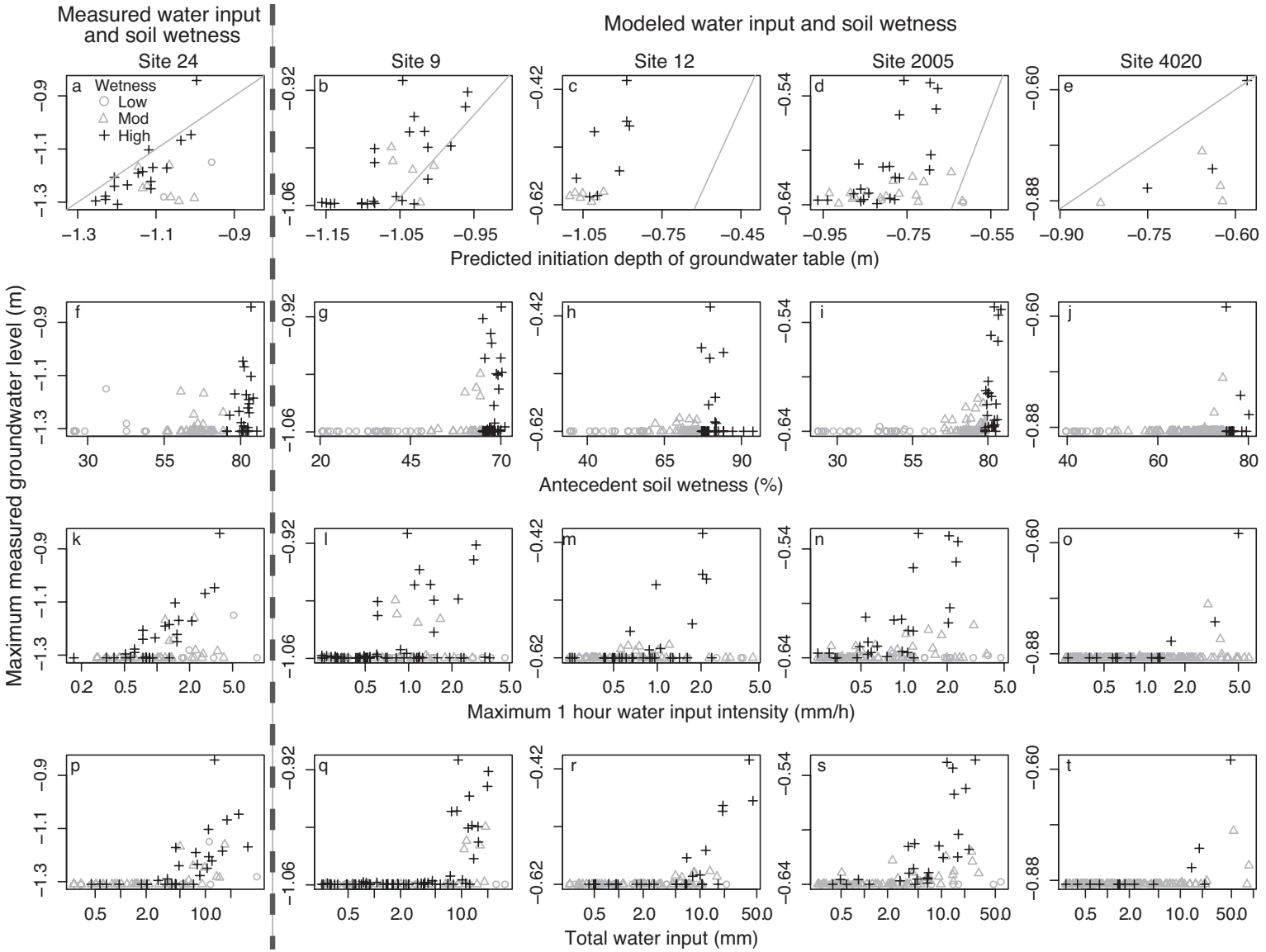
Measured water input and soil wetness
Modeled water input and soil wetness
Site 24
Site 9
Site 12
Site 2005
Site 4020
a Wetness
Low
Mod
High
Predicted initiation depth of groundwater table (m)
Antecedent soil wetness (%)
Maximum 1 hour water input intensity (mm/h)
Total water input (mm)
Maximum measured groundwater level (m)

Figure 4.3. Previous page. Maximum measured groundwater level and (a-e) predicted initiation depth of the groundwater table (grey lines are the 1:1 relation), (f-j) antecedent soil wetness, (k-o) maximum 1 hour water input intensity, and (p-t) total water input for the sites with decreasing saturated hydraulic conductivity (K_s) profiles. Sites with modeled water inputs and soil wetness are indicated at the top of the figure. Apparent antecedent wetness thresholds should be interpreted with caution for the modeled sites, as seasonal variation in the soil wetness data was captured well by the modelling, but the absolute values were biased upwards for periods with low or moderate wetness.

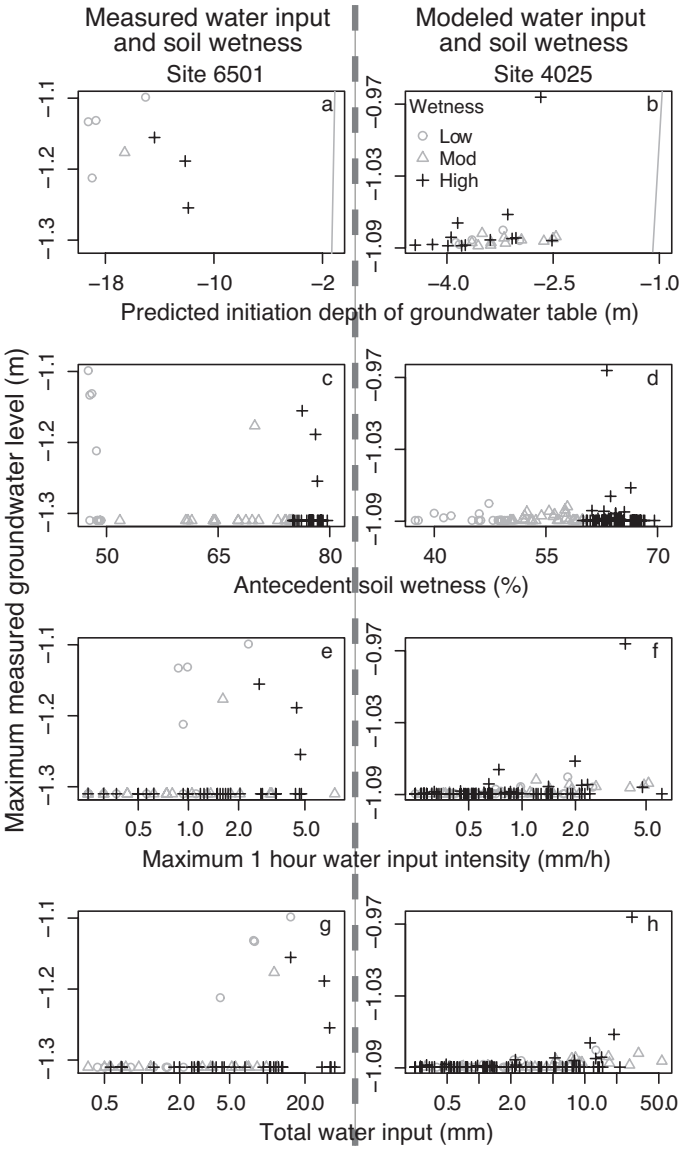

Figure 4.4. Maximum measured groundwater level and (a-b) predicted initiation depth of the groundwater level (grey lines are the 1:1 relation), (c-d) antecedent soil wetness, (e-f) maximum 1 hour water input intensity, and (g-h) total water input for the sites with non-decreasing saturated hydraulic conductivity (K_s) profiles. The site with modeled water inputs and soil wetness is indicated at the top of the figure. The apparent antecedent wetness threshold should be interpreted with caution for the modeled site, as seasonal variation in the soil wetness data was captured well by the modelling, but the absolute values were biased upwards for periods with low or moderate wetness.

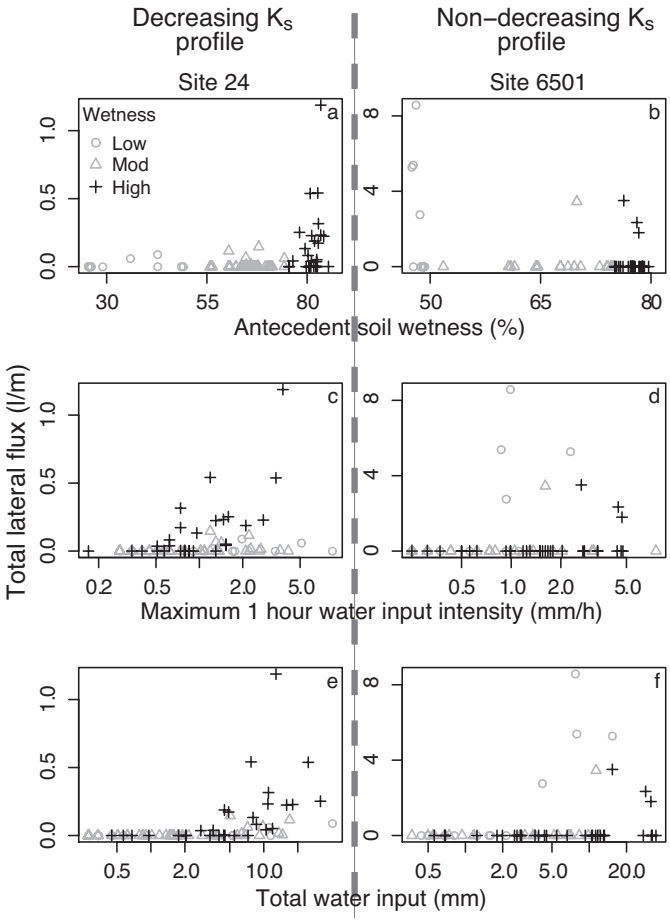

Figure 4.5. Total lateral flux and (a-b) antecedent soil wetness, (c-d) maximum 1 hour water input intensity, and (e-f) total water input for the sites with measured water inputs. The site number and corresponding saturated hydraulic conductivity (K_s) profile pattern is indicated at the top of the figure. The apparent antecedent wetness threshold should be interpreted with caution for the modeled site, as seasonal variation in the soil wetness data was captured well by the modelling, but the absolute values were biased upwards for periods with low or moderate wetness.

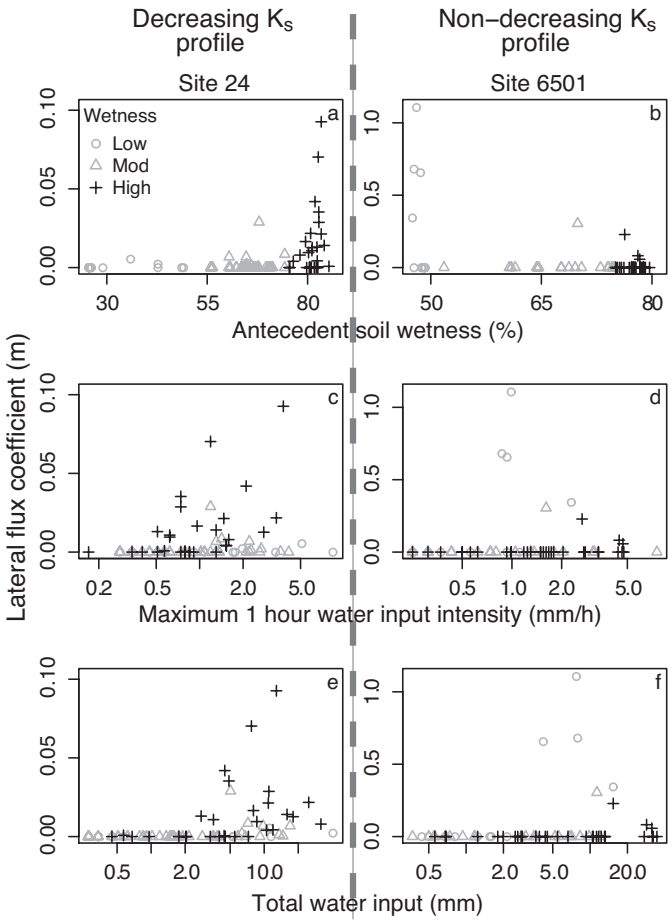

Figure 4.6. Lateral flux coefficient as a function of (a-b) antecedent soil wetness, (c-d) maximum 1 hour water input intensity, and (e-f) total water input for the sites with measured water inputs. The site number and corresponding saturated hydraulic conductivity (K_s) profile pattern is indicated at the top of the figure. The apparent antecedent wetness threshold should be interpreted with caution for the site with modeled soil wetness, as seasonal variation in the soil wetness data was captured well by the modelling, but the absolute values were biased upwards for periods with low or moderate wetness.

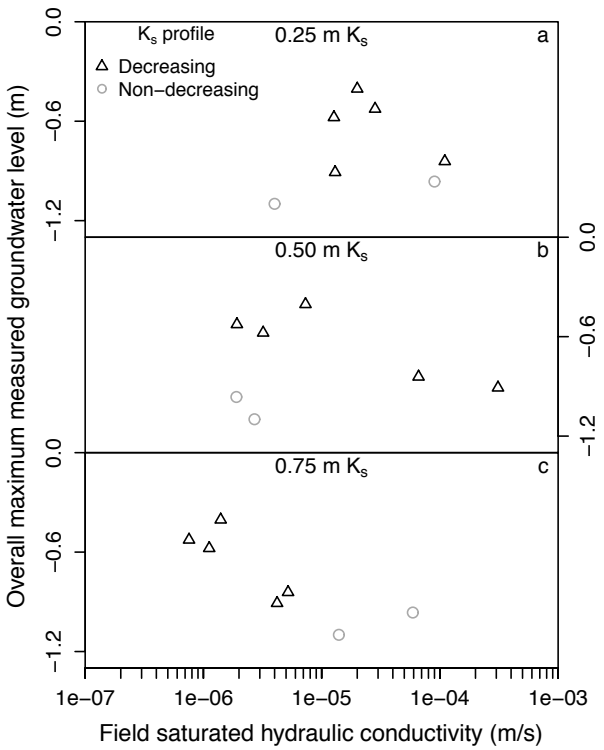

Figure 4.7. Overall maximum measured groundwater level at each site during the period of record and field saturated hydraulic conductivity (K_s) at the respective site measured at approximately (a) 0.25 m, (b) 0.50 m, and (c) 0.75 m soil depths for sites with decreasing and non-decreasing K_s profiles.

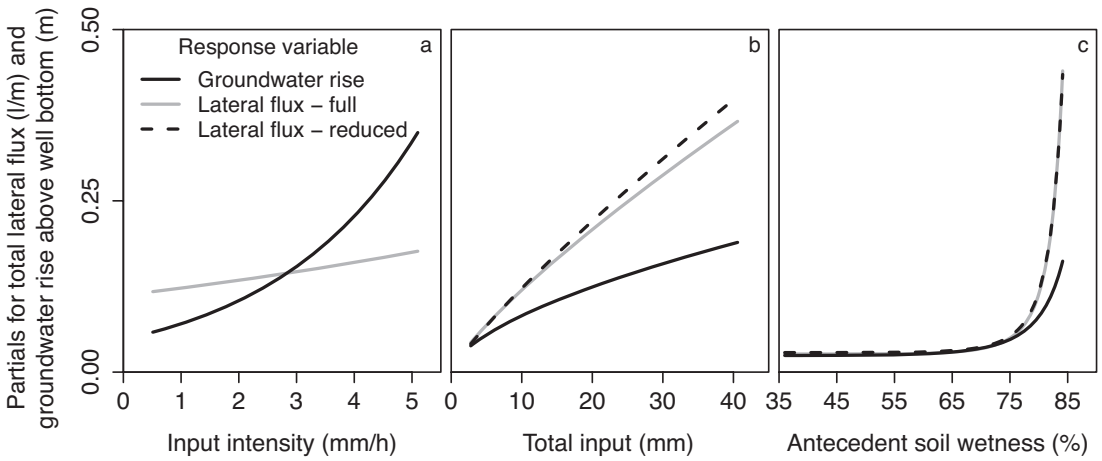

Figure 4.8. Partial responses for maximum measured groundwater rise above the well bottom and total lateral flux for site 24 based on the regression models in Table 4.2. For calculating each set of partial response values, all predictor variables other than the variable of interest were held at their respective median values.

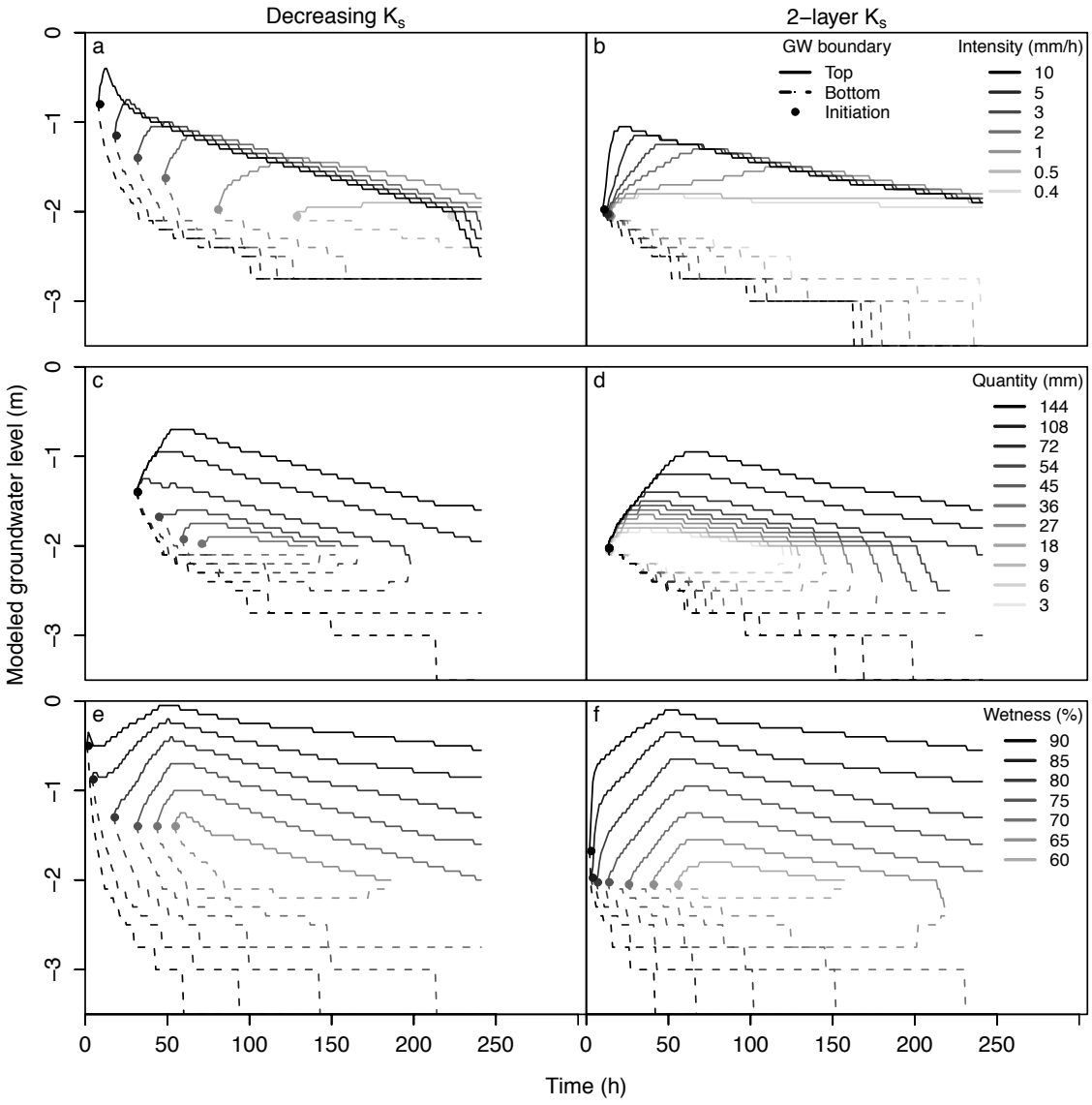

Figure 4.9. Modeled groundwater level and time since the start of rainfall for modeled events with varying (a-b) water input intensity, (c-d) total water input, and (e-f) antecedent soil wetness for a decreasing saturated hydraulic conductivity (K_s) profile and a 2-layer K_s profile.

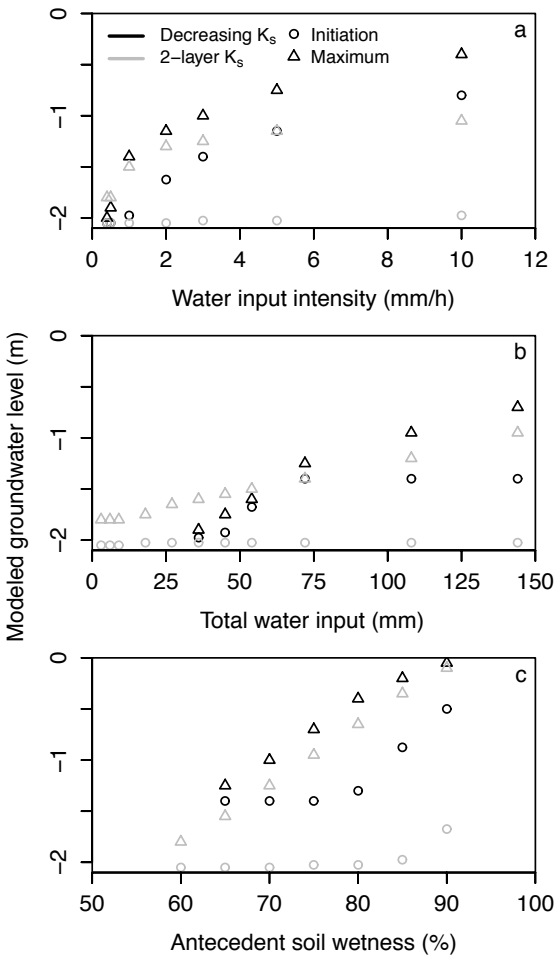

Figure 4.10. Modeled groundwater initiation depth and maximum groundwater level as a function of (a) water input intensity, (b) total water input, and (c) antecedent soil wetness for modeled rainfall events applied to a decreasing saturated hydraulic conductivity (K_s) profile and a 2-layer K_s profile. For each event, the groundwater initiation level and the maximum groundwater level are both indicated.

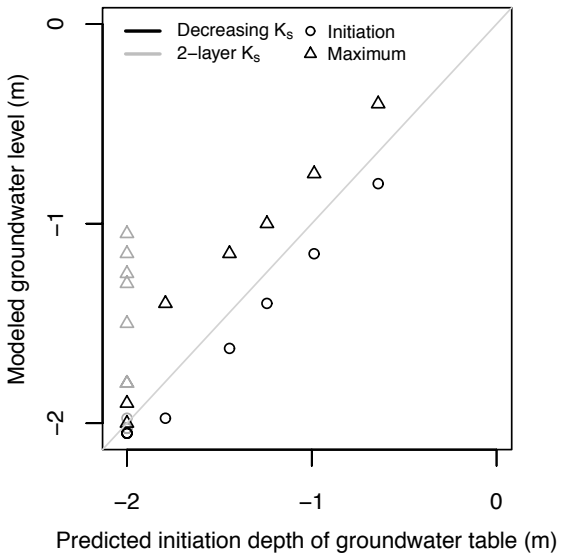

Figure 4.11. Modeled groundwater level and predicted initiation depth of the groundwater table for modeled water input events applied to the decreasing saturated hydraulic conductivity (K_s) profile and the 2-layer K_s profile (Figure 4.1). For each event and profile pairing, the groundwater initiation level and the maximum groundwater level are both indicated.

5 Controls on groundwater response and runoff source area dynamics

5.1 Introduction

Runoff generation has been a prominent research theme in hydrology for decades. For rainfall-dominated catchments, conceptual models of runoff source area dynamics have typically emphasized the influences of topography and soil characteristics on the downslope flow of water, particularly in relation to flow convergence and the connectivity of hillslope flow paths [*Dunne and Black*, 1970a; b; *Freeze*, 1972; *Hewlett and Hibbert*, 1963; 1967; *Sidle et al.*, 2000]. For example, the hydrogeomorphic concept articulated by Sidle *et al.* [2000] focuses on the activation of different hydrogeomorphic units as a function of catchment wetness. The "fill and spill" concept similarly examines runoff generation in relation to the effects of soil wetness on flow path continuity [*Tromp-van Meerveld and McDonnell*, 2006a; b].

The role of spatial variability in water inputs on runoff source area dynamics has generally not received as much attention as topography and soils, particularly at the scale of headwater catchments where much of the research on rainfall runoff processes has been conducted. The influence of topography and forest cover on snow surface energy exchanges can result in de-synchronization of snowmelt throughout a catchment [*Boyer et al.*, 2000; *Jost et al.*, 2007], complicating the space-time patterns of runoff generation. Further complexity arises because some physiographic variables can exert contrasting influences on snowmelt runoff. For instance, sites with high insolation might experience more evapotranspiration throughout the growing season and more sublimation throughout the winter season, resulting in drier soils and less snow cover prior to spring melt, respectively. However, the same sites might also experience more rapid snowmelt due to greater energy inputs and, therefore, potentially more rapid runoff response once soils are sufficiently wet. On the other hand, the influences of drier antecedent soil wetness and less snow as water input to the soil could overwhelm the influence of higher melt rates in some circumstances.

Since runoff generation in forested catchments typically depends on the development of phreatic conditions within the soil, understanding shallow groundwater (used here to refer to near-surface soil saturation) dynamics is important for understanding runoff source area dynamics [*Anderson and Burt*, 1978; *Jencso et al.*, 2009; *Kuras et al.*, 2008; *Monteith et al.*, 2006a; b; *Seibert et al.*, 2003]. Among studies that investigated groundwater related runoff source area dynamics in snowmelt-dominated forested catchments, most have been conducted in small catchments (e.g. 0.3-50 ha) with limited elevation ranges (e.g. 20-200 m of relief) [*Buttle et al.*, 2004; *Dunne and Black*, 1971; *Flerchinger and Cooley*, 2000; *Laudon et al.*, 2004; *McDaniel et al.*, 2008; *McNamara et al.*, 2005; *Monteith et al.*, 2006a; b; *Seibert et al.*, 2003], which would have limited the spatial variability in the timing, quantity, and intensity of snowmelt water inputs and associated impacts on runoff generation patterns. Larger or higher-relief catchments with complex terrain and variable land cover would experience large gradients in meteorological and snowpack conditions that could generate asynchronous snowmelt, leading to isolated areas of groundwater response. Only a few studies have addressed groundwater dynamics within the context of asynchronous water inputs that can occur under snowmelt conditions [*Boyer et al.*, 1995; 1997; 2000; *Deng et al.*, 1994; *Kuras et al.*, 2008] and several of these focused more on the flushing of dissolved organic carbon than on runoff generation processes [*Boyer et al.*, 1995; 1997; 2000].

This chapter focuses on shallow groundwater dynamics and their implications for runoff generation in the UEC catchment. Unlike some other study sites that have relatively shallow soils [*Freer et al.*, 2002; *McGlynn et al.*, 1999; *Sidle et al.*, 2000], UEC is mantled by glacial tills typically 2-8 m or more in depth. It is hypothesized that, at sites like UEC, surface topography may be less important in controlling runoff source area dynamics than other factors. Instead, deep soil (e.g. 0.5 to 2 m depth) hydraulic conductivity should be an important control on the overall occurrence of shallow groundwater response during all streamflow periods due to its influence on the partitioning of vertical versus lateral soil water fluxes, with locations having greater deep soil hydraulic conductivity experiencing deeper percolation and, thus, less shallow

groundwater response. Moreover, it is hypothesized that the dominant controls on groundwater response differ between snowmelt and non-snowmelt periods, and that the dominant controls also vary with time during each period. Upslope drainage area and hillslope gradient are expected to be dominant controls on the spatial distribution of groundwater response throughout non-snowmelt periods due to their influences on flow path convergence, and that they counteract each other in their influence on the persistence of groundwater response, with the former having a positive relation and the latter having a negative relation. It is further expected that the localized influences of elevation, insolation, and vegetation on energy inputs to the snowpack overwhelm the influences of upslope drainage area and slope gradient on the spatial distribution of groundwater response during snowmelt periods, and that locations with greater solar radiation incident on the snow surface experience greater groundwater response during the early melt periods and locations with lower solar radiation incident on the snow surface experience greater groundwater response during later melt periods.

5.2 Data analysis

5.2.1 Site parameters

Table 5.1 provides a list of site parameters that were measured or calculated to characterize each site and used in subsequent statistical analyses to investigate the influences of site physiography on groundwater response. ArcGIS 9.3.1 (ESRI) was used for delineating and calculating the upslope drainage area (using a D8 grid) for the hillslope sites and for manually determining the elevation rise and fall to the upslope ridge and downslope channel (along the flow path), respectively. Rivertools 3.0 (Rivix LLC) was used for calculating surface curvature (mean, plan, and profile). The topographic wetness index was calculated for each site using the upslope drainage area per unit contour width of the DEM (5 m) and the mean hillslope gradient from field observations. To account for the effects of site aspect and hillslope shading on energy inputs, potential solar radiation (direct and diffuse) was modeled for each day of the year for each hillslope site using ArcGIS 9.3.1 (ESRI). To incorporate the seasonal variation

in potential solar radiation within statistical analyses, radiation was averaged for three seasons of the year: the snow accumulation season (November through March), the snowmelt season (April and May), and the snow-free season (June through October). Forest cover basal area was calculated for each site using the forest cover survey data. For calculating the portion of the upslope drainage area that is logged, all areas in an early stage of regeneration were grouped together.

5.2.2 Statistical analysis

Streamflow monitoring at the UEC main gauging station commenced in April 2005 and all hillslope monitoring sites were established during October 2005 and August 2006; however, the final well depths were not established until October 2007, as multiple attempts were made during 2006 and 2007 to increase the depth of groundwater wells where responses were negligible during the preceding spring freshets. Because of these changes to the groundwater infrastructure, the period of record for the streamflow and groundwater datasets was limited to the period from November 1, 2007, to September 20, 2008. Notwithstanding the fact that data from late September and all of October are missing from the period of record, inference is made as though the period of record incorporates an entire year since the autumn period is hydrologically relatively inactive in the UEC catchment.

Groundwater dynamics throughout the catchment included persistent, transient, and unresponsive (i.e. no formation of a saturated layer within the soil profile) behaviour. Groundwater responses were temporally discontinuous at most sites and detectible groundwater responses were never recorded at 13 of the 50 hillslope sites. Due to this data censoring, statistical analysis methods such as ordinary regression could not be applied without removing the sites that did not experience groundwater responses, which would have led to a substantial loss of spatial information. As a result, the analyses were based on an ordered classification of the groundwater response data and ordinal logistic regression (OLR) was applied to predict the probability of a site meeting or exceeding each ordered class using the selected site parameters (Table 5.1) as predictors. OLR is an

extension of binary logistic regression (LR). LR forms a linear regression between the natural logarithm of the odds ratio (*O*) for a response variable and one or more predictor variables:

$$\ln(O) = a + \mathbf{b} \cdot \mathbf{x} \tag{5.1}$$

where *a* is a constant, **b** is a vector of slope coefficients, and **x** is a vector of predictor variables. The odds ratio for the response is the probability of being in one group divided by the probability of being in the other group,

$$O = \frac{p}{1-p} \tag{5.2}$$

where *p* is the probability that a particular sample point is in a specific category of the response variable. In OLR, the response variable has more than two categories of outcome that are ranked so that the p in equation 5.2 is with respect to the probability of a response being equal to or greater than a particular category. An extensive review of OLR can be found in McCullagh [1980].

The period of record was separated into eight streamflow periods to investigate, via OLR, temporal variability in the spatial patterns of groundwater response that correspond with seasonal changes in catchment hydrologic conditions. Each streamflow period was intended to represent a distinct phase of water input (related to variability in meteorological conditions) and resulting runoff response (Figure 5.1): (1) a fall transition period when the catchment experienced limited soil water recharge following the previous summer drought, (2) a winter low flow period when the catchment experienced minimal water input, (3) an early-melt transition period when the catchment began experiencing active snowmelt input that generated a small streamflow response, (4) a rising limb period when snowmelt in the catchment generated a rapid rise in the streamflow response, (5) a peak flow period when the streamflow response reached its maximum, (6) a falling limb period when the streamflow decreased quickly and the last of the remaining snow covered areas within the catchment were melting rapidly, (7) a

post-melt transition period when no snow remained in the catchment and streamflow continued decreasing at a moderate rate, and (8) a summer low flow period when streamflow responded to occasional intense rainstorm events.

Three types of response variables were defined: (1) occurrence, in which a well was assigned a value of 1 if a groundwater response was observed during the period of record and 0 if not; (2) duration, computed by determining the fractional portion of time that a water table was recorded in a well, and then reducing this interval measure to ordered classes for each time period; and (3) timing, in which the date/time (in decimal days since January 1) of first response and maximum response were classified into ordered classes. Duration classes were defined for the eight streamflow periods individually, then to the melt period after aggregating streamflow periods 3 through 6, and again to the annual period after aggregating all eight streamflow periods. Ordinal logistic regression analyses were applied to all three levels of aggregation. Observations of both transient perched groundwater and continuously persistent groundwater, which may extend deep into the subsurface, were treated as one population for the analyses regardless of the lower extent of saturation. OLR requires that the number of cases within each response class exceed the number of predictor terms in the model, which restricted the number of classes that could be defined to two or three. As much as possible, natural breaks in the distribution of the response data were used to define class thresholds, but it was necessary to adjust the thresholds slightly for each streamflow period to meet the necessary sample size for each class based on the distribution of durations in the response data. Table 5.2 provides a summary of the classes for each period. Applying an ordered classification to the duration data also led to a loss of information since duration does not account for variation in groundwater response intensity (e.g. maximum groundwater level, rate of rise or fall); however, it was considered more important in this study to maximize the spatial coverage than to capture more details of the groundwater dynamics.

In total, 36 site parameters were considered as candidate predictors in the OLR models (Table 5.1). For each parameter, a frequency histogram was used to verify whether or not the data were normally distributed and an appropriate transformation was applied, if

necessary. Although logistic regression does not assume any particular sampling distribution, it is known to perform better in some circumstances when the predictor variables are normally distributed [*Tabachnick and Fidell*, 2007], and this finding was true for the current study. All predictor variables were standardized to minimize multicollinearity and to enhance interpretation of the model coefficients. To reduce the number of potential predictor variables for each model, the classified response data were fit to each potential predictor variable separately and the strongest predictor variable from each parameter group (e.g. forest cover group, soil constituent group; Table 5.1) was selected to enter the model first. Individual variables and variable interactions were then added, removed, or replaced to achieve a final model for each streamflow period. Any effects that were not physically meaningful or possible were removed from the models. Since the groundwater wells were installed to varying depths, well depth was included as a potential predictor variable to assess whether or not the well installation depths biased the observed responses.

Several tools were used for model evaluation and for selecting the final models. The Wald test statistic [*Engle*, 1983], the AIC [*Akaike*, 1987], and the Bayesian information criterion (BIC) [*Schwarz*, 1978] were all used for variable selection, with an emphasis on BIC, as it led to the most parsimonious models. OLR assumes that the coefficients that describe the relationship between the predictor variables and the response category are the same for each response category in a model, which is called the proportional odds assumption or the parallel regression assumption. If this assumption were not true, different sets of predictor coefficients would be required to describe the relationship with each response category. Like binary LR, OLR also assumes that the relationship between the predictor variables and the natural logarithm of the odds ratio of the response (equation 5.1) is linear. Plots of partial residuals were used to confirm that the proportional odds assumption was met, to check that predictors behaved linearly, and to check for potential outliers. Lastly, a bootstrap resampling validation procedure generating Somers' D rank correlation [*Somers*, 1962] and R^2 index statistics was applied to assess predictive performance. For LR, R^2 is referred to as an index because the residuals in LR are always the difference between a binary value (0 or 1) and the

calculated probability and, therefore, R^2 is not strictly the same in LR as in ordinary linear regression. R statistical software [*R Development Core Team*, 2010] was used for all statistical analyses.

5.3 Results

5.3.1 Space-time patterns of water inputs to the catchment

Figure 5.2 shows spatially distributed mean annual potential solar radiation for the UEC catchment to highlight the catchment locations that likely experience higher rates of evapotranspiration, sublimation, and snowmelt due to greater energy inputs. Locations within the valley bottoms receive low amounts of solar energy regardless of the slope aspect due to hillslope shading. The snow cover retreated quickly during the 2008 melt and only one snow cover survey captured the catchment in a state of partial snow cover. It was observed during field investigations over three years that the snowline retreat patterns were generally consistent from year to year, but with differences in timing; thus, Figure 5.2 shows the snow cover retreat patterns for both 2007 and 2008 to illustrate the typical spatial progression within the UEC catchment. The general spatial pattern of spring snowline retreat and, thus, the spatial shifting of the lower extent of snowmelt input to the soil progresses as follows: (1) south-facing, low elevation clearcut areas; to (2) south-facing, middle-elevation forest and clearcut areas; to (3) south-facing, high elevation forest areas; and north-facing, low and middle elevation forest and clearcut areas; to (4) north-facing, high elevation forest areas.

5.3.2 Groundwater response occurrence and duration for the melt period and the annual cycle

Groundwater responses were never observed at 13 of the 50 hillslope sites in the UEC catchment. The probability of a groundwater response occurring increased with increasing upslope drainage area or with increasing melt period mean daily solar radiation (hereafter referred to as *insolation*), but decreased with increasing slope

gradient or with increasing 75 cm depth K_s (hereafter referred to as *deep soil K_s*; refer to Table 5.3 for the OLR models and Figure 5.3 for the change in probability along each variable gradient). The odds ratio of the main effect for each predictor variable (using the difference between the 25th and 75th percentile values for each predictor variable) showed that deep soil K_s was the most important variable in determining the probability of a groundwater response occurrence followed by upslope drainage area, insolation, and slope gradient, in order of importance (refer to Figure 5.4 for the strengths of the variable effects). However, accounting for variable interactions, slope gradient was found to have a highly negative effect on the probability of occurrence among low insolation sites and a weakly positive effect among high insolation sites (Figures 5.3 and 5.4). Insolation had a strongly positive effect on the probability of occurrence among high slope gradient sites and a slightly weaker negative effect among low slope gradient sites. Inspection of the locations of the sites that did not respond (indicated by "·" symbols in Figure 5.5) shows that unresponsive sites tended to be on middle or upper hillslope locations among areas with planar surface curvature and on ridges, which is consistent with the model results. The spatial distribution of deep soil K_s was also generally consistent with the model results based on a manual comparison. The absence of unresponsive sites within the south-facing clearcut area suggests that forest cover might also be an important variable, but none of the forest cover parameters was significant in the model, possibly due to being overwhelmed by the influence of insolation or due to statistical limitations associated with the sample size.

Over the annual period, the probability of a higher response duration increased with increasing upslope area or insolation, but decreased with increasing slope gradient, maximum tree diameter, or deep soil K_s (Figure 5.3). In order of importance, the main effects were strongest for maximum tree diameter and upslope area, somewhat weaker for deep soil K_s and slope gradient, and much weaker for insolation (Figure 5.4). Interaction effects showed that slope gradient had a stronger negative effect among sites with low insolation, and a weakly positive effect among sites with high insolation (Figures 5.3 and 5.4). Insolation had a much stronger positive effect among sites with high slope gradient and a strongly negative effect among sites with low slope gradient.

Inspection of the spatial distribution of annual response durations (indicated by symbol size in Figure 5.5) shows that sites with persistent responses tended to be located near streams or in hillslope hollows, particularly those with low slope gradients. Moreover, 36% of the clearcut sites experienced a 0.75-1.0 response (i.e. a water table was measured within the well 75% to 100% of the time; largest symbol size in Figure 5.5), whereas only 11% of the forested sites experienced a >0.75 response.

When OLR was applied to the duration of groundwater response throughout the melt period (defined as April 11 – June 7 for the streamflow duration data), the variables in the model, their interactions, and their signs (i.e. positive or negative effects) were the same as for the annual duration model, but the order of importance varied (Figures 5.3 and 5.4). In particular, slope gradient and deep soil K_s had stronger effects than both maximum tree diameter and upslope area. Moreover, the overall strengths of the main and interaction effects were stronger for slope gradient and weaker for maximum tree diameter and upslope area. Compared to the persistence of response on an annual basis, some sites that were distant from the stream network and not in well defined hillslope hollows experienced more persistent responses (Figure 5.5).

5.3.3 Response timing analysis

For sites with groundwater responses that persisted through the winter, the date/time of the start of the first distinct rise in the water table level during the spring melt was used as the timing of first response. For other sites, the first response was defined as the date/time that a water table was first recorded in the well. The fitted OLR model showed that the timing of first response was advanced with increasing upslope drainage area or with a greater portion of the upslope area being logged, whereas the timing of first response was delayed with increasing elevation, deep soil K_s, or silt fraction (refer to Figure 5.6 for the change in probability along each variable gradient and Table 5.4 for the strengths of the variable effects). The main effects were strongest for upslope drainage area followed by elevation, silt fraction, deep soil K_s, and upslope logging (Table 5.4). No interaction effects were significant in the model. Inspection of the spatial distribution of first

response (indicated by symbol size in Figure 5.5) shows that sites with an early first response tended to be located near streams and in hillslope hollows, and in the low elevation south-facing clearcut.

When the date/time of maximum groundwater level was used as a response variable, the fitted OLR model showed that the timing of maximum response was advanced with increasing insolation and clear-sky fraction, but delayed with increasing silt fraction (Figure 5.6). Clear-sky fraction was the strongest effect with much weaker effects from insolation and silt fraction, in order of importance (Table 5.4). No interaction effects were significant in the model. Inspection of the spatial distribution of the maximum response (indicated by symbol size in Figure 5.5) shows that sites with an early maximum response tended to be located in the low elevation south-facing clearcut.

5.3.4 Response during individual streamflow periods

For the individual streamflow periods, OLR models for response duration included two or more of the following variables: upslope drainage area, slope gradient (mean of upslope and downslope directions or downslope direction only), deep soil K_s, maximum tree diameter, and insolation (Table 5.3 and Figure 5.7). Three out of eight models also incorporated interactions between slope gradient and insolation. Other variables from the list of parameters that were tested (Table 5.1) were either not significant in the models, explained smaller amounts of variance in the data than the associated variables that were selected, or their effects were not physically meaningful or possible. Well depth was not significant in any model. Upslope drainage area and slope gradient were important in all periods, with each holding either first or second place in terms of importance (Figure 5.4), except in period 3 (early-melt transition) and period 4 (rising limb) when maximum tree diameter and deep soil K_s had the strongest effects relative to other variables, respectively. The main effects of upslope area and slope gradient were positive and negative during all periods, respectively, and were at their weakest levels during periods 3 and 4, respectively (Figures 5.4 and 5.7).

Deep soil K_s had the third strongest main effect in periods 1 through 3 and 8, and the strongest effect in period 4, but was not significant in the models during periods 5 through 7 when the catchment was wet throughout and draining. Maximum tree diameter was significant in the model only during periods 1 through 4 with its importance rising to a maximum during period 3 (early-melt transition). The effects of deep soil K_s and maximum tree diameter were negative during all relevant periods. Insolation was significant in the models only during periods 3 through 5 when snowmelt was widespread throughout the catchment. The main effect of insolation was weakly positive during period 3 (early-melt transition), moderately positive during period 4 (rising limb), and moderately negative during period 5 (peak flow), showing the spatial shifting of dominant water input source areas from high insolation sites in periods 3 and 4 to low insolation sites in period 5. Moreover, the effect of insolation was strongly negative among low slope gradient sites and strongly positive among high slope gradient sites during periods 3, 4, and 5 (Figures 5.4 and 5.7). During periods 3 through 5, the effect of slope gradient was strongly negative among sites with low insolation. Among sites with high insolation, the effect of slope gradient was weakly positive during periods 3 (early-melt transition) and 4 (rising limb), and moderately positive during period 5 (peak flow). Interestingly, sites with low slope gradient and high insolation and sites with high slope gradient (regardless of insolation) had lower overall shallow soil saturation (mean of 10-40 cm soil depth) at the start of the spring melt compared to sites with low slope gradient and low insolation (Figure 5.8).

By examining the relative positions of the main effects along the respective x-axes in Figure 5.7, one can observe that the relations shift to higher or lower values of the predictor variables sequentially between periods. To investigate this variation in more detail, the 0.1 and 0.5 probabilities of a persistent response are plotted for each predictor variable (except insolation since the direction of its effect, i.e. positive versus negative, changes between period 4 and period 5) and period in Figure 5.9. Compared to the 0.1 probability, the 0.5 probability had a higher upslope area and lower slope gradient, deep soil K_s, and maximum tree diameter in any given period. These relative positions are consistent with the positive main effect of upslope area versus the negative main effects

of slope gradient, deep soil K_s, and maximum tree diameter on the duration of groundwater response (Figures 5.4 and 5.7). Examining a constant probability of a persistent response (e.g. 0.5), the minimum upslope area required to generate persistent groundwater responses reached a maximum in period 2 or 3 and a minimum in period 4. During period 4, probabilities of experiencing persistent groundwater responses of 0.1 and 0.5 were associated with upslope areas of approximately 90 m^2 and 1120 m^2, respectively. In contrast, the same probabilities were associated with upslope areas of approximately 1.6 ha and 140 ha during period 3, respectively. Similarly, the slope gradient associated with a particular probability of a persistent groundwater response (e.g. 0.5) reached a maximum in period 4 and a minimum in periods 2 or 3. During period 4, probabilities of 0.1 and 0.5 were associated with slope gradients of approximately 68% and 32%, respectively, whereas the same probabilities were associated with slope gradients of approximately 20% and 9% during period 3. This expansion of the runoff generation areas to locations with higher slope gradients and smaller upslope drainage areas (i.e. planar hillslopes and ridges) followed by contraction of the runoff generation areas can be confirmed by observing variation in the spatial distribution of 0.75-1.0 duration sites (i.e. responded during 75% to 100% of the period) between each period in Figure 5.10. The most widespread distribution occurred in period 5. It is also possible to observe that from period 3 through period 5, moderate and high elevation sites were sequentially added to the portion of sites that experienced persistent responses while a small number of low elevation sites stopped contributing.

The limiting effect of deep soil K_s on groundwater response (Figure 5.9) was greatest in period 1 (i.e. only sites with very low values of K_s were likely to experience persistent groundwater responses) when the catchment was relatively dry and streamflow was low following the summer drought, and decreased (i.e. higher K_s value) in subsequent periods. Deep soil K_s was the least limiting (i.e. even sites with high values of K_s were likely to experience persistent groundwater responses) in period 4 during widespread snowmelt and was insignificant in the models for periods 5 through 7. During period 1, probabilities of 0.1 and 0.5 were associated with deep soil K_s values of approximately

$9 \cdot 10^{-9}$ m/s and $5 \cdot 10^{-10}$ m/s, whereas the same probabilities were associated deep soil K_s values of approximately $4 \cdot 10^{-5}$ m/s and $4 \cdot 10^{-6}$ m/s during period 4, respectively.

Maximum tree diameter was most limiting (i.e. only sites with small or no trees were likely to experience persistent groundwater responses; Figure 5.9) during period 1 when the catchment was relatively dry and streamflow was low. Maximum tree diameter was least limiting (i.e. sites with small through large diameter trees were likely to experience persistent groundwater responses) in period 4 during widespread snowmelt and was insignificant in the models for periods 5 through 8. During period 1, sites with forest cover had probabilities of experiencing persistent groundwater responses that were less than 0.1, whereas probabilities of 0.1 and 0.5 were associated with maximum tree diameters of approximately 72 cm and 33 cm during period 4, respectively. The limiting effects of forest cover on melt can be observed for period 3 when sites within the low elevation south-facing clearcut area experienced persistent groundwater responses, but sites in adjacent forested areas of similar or lower elevation and similar insolation did not respond or responded minimally (Figure 5.10). For periods 4 and 5, one can observe that sites with persistent groundwater responses were distributed throughout both forested and clearcut areas.

5.4 Discussion

5.4.1 Controls on the spatial distribution of groundwater occurrence

Deep soil K_s (measured at 75 cm depth) was the most important variable for predicting whether or not a site experiences any detectable groundwater response within the range of soil depths that were monitored (i.e. groundwater well depths ranged between 0.50 m and 1.64 m). Moreover, the finding that a groundwater response is more likely to occur at high slope gradient sites with high insolation compared to high slope gradient sites with low insolation, despite having negligible differences in shallow soil wetness at the start of the spring melt, suggests that water input intensity is also an important influence on the spatial distribution of the occurrence of groundwater response. These results are

consistent with the percolation-excess runoff generation mechanism described by Redding and Devito [2008; 2010], who found that water input intensity was a first-order control on the occurrence and amount of lateral flux in glacial till soils due to its influence on vertical versus lateral flux partitioning. Similar results were found for the UEC catchment, as described in chapter 4. In the statistical models for this study, deep soil K_s likely accounts for variation in the depth of the percolation-limiting layer.

Upslope drainage area and slope gradient were also found to be important in determining whether or not a site experiences a detectable groundwater response. This finding suggests that some sites with large upslope areas will experience a shallow groundwater response regardless of the K_s of the surficial soils due to high rates of flow accumulation. Jencso *et al.* [2009] found that some sites in a snowmelt-dominated catchment in Montana experienced little or no groundwater response and they attributed the lack of response to small upslope drainage areas, but without detailed evaluation of the influences of deep soil conductivity and water input intensity on vertical versus lateral flux partitioning. Notwithstanding the findings related to flow accumulation, the current study suggests that the underlying geology and the various physiographic influences on snowmelt intensity might be as important or more important than topographic convergence in determining the spatial distribution of responsive sites.

5.4.2 Controls on the space-time distribution of groundwater persistence

During the early phases of the spring freshet, while the catchment is relatively dry (except along riparian corridors) and snow covered, increasing energy inputs begin to generate melt in low elevation, high insolation locations of the catchment. Under these conditions, the OLR models suggest that vertical controls (i.e. localized energy and mass inputs, and vertical versus lateral flux partitioning expressed by maximum tree diameter and deep soil K_s) dominate the patterns of persistent groundwater response due to the influence of locally generated snowmelt. Once snowmelt expands throughout the catchment and most of the catchment is wet and hydrologically connected, lateral controls (i.e. lateral hydraulic gradient and flow path convergence expressed by slope

gradient and upslope contributing area) begin to dominate the persistence of groundwater response, which continues throughout the peak flow period and throughout the summer, autumn, and winter low-flow periods while the catchment drains. These findings are supported by those of Jencso *et al.* [2009] and Kuras *et al.* [2008] for other snowmelt-dominated montane catchments, and by those of Szeftel [2010] for the CCEW. These findings also corroborate the applicability of the generally accepted relations between soil wetness and various topographic indices [*Beven and Kirkby*, 1979; *Quinn et al.*, 1995], as well as the importance of topographic position as a controlling factor in runoff generation dynamics [*Dunne and Black*, 1970a; b; *Freeze*, 1972; *Hewlett and Hibbert*, 1963; 1967; *Sidle et al.*, 2000], except during the early-melt and rising limb periods of the spring freshet.

The contrast in the dominance of vertical versus lateral controls is also highlighted by the positive influence of insolation on the persistence of groundwater response at high slope gradient sites during the early-melt, rising limb, and peak flow periods compared to the negative influence at low slope gradient sites during the same periods. The same patterns exist regarding the probability of groundwater response occurrence. Low slope gradient sites on low insolation hillslopes are generally wetter at the start of the spring melt compared to low gradient sites on high insolation hillslopes (Figure 5.8), likely due to lower rates of pre-melt evapotranspiration (particularly before snowpack development) and, thus, greater pre-melt accumulated soil wetness in low insolation areas than in high insolation sites. These differences appear to make low gradient, low insolation sites more responsive to water inputs than low gradient, high insolation sites, which is corroborated by field observations that north-facing areas are generally wetter throughout the snow-free season and have a higher density of streams compared to south-facing areas. In contrast, the high rates of soil drainage at high slope gradient sites likely limit the potential for evapotranspiration differences to generate large differences in antecedent soil wetness at the start of the spring melt. Thus, higher rates of snowmelt on high slope gradient, high insolation sites have a greater ability to generate a groundwater response compared to relatively lower rates of snowmelt on high slope gradient, low insolation sites. In essence, controls on antecedent wetness and flow path convergence overwhelm

controls on water input intensity and vertical versus lateral flux partitioning among low slope gradient sites, but not among high slope gradient sites.

The fact that maximum tree diameter is the most important variable in determining the persistence of groundwater response over the annual cycle is consistent with the hypothesis that forest cover removal increases groundwater levels via its negative influence on evapotranspiration and, thus, positive influence on water input.

5.4.3 Controls on groundwater response timing

The timing of first groundwater response is controlled by parameters influencing the upslope hydrologic conditions and lateral redistribution (e.g. the upslope drainage area, the portion of the upslope area that is logged), the local soil hydraulics (e.g. deep soil K_s, silt fraction), and the localized energy inputs and/or snowpack depth (e.g., as influenced by elevation). The strong importance of upslope drainage area shows that when the upslope area is large, even small amounts of melt can generate an initial groundwater response, likely due to the influence of lateral redistribution of soil water on antecedent wetness. The influence of upslope logging on the timing of first response is likely related to controls on both the early melt energy and mass flux dynamics distributed throughout the upslope drainage area and the antecedent wetness remaining from the previous growing season. A high value of deep soil K_s means that more storage capacity must be satisfied (i.e. due to greater depth to the percolation-limiting layer) before the first groundwater response can occur. The silt fraction likely influences the absolute soil storage capacity and the retention of soil water in the unsaturated zone through the winter, and, thus, the unsaturated hydraulic conductivity, which would all influence the rate of percolation and the amount of water input necessary to satisfy the unsaturated soil storage capacity before forming or contributing to the first groundwater response.

The timing of maximum groundwater response appears to be controlled primarily by parameters influencing the localized energy inputs (e.g. clear-sky fraction, insolation) with less control by parameters influencing the local soil hydraulics (e.g. only silt fraction

is important) and negligible control related to lateral redistribution. Neither upslope drainage area nor slope gradient are important controls on the timing of maximum groundwater response, suggesting that the timing of maximum response is determined more by vertical process controls than by lateral process controls, which is consistent with the maximum response being controlled more by surface processes. The importance of clear-sky fraction and insolation in controlling the timing of maximum response illustrates the importance of localized energy and mass flux dynamics on the differential timing, intensity, and quantity of snowmelt and their subsequent influences on the timing of response. Overall, the controls on both timings (i.e. first and maximum groundwater responses) have some consistency with the controls on snow accumulation and melt processes, particularly for the timing of maximum groundwater response.

5.4.4 Implications for runoff source area dynamics and catchment modelling

Sites with high values of deep soil K_s that do not generate a shallow groundwater response should experience deep percolation and likely generate runoff via slow response pathways resulting in continual drainage throughout the recession and low flow periods. These findings are supported by two points: (1) precipitation exceeds actual evapotranspiration in the UEC catchment and, therefore, all sites must experience runoff (ignoring the influences of wind redistribution, which is negligible under a forest canopy, on the water balance); and (2) rapid response pathways within the deep subsoil, such as deep soil cracks in clay or bedrock [*Montgomery et al.*, 2002; *Montgomery et al.*, 1997; *Tromp-van Meerveld et al.*, 2007], are likely limited in abundance since the soils are typically 2-8 m or more in depth with only small amounts of clay and minimal bedrock. Thus, the spatial distribution of surficial soil K_s is an important control on the distribution of sites that generate rapid runoff versus sites that generate slow runoff. Kuras *et al.* [2008] found that runoff source area dynamics during low flow periods were not explained well by surface topography and suggested that deep, disconnected flows dominate runoff generation during these periods. Moreover, sites with large upslope drainage areas and high values of soil K_s that also experience a shallow groundwater

response would be capable of transmitting water to the stream network at a high rate and, thus, would be critical in the connectivity of runoff source areas to streams.

The amount of incident solar radiation differentiates runoff source areas during the early-melt period and, to a lesser extent, during the rising limb and peak flow periods. However, its influence weakens as active snowmelt zones shift into more shaded (via topography and/or forest cover) locations. Peak streamflow occurs when snowmelt and runoff are being generated throughout most areas of the catchment, including locations with low insolation, with mature forest cover, with high slope gradients, with convex topography (i.e. ridges), and with high elevations (Figures 5.9 and 5.10). This expansion and contraction of the runoff source areas is analogous to the patterns described by conceptual rainfall runoff models [*Dunne and Black*, 1970a; b; *Freeze*, 1972; *Hewlett and Hibbert*, 1963; 1967; *Sidle et al.*, 2000], and is consistent with the findings of Jencso *et al.* [2009], Kendall *et al.* [1999], and Kuras *et al.* [2008].

Topography-based indices [*Beven and Kirkby*, 1979; *Quinn et al.*, 1995] and the various rainfall runoff conceptual models [*Dunne and Black*, 1970a; b; *Freeze*, 1972; *Hewlett and Hibbert*, 1963; 1967; *Sidle et al.*, 2000] should be reliable predictors of runoff source area dynamics in snowmelt-dominated montane catchments during peak flow, recession flow, and low flow periods since upslope area and slope gradient were dominant in the statistical models during these periods [*Jencso et al.*, 2009; *Kuras et al.*, 2008; *Szeftel*, 2010]. However, they would likely be poor predictors of runoff source area dynamics during early phases of the spring freshet without adequately addressing the space-time variability of water input intensity (i.e. controls on snowpack conditions and surface energy fluxes). Kuras *et al.* [2008] found that differential snowmelt timing between clearcuts and forested areas was responsible for generating different streamflow peaks. Moreover, for glacial till catchments with spatially variable soil K_s profiles or for catchments with varying soil depths, catchment models must address the spatial distribution of controls on vertical versus lateral flux partitioning in the soil coupled with the distribution of controls on the rate of percolation to adequately explain runoff source area dynamics during all periods, including differentiation of rapid runoff response areas

from areas that contribute primarily to sustaining low flows [*Redding and Devito*, 2008; 2010].

5.5 Conclusions

The spatial controls on the occurrence, timing, and persistence of shallow groundwater response in glacial till montane catchments that are snowmelt-dominated are complex and vary not only between seasons, but also intra-seasonally. The K_s of the soil at 75 cm depth was found to be a first-order control on the distribution of sites that generate shallow groundwater response versus sites that experience only deep percolation. Moreover, the study findings suggest that sites with highly permeable surface soils, large upslope contributing areas, and low slope gradients would be important links in the connectivity of runoff source areas to streams. Upslope contributing area and slope gradient are first-order controls on the persistence of groundwater response during peak flow, recession flow, and low flow periods. Runoff source areas expand and contract throughout these periods according to an interplay between catchment wetness and the spatial patterns of topographic convergence; however, controls on the differential timing, intensity, and quantity of snowmelt and controls on vertical versus lateral flux partitioning in the soil overwhelm the influence of topographic convergence on runoff source area dynamics during early spring freshet periods. These findings suggest that various topographic indices and topography-based rainfall runoff models are not directly applicable to modelling snowmelt runoff source area dynamics during all streamflow periods. Topography-based indices would likely be poor predictors of runoff source area dynamics during early phases of the spring freshet without adequately addressing controls on the space-time variability of water input intensity and the spatial distribution of controls on vertical versus lateral flux partitioning in the soil and rate of percolation.

Table 5.1. Table of physiographic parameters and corresponding transformations applied for the logistic regression analyses. Parameter symbols are used in Table 5.3.

Parameter group	Parameter name	Transformation	Symbol
Well depth	Well depth		
Forest cover	Tree height – mean	$(x+1)^{1/3}$	
	Tree height – median	$(x+1)^{1/3}$	
	Tree height – 75th percentile		
	Tree height – 90th percentile		
	Tree height – maximum		
	Tree diameter – mean		
	Tree diameter – median	$(x+1)^{1/2}$	
	Tree diameter – 75th percentile		
	Tree diameter – 90th percentile		
	Tree diameter – maximum	$(x+1)^{1/2}$	D_{max}
	Tree basal area	$(x+1)^{1/2}$	
	Logged portion of upslope area		L
	Clear-sky fraction	ln(x)	CS
Slope gradient	Slope gradient – upslope	$x^{1/2}$	
	Slope gradient – downslope	$x^{1/2}$	S_{down}
	Slope gradient – mean	ln(x)	S_{mean}
Flow path convergence	Surface curvature – plan		
	Surface curvature – profile		
	Surface curvature – mean	$(x+5.5)^{1/2}$	
	Upslope drainage area	ln(x)	A
Topographic position	Elevation		E
	Elevation above channel	$x^{1/3}$	
	Elevation below ridge	$x^{1/3}$	
Insolation	Insolation – accumulation season		
	Insolation – melt season	x^2	R_{melt}
	Insolation – snow-free season		
Soil constituent	Porosity		
	Sand fraction		
	Silt fraction		SI
	Clay fraction		
	Organic fraction	ln(x)	
	Coarse fragment fraction		
Soil conductivity	K_s at 25 cm soil depth	ln(x)	
	K_s at 50 cm soil depth	ln(x)	
	K_s at 75 cm soil depth	ln(x)	K_{75}

Table 5.2. Breakdown of groundwater response classes for the occurrence of response, the duration of response (annual period, melt period, and periods 1 through 8), and the timing of response (first response or maximum response). Units for duration data are portion of period. Units for timing data are decimal day of year.

Period/timing	Range of responses		
	Class 0	**Class 1**	**Class 2**
Occurrence	0	NA	1
Annual	0	0.01 – 0.32	0.36 – 1
Melt season	0	0.01 – 0.46	0.56 – 1
1	0	0.01 – 0.40	1
2	0	NA	0.35 – 1
3	0	0.01 – 0.45	0.59 – 1
4	0	0.03 – 0.37	0.58 – 1
5	0	0.05 – 0.83	1
6	0	NA	0.66 – 1
7	0	0.34 – 0.80	0.93 – 1
8	0	0.01 – 0.53	0.73 – 1
Start	102.6 – 105.6	119.6 – 127.0	137.7 – 140.9
Maximum	105.7 – 128.6	136.7 – 139.8	141.5 – 151.6

Table 5.3. Ordinal logistic regression models for the occurrence of response, the duration of response (annual period, melt period, and periods 1 through 8), and the timing of response (first response or maximum response). See Table 5.1 for definition of the predictor variable symbols.

Period/timing	Model	R^2	p-value
Occurrence	$\ln(O) = 1.92 - 1.08 \cdot S_{mean} + 1.43 \cdot A - 2.83 \cdot K_{75} + 0.88 \cdot R_{melt} + 1.43 \cdot S_{mean} \cdot R_{melt}$	0.71	< 0.001
Annual	$\ln(O) = -7.75 - 2.27 \cdot S_{mean} + 2.80 \cdot A - 2.85 \cdot K_{75} + 0.48 \cdot R_{melt} - 2.79 \cdot D_{max} + 2.43 \cdot S_{mean} \cdot R_{melt}$	0.88	< 0.001
Melt	$\ln(O) = -2.44 - 3.16 \cdot S_{mean} + 1.90 \cdot A - 2.66 \cdot K_{75} - 0.62 \cdot R_{melt} - 1.93 \cdot D_{max} + 3.26 \cdot S_{mean} \cdot R_{melt}$	0.86	< 0.001
1	$\ln(O) = -7.39 - 5.26 \cdot S_{down} + 4.36 \cdot A - 2.18 \cdot K_{75} - 1.35 \cdot D_{max}$	0.88	< 0.001
2	$\ln(O) = -5.49 - 3.51 \cdot S_{down} + 2.68 \cdot A - 2.26 \cdot K_{75} - 1.67 \cdot D_{max}$	0.86	< 0.001
3	$\ln(O) = -2.96 - 1.91 \cdot S_{down} + 1.14 \cdot A - 2.39 \cdot K_{75} + 0.31 \cdot R_{melt} - 3.22 \cdot D_{max} + 1.64 \cdot S_{down} \cdot R_{melt}$	0.85	< 0.001
4	$\ln(O) = 0.09 - 1.24 \cdot S_{mean} + 2.02 \cdot A - 2.73 \cdot K_{75} + 1.15 \cdot R_{melt} - 1.21 \cdot D_{max} + 1.78 \cdot S_{mean} \cdot R_{melt}$	0.76	< 0.001
5	$\ln(O) = -0.25 - 2.29 \cdot S_{mean} + 1.88 \cdot A - 1.23 \cdot R_{melt} + 2.76 \cdot S_{mean} \cdot R_{melt}$	0.69	< 0.001
6	$\ln(O) = -1.80 - 3.70 \cdot S_{down} + 3.94 \cdot A$	0.84	< 0.001
7	$\ln(O) = -3.53 - 2.80 \cdot S_{down} + 2.68 \cdot A$	0.75	< 0.001
8	$\ln(O) = -4.48 - 2.89 \cdot S_{down} + 3.27 \cdot A - 2.36 \cdot K_{75}$	0.82	< 0.001
First	$\ln(O) = -3.44 - 3.63 \cdot A + 2.51 \cdot K_{75} + 2.54 \cdot E - 2.41 \cdot L + 2.95 \cdot SI$	0.83	< 0.001
Maximum	$\ln(O) = -1.09 - 1.04 \cdot R_{melt} - 2.73 \cdot CS + 1.09 \cdot SI$	0.70	< 0.001

Table 5.4. Ranked main effect sizes for the logistic regression models predicting response timing. Effect sizes were calculated by taking the exponential of the product of the coefficient and the range in the data between the 25th and 75th percentile values for each respective predictor variable.

Effect size	**Streamflow response timing**	
	Start	**Maximum**
>100	– Area upslope	– Clear-sky fraction
50-100		
10-50	+ Elevation + Silt fraction + 75 cm K_s – Upslope logging	
5-10		– Solar
1-5		+ Silt fraction

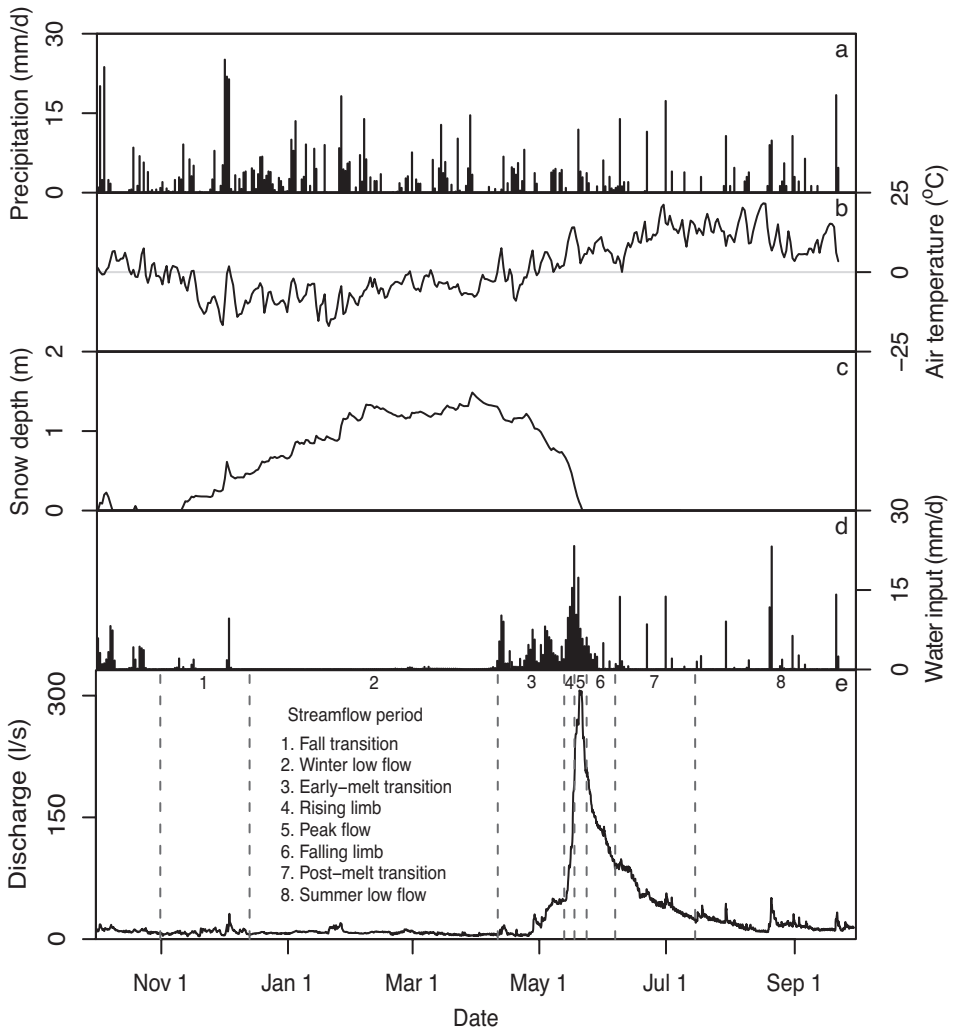

Figure 5.1. Precipitation and snow depth at the UC climate station throughout the period of record, air temperature and water input as means among all six lysimeter sites in the UEC catchment, and streamflow and corresponding periods throughout the period of record at the UEC catchment outlet. The annual streamflow period is the sum of periods 1 through 8. The spring melt streamflow period is the sum of periods 3 through 6.

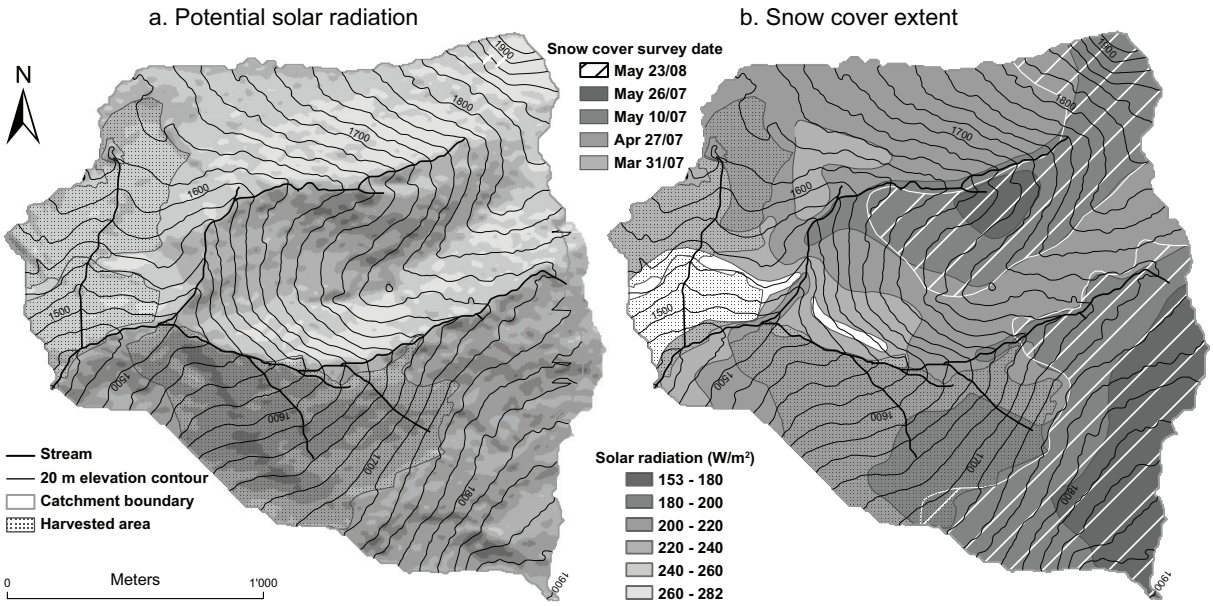

Figure 5.2. Mean annual potential solar radiation (a) and snow cover extent during the spring melt periods of 2007 and 2008 (b).

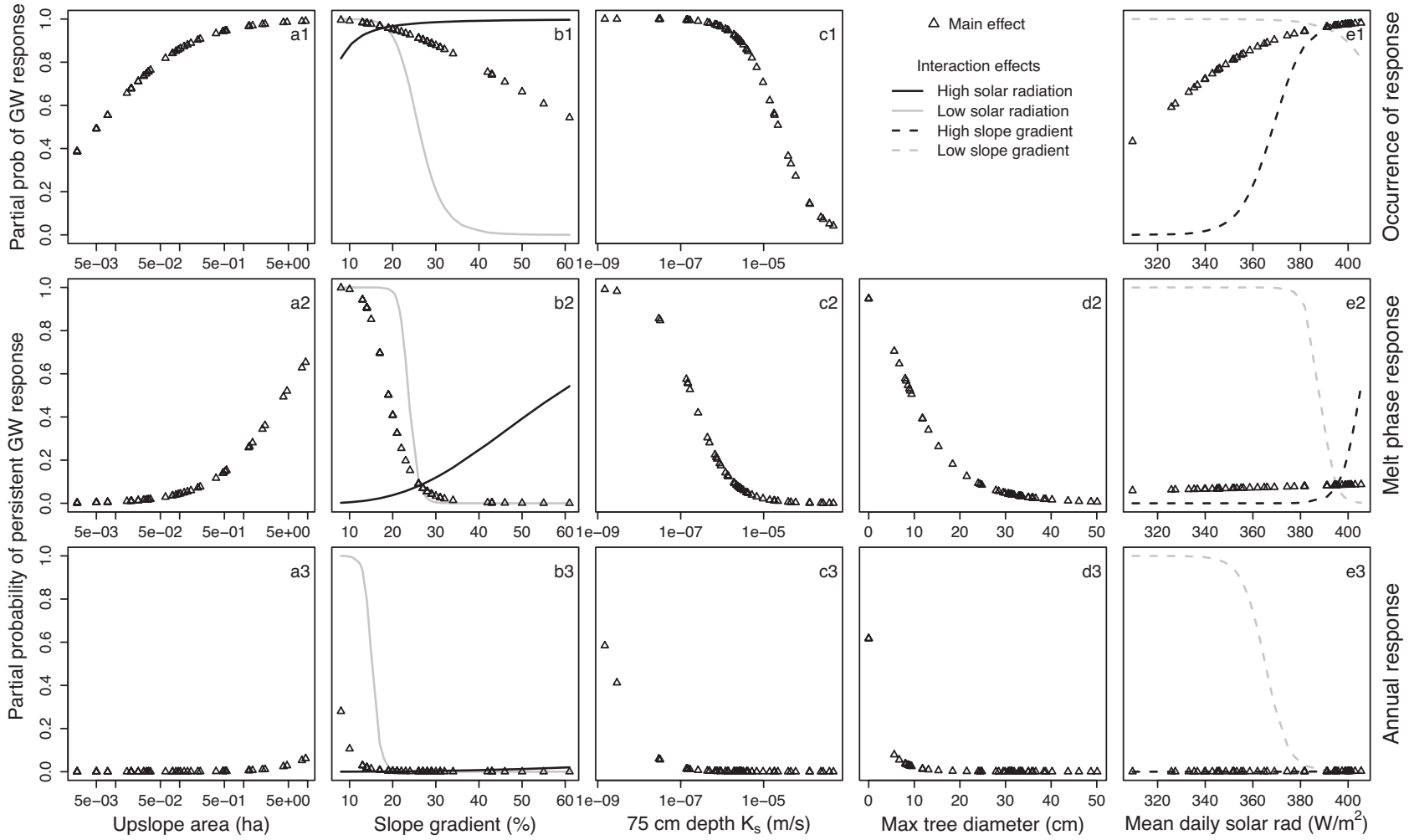
Partial prob of GW response
Partial probability of persistent GW response
Occurrence of response
Melt phase response
Annual response
Main effect
Interaction effects
High solar radiation
Low solar radiation
High slope gradient
Low slope gradient
a1
b1
c1
e1
a2
b2
c2
d2
e2
a3
b3
c3
d3
e3
Upslope area (ha)
Slope gradient (%)
75 cm depth K_s (m/s)
Max tree diameter (cm)
Mean daily solar rad (W/m^2)

Figure 5.3. Previous page. Partial probability of groundwater response for each variable in the respective logistic regression models. Response periods are indicated on the far right side of each row. Response variable for row 1 is the occurrence of a groundwater response. Response variables for rows 2 and 3 are the persistence of groundwater response. For calculating the partial probabilities, all predictor variables were held at their respective mean (geometric mean for K_s) values except any relevant interaction predictor variables, which were held at their respective minimum or maximum values.

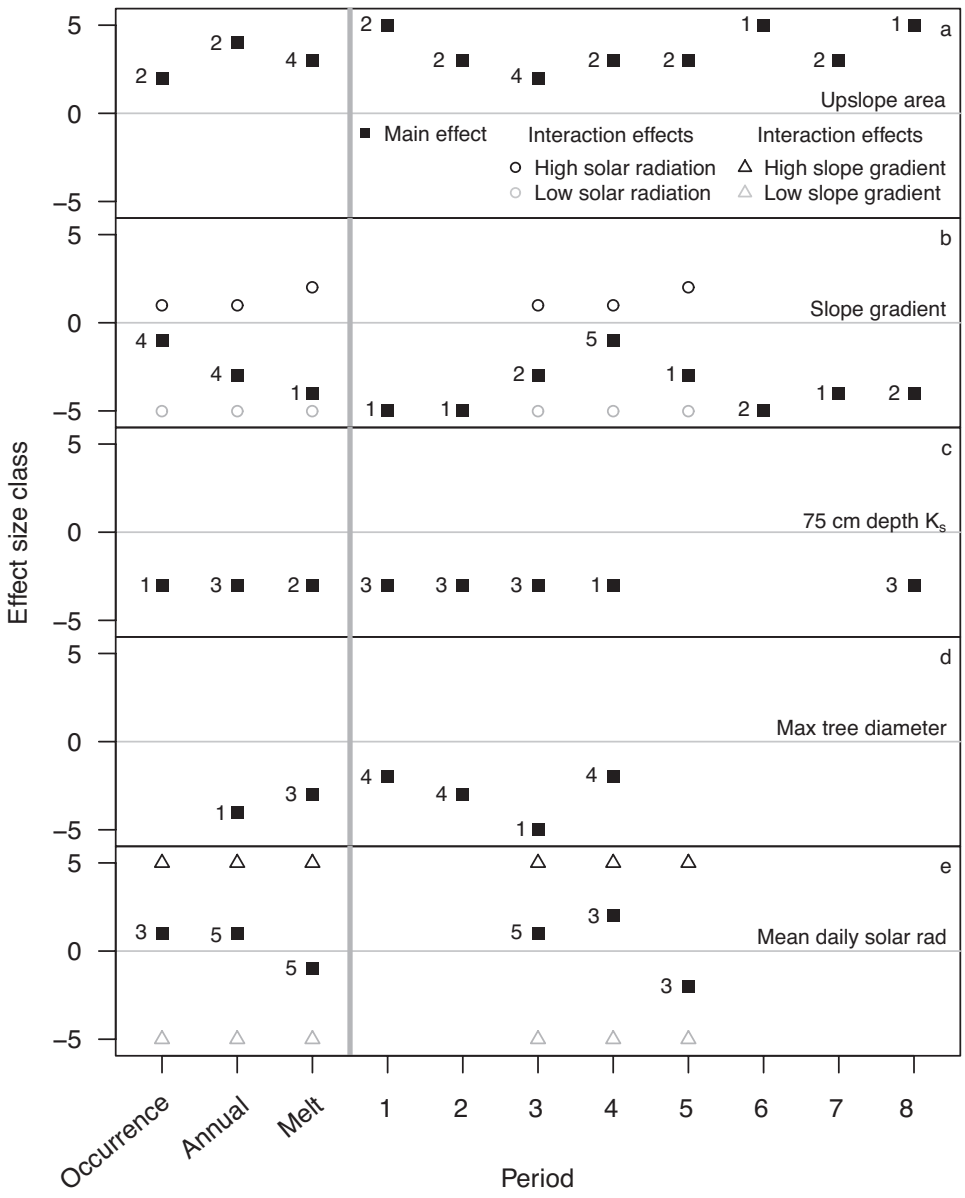

Figure 5.4. Effect size class (effect size for each class: 1: 1-5, 2: 5-10, 3: 10-50, 4: 50-100, 5: >100), direction of effect (positive or negative), and effect rank (indicated to the left of each point) for the predictor variables in the logistic regression models. Effect sizes were calculated by taking the exponential of the product of the coefficient and the range in the data between the 25th and 75th percentile values for each respective predictor variable. Interaction terms were ignored for calculating the main effects. For calculating the interaction effects, relevant interaction predictor variables were held at their respective minimum or maximum values.

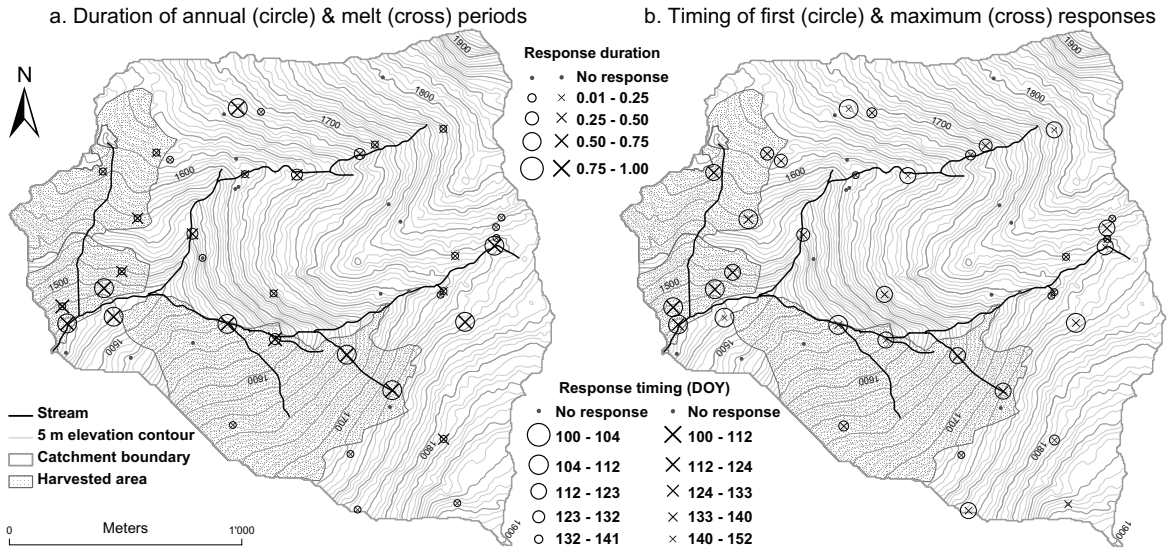

Figure 5.5. Groundwater response duration (as a portion of the total duration of response in the period) at the hillslope sites for the annual and spring melt periods (a) and groundwater response timing (day of the year, DOY) at the hillslope sites for the first and maximum responses. The timing of each period is indicated in Figure 5.1.

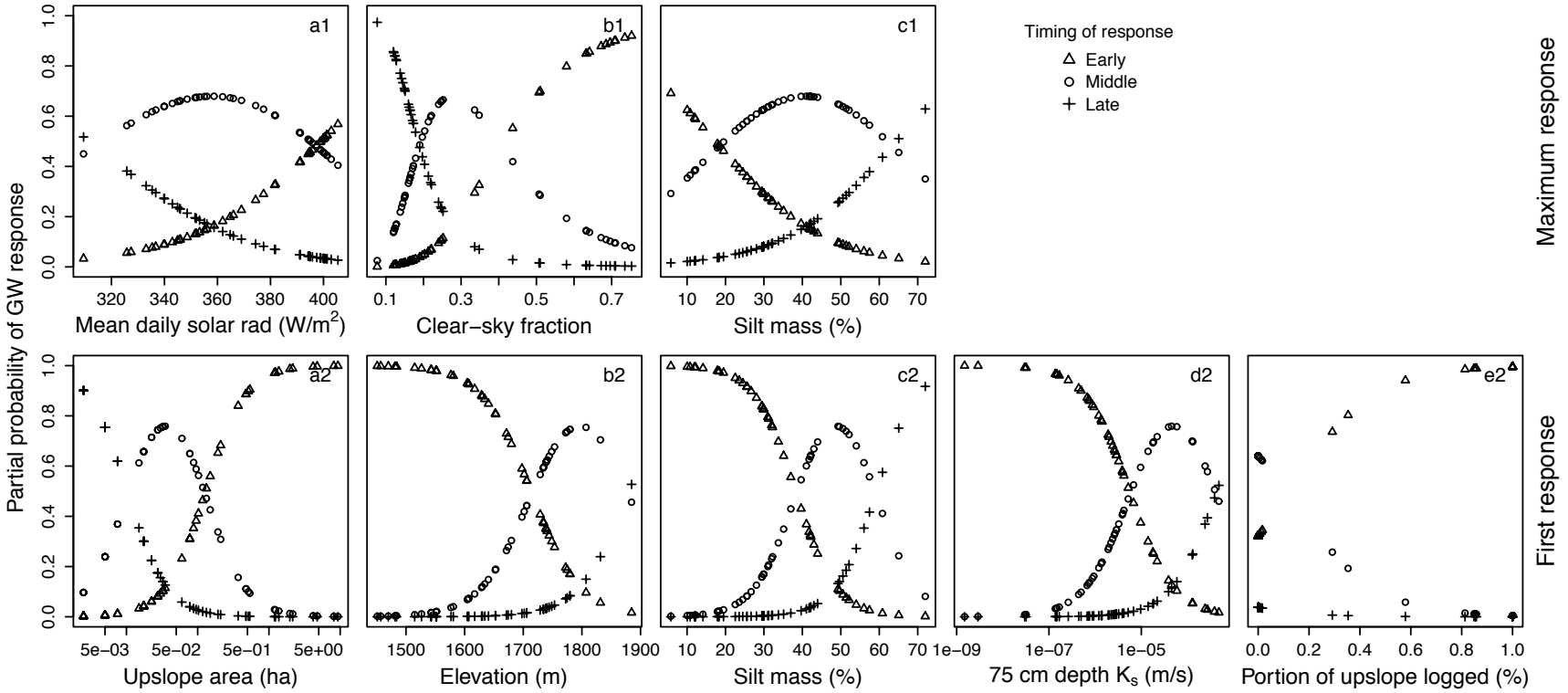

Figure 5.6. Partial probability of groundwater response for each variable in the respective logistic regression models (indicated on the far right side of each row) predicting the timing of maximum response and the timing of first response. The timing of response (early, middle, or late in the spring melt) with the highest partial probability at any corresponding value of a predictor variable is the most likely outcome.

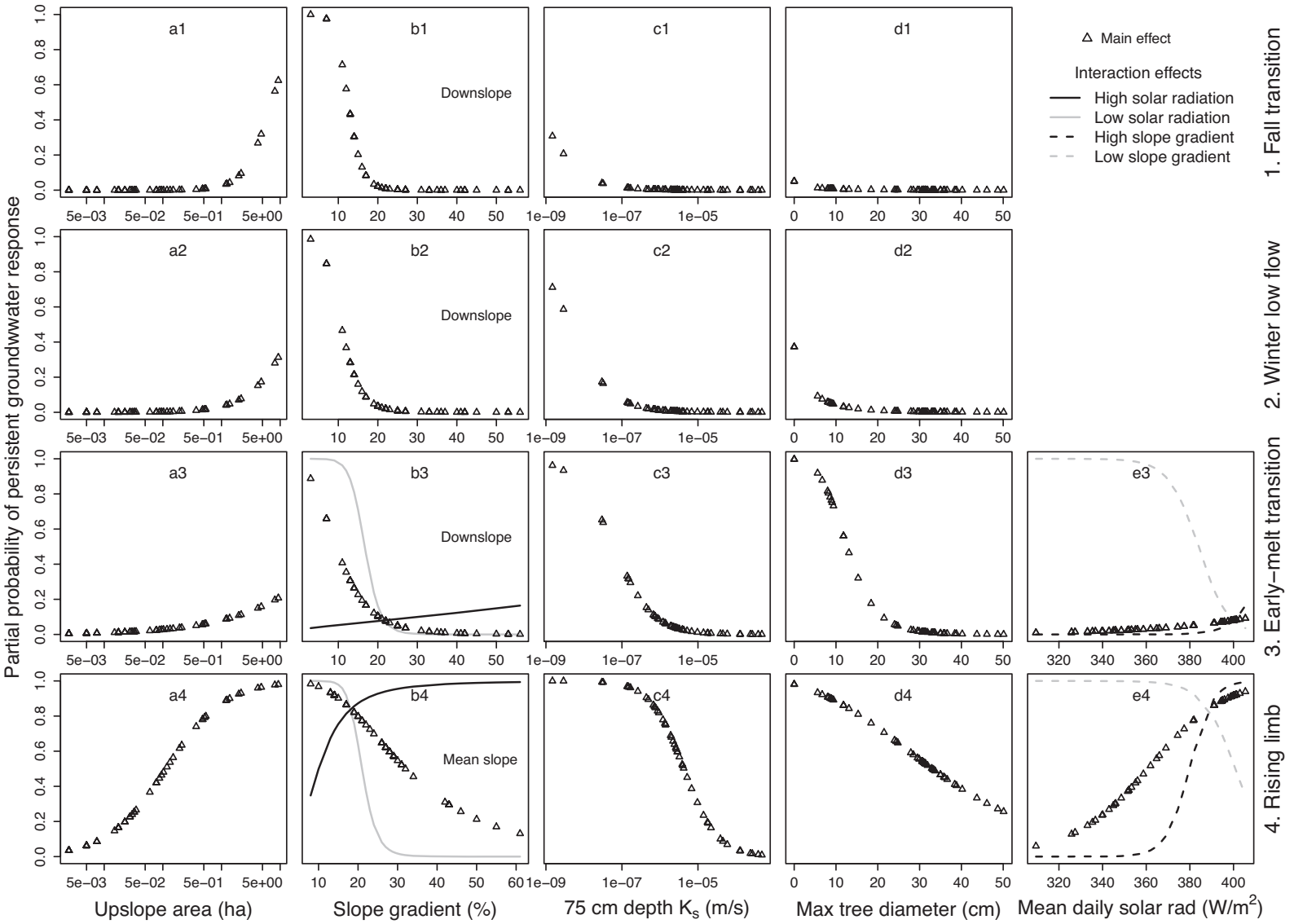
Partial probability of persistent groundwater response
a1
b1
Downslope
c1
d1
a2
b2
Downslope
c2
d2
a3
b3
Downslope
c3
d3
e3
a4
b4
Mean slope
c4
d4
e4
Main effect
Interaction effects
High solar radiation
Low solar radiation
High slope gradient
Low slope gradient
1. Fall transition
2. Winter low flow
3. Early−melt transition
4. Rising limb
Upslope area (ha)
Slope gradient (%)
75 cm depth K_s (m/s)
Max tree diameter (cm)
Mean daily solar rad (W/m^2)

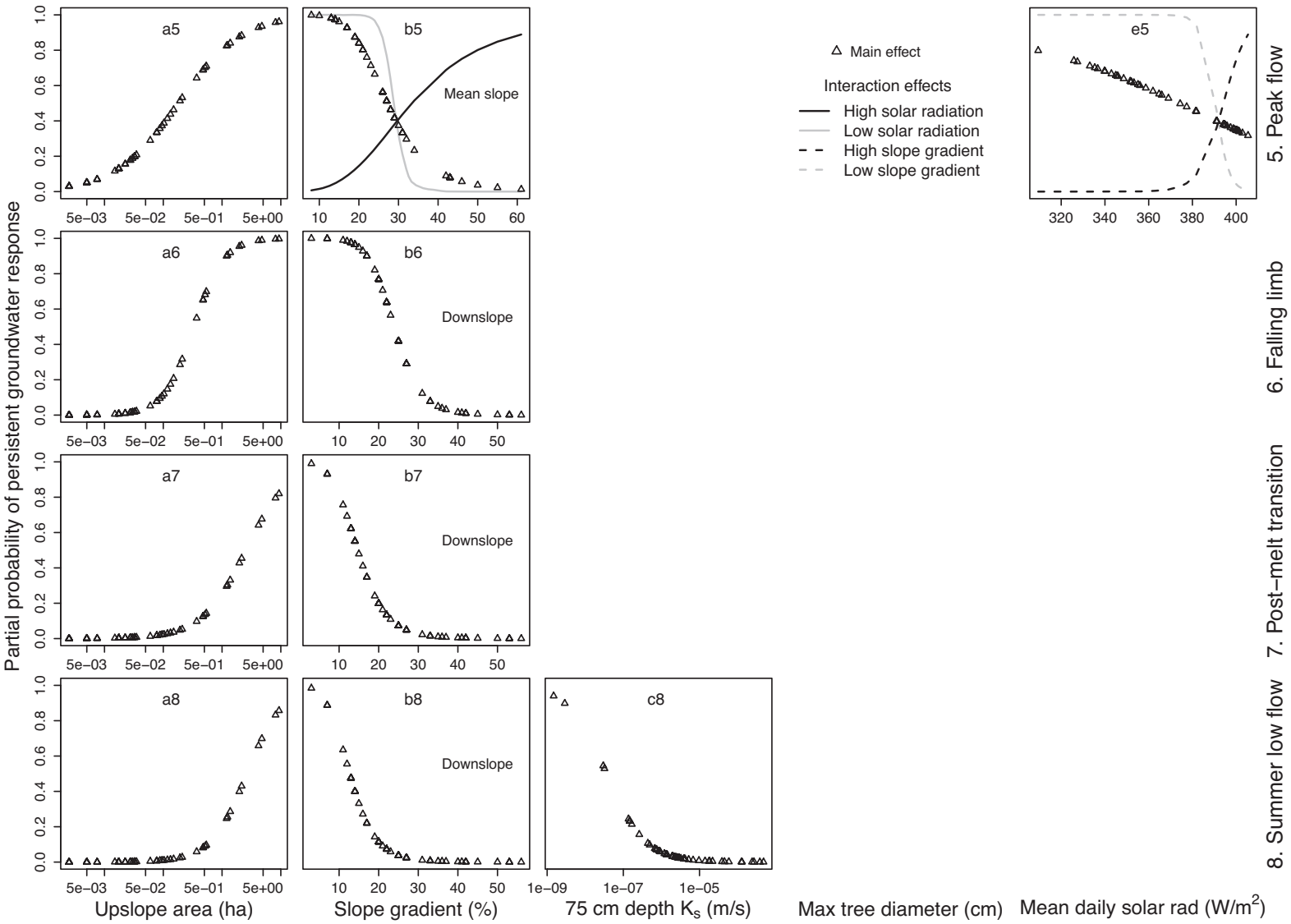
Partial probability of persistent groundwater response
a5
b5
Mean slope
a6
b6
Downslope
a7
b7
Downslope
a8
b8
Downslope
c8
e5
Main effect
Interaction effects
High solar radiation
Low solar radiation
High slope gradient
Low slope gradient
5. Peak flow
6. Falling limb
7. Post−melt transition
8. Summer low flow
Upslope area (ha)
Slope gradient (%)
75 cm depth K_s (m/s)
Max tree diameter (cm)
Mean daily solar rad (W/m^2)

Figure 5.7. Previous two pages. Partial probability of groundwater response for each variable in the respective logistic regression models. For slope gradient, mean gradient versus downslope gradient is indicated. Response periods are indicated on the far right side of each row. Response variables for all rows are the persistence of groundwater response. For calculating the partial probabilities, all other predictor variables were held at their respective mean (geometric mean for K_s) values except any relevant interaction predictor variables, which were held at their respective minimum or maximum values.

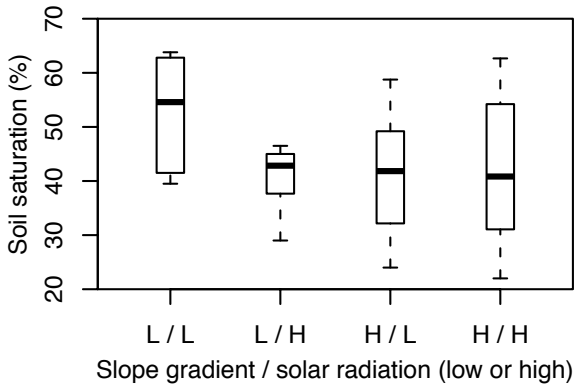

Figure 5.8. Boxplots of soil saturation (mean of 10-40 cm soil depth) on April 6-8, 2008, combining sites of low or high mean slope gradient (i.e. less than or greater than the mean gradient) with sites of low or high spring melt potential solar radiation (i.e. less than or greater than the 25th or 75th percentile radiation, respectively) throughout the snow-free season.

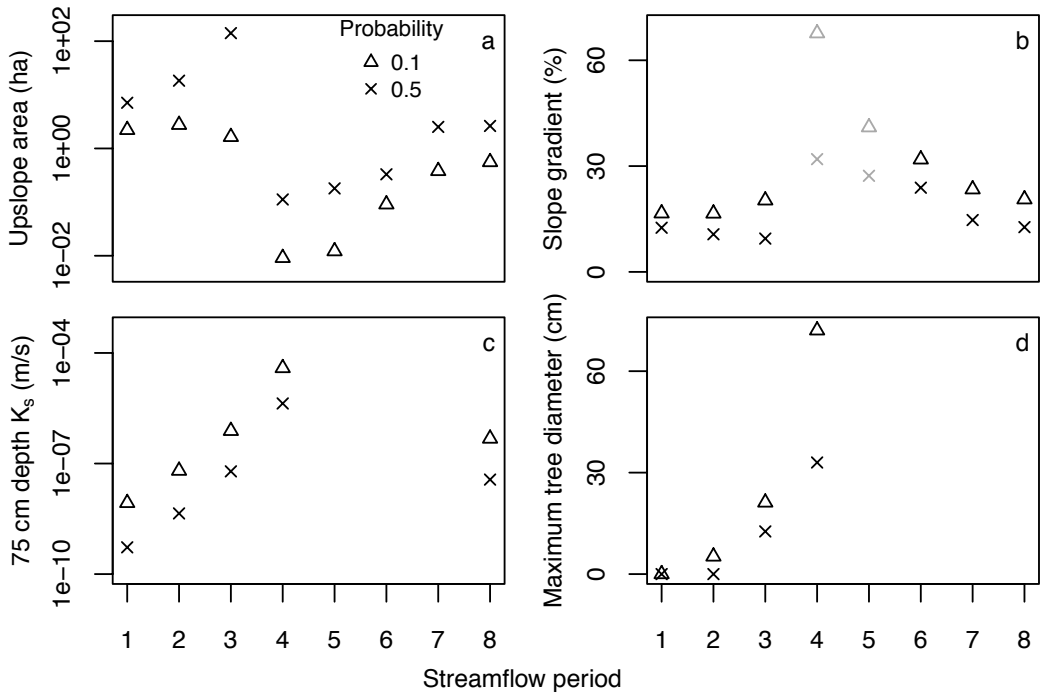

Figure 5.9. Variation in the predicted values of (a) upslope drainage area, (b) slope gradient (downslope gradient in black, mean slope gradient in gray), (c) deep soil K_s, and (d) maximum tree diameter for the 10% and 50% partial probabilities of persistent groundwater responses. For calculating the partial probabilities, all other predictor variables were held at their respective mean (geometric mean for K_s) values.

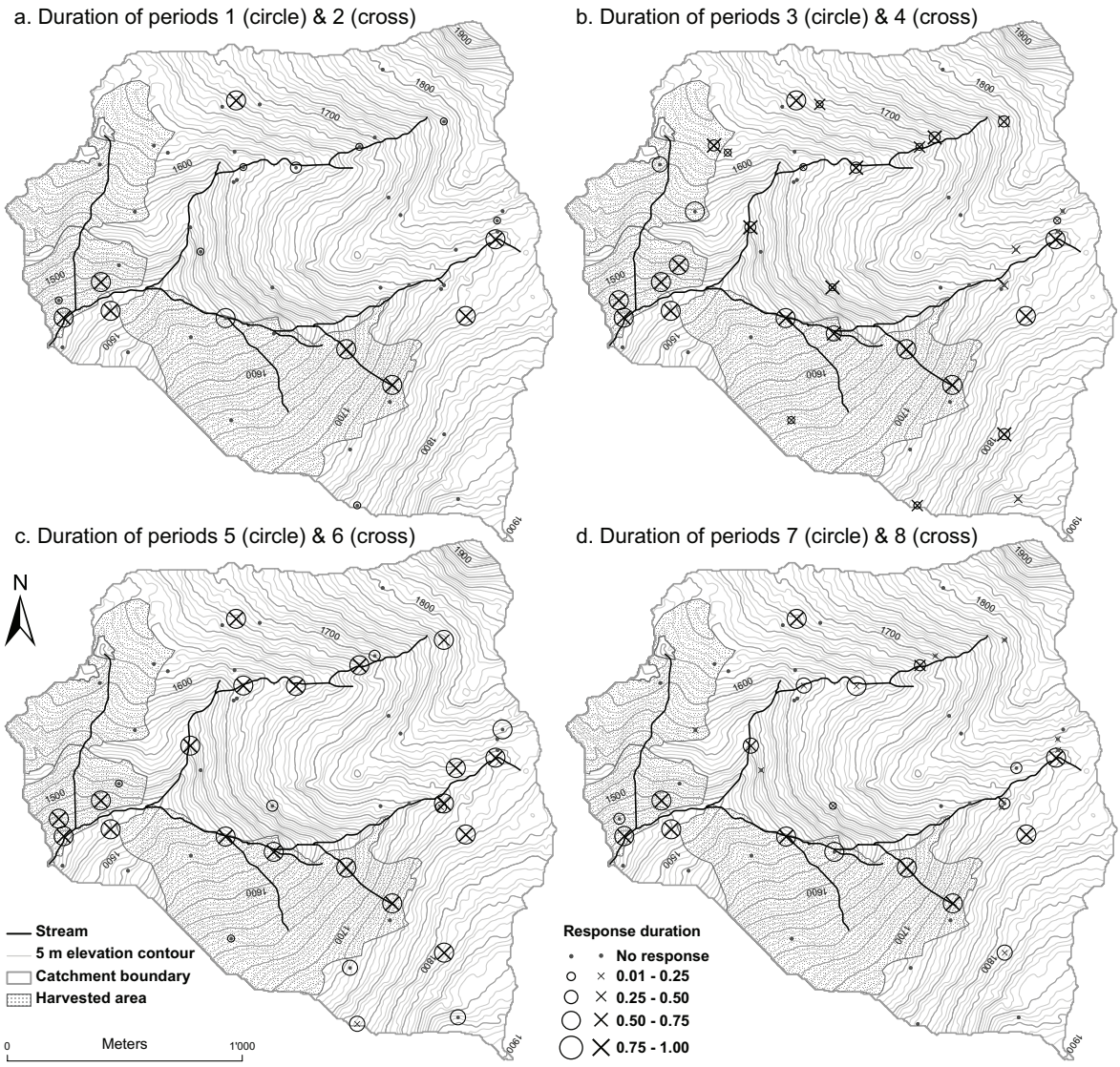

Figure 5.10. Groundwater response duration (as a portion of the total duration of response in the period) at the hillslope sites. The timing of each period is indicated in Figure 5.1.

6 Conclusions and recommendations

This study investigated the extensive space-time variability of water inputs that is unique to snowmelt-dominated montane catchments and interactions with subsurface processes that are important in controlling runoff source area dynamics at the catchment scale. The following sections provide a summary of important findings, a conceptual model for runoff source area dynamics in snowmelt-dominated montane catchments, and an outline of opportunities for future research.

6.1 Summary of important findings

The midwinter snowmelt results in chapter 3 provide a unique account of the potential for continuous and widespread melt to occur under extreme cold weather conditions. Multiple lines of circumstantial evidence suggest that much of the melt resulted from soil heat flux and, thus, can be considered ground melt, and that the development of a deep insulating snowpack over frozen soils can inhibit ground melt. Accumulated snowpack losses throughout midwinter 2007 comprised between 3% and 27% of the winter snowfall and between 1% and 14% of the annual water budget. Midwinter melt increased with increasing early-winter soil temperature and wetness, and increasing midwinter air temperature, which formed important controls on the spatial variability of melt. Synoptic air temperature patterns formed an important control on the temporal variability. Lateral advection of soil heat via groundwater flow might have also increased midwinter melt. Though the rates of melt varied considerably between sites, the positive influence of early-winter soil temperature and wetness on midwinter melt might enhance early-spring hillslope hydrologic connectivity and associated spring runoff response. The weather and snowpack conditions leading to high rates of melt during midwinter 2007 do not appear unusual for the study region.

Chapter 4 examines the development of transient perched shallow groundwater and associated vertical versus lateral flux partitioning in the soil via percolation-excess runoff generation. The results suggest that, at locations where K_s decreases gradually with

depth, the initiation depth and maximum level of the perched groundwater might vary according to an interplay between the K_s profile and the water input intensity dynamics during an event, and can be predicted by relating the K_s profile to the water input intensity dynamics. Input intensity may strongly influence maximum stormflow response due to its influence on maximum groundwater level and, thus, soil transmissivity. At sites where K_s does not decrease gradually with depth, water input intensity does not appear to influence the depth of groundwater initiation due to a stationary lower restricting layer. The spatial distribution of various K_s profiles appears to influence the spatial distribution of runoff response within the UEC catchment, and may supersede the influence of topography on groundwater response at locations with deep, highly conductive soils.

Chapter 5 addresses temporal variation in the relative importance of spatial controls on the occurrence, timing, and persistence of shallow groundwater response. The K_s of the soil at 75 cm depth was found to be a first-order control on the distribution of sites that generate shallow groundwater response versus sites that experience only deep percolation and, thus, provides evidence that the findings in chapter 4 are relevant at the catchment scale. Upslope contributing area and slope gradient are first-order controls on the persistence of groundwater response during peak flow, recession flow, and low flow periods. Runoff source areas expand and contract throughout these periods according to an interplay between catchment wetness and the spatial patterns of topographic convergence. However, controls on the differential timing, intensity, and quantity of snowmelt and controls on vertical versus lateral flux partitioning in the soil overwhelm the influence of topographic convergence on runoff source area dynamics during early spring freshet periods. These findings suggest that various topographic indices and topography-based rainfall runoff models are not necessarily applicable to modelling snowmelt runoff source area dynamics during all streamflow periods.

6.2 Conceptual model

A hydrogeomorphic conceptual model for snowmelt-dominated montane catchments is presented based on research findings in the CCEW [*Jost et al.*, 2007; *Jost et al.*, 2009; *Szeftel*, 2010], including chapters 3 through 5 of the current study. It illustrates the seasonal progression of spatially distributed water inputs and associated runoff generation dynamics, and integrates findings from other runoff studies focused on snowmelt-dominated catchments [*Jencso et al.*, 2010; *Jencso et al.*, 2009; *Kuras et al.*, 2008; *McNamara et al.*, 2005].

During midwinter, water inputs are minimal where the soil surface is frozen except during infrequent surface melt events. However, where the soil surface is unfrozen beneath a deep insulating snowpack, ground melt may occur and is concentrated in areas with warm and wet soils and relatively high air temperatures (e.g. riparian areas, hillslope hollows, and canopy openings of low to middle elevation) (Figure 6.1a). Lateral flux is negligible throughout most of the catchment except in riparian areas and hillslope hollows with large upslope drainage areas, which are fed by deep lateral flow. In these areas, shallow groundwater persists for much of the year, particularly in locations without forest cover and with well developed perolation-limiting soil layers. Ongoing water inputs from ground melt may augment lateral flux in these areas, and help maintain hillslope hydrologic connectivity through the winter.

Once air temperatures rise above freezing in the spring, active surface melt initiates in low elevation, high insolation areas (Figure 6.1b). In areas without forest cover, early spring melt extends across a larger range of elevations and aspects. Within the melt areas, groundwater response occurs first in locations having large upslope drainage areas, well developed percolation-limiting layers, minimal soil water storage capacity, and extensive upslope open areas, but is most persistent in locations with high melt intensities (due to high insolation). Upslope groundwater response only contributes to streamflow once downslope pockets of dry soil are wetted sufficiently to breach any hydrologic disconnects, either via localized water inputs or via cascading groundwater.

As overall energy inputs increase through the spring, active surface melt shifts into higher elevation areas and areas with low insolation caused by topographic and/or forest cover shading (Figure 6.1c and 6.1d). Along with the spatial shifting of melt areas, groundwater response expands into areas with smaller upslope drainage areas, steeper slope gradients, more mature forest cover, and higher deep soil hydraulic conductivity to eventually include small hollows, linear hillslopes, and ridge sites. Unchannelized overland flow occurs in hollows, localized depressions, and riparian areas where the water table intersects the soil surface. The stream network expands into reaches that experience only seasonal flow. Despite the general expansion of runoff generation areas in the catchment, areas that melted early become snow-free and runoff generation contracts in those areas. Factors influencing the distribution of flow accumulation processes (i.e. upslope drainage area and slope gradient) gradually become more important in controlling the distribution of runoff generation areas relative to factors influencing the distributions of insolation (i.e. topographic and forest cover shading) and percolation processes (i.e. hydraulic conductivity and soil texture). Peak streamflow occurs once runoff generation areas have reached their maximum spatial extent (Figure 6.1d); however, some areas with high values of deep soil hydraulic conductivity never experience a shallow groundwater response, particularly those with low melt intensities, due to the lack of percolation-excess processes. Rather, they experience deep percolation and store water for maintaining subsequent low flows.

As the catchment melts out and water inputs become limited to high elevation, low insolation, forested areas, the extent of runoff generation areas and the stream network contract rapidly (Figure 6.1e). Once melt-out is complete (Figure 6.1f), the catchment continues to drain and controls on the distribution of runoff generation areas are dominated almost exclusively by factors influencing flow accumulation rather than factors influencing vertical processes (i.e. insolation and percolation), although the overall persistence of runoff generation decreases with increasing forest cover maturity. Deep percolation sites that experience little or no shallow groundwater response during spring melt become increasingly important for maintaining streamflow via deep lateral

flow as the catchment returns to a low flow state. Occasional rainfall events generate relatively short-term streamflow responses. Runoff generation dynamics during these events are consistent with rainfall runoff conceptual models described by previous authors [*Sidle et al.*, 2000].

6.3 Future research

The midwinter snowmelt results in chapter 3 highlight the need for more detailed monitoring of soil and snowpack conditions in montane catchments during cold winter periods to improve our understanding of interactions between soil, snow, and meteorological conditions, and their potential impacts on catchment hydrology. In particular, coupling snowmelt lysimeters with more detailed measurements of meteorology, heat flux, and temperature within the soil and the snow, and local and upslope soil matric potential would provide opportunities to better understand ground melt processes and interactions with the surface and subsurface environments. Specific topics that require further investigation include the spatial and temporal occurrence of ground melt under various physiographic conditions, interactions with laterally advected heat via groundwater flow, feedback responses between soil wetness and ground melt inputs, and mechanisms coupling basal snowpack temperatures to the atmosphere. Further investigations incorporating ground melt processes within a spatially distributed physically based model could help to improve our understanding of the broader hydrologic significance of midwinter ground melt in snowmelt-dominated catchments. For instance, investigations could address the influences of subsurface flow accumulation due to topographic convergence on soil heat flux and resulting spatial distribution of ground melt rates, the influences of ground melt patterns on the spatial organization of late-winter soil wetness and hydrologic connectivity, and the influences of forest cover distribution on early-winter soil hydrothermal conditions and subsequent ground melt processes.

The percolation-excess runoff generation results in chapter 4 identified the need for additional investigations incorporating measurements of soil matric potential to further

establish the occurrence and space-time distribution of percolation-excess processes. As deep glacial tills exist throughout many areas of the world, it is conceivable that percolation-excess runoff generation is a widespread, but poorly understood phenomenon. In particular, measuring matric potential while applying a range of water input rates via a rainfall simulator [*Redding and Devito*, 2008; 2010] for multiple sites would help to verify the potentially dynamic nature of perched groundwater initiation and vertical versus lateral flux partitioning in soils with gradually changing K_s. It would also help determine the importance of the K_s profile to controlling the occurrence and space-time distribution of percolation-excess runoff generation processes, and the characteristics and distribution of sites that generate shallow groundwater response versus sites that experience only deep percolation. To further investigate the significance of percolation-excess runoff generation to catchment response, the distribution of various K_s profiles could be varied within a spatially distributed runoff model while evaluating the influence of percolation-excess processes on the spatial patterns of predicted lateral flux and hydrologic connectivity. Interactions with other physiographic properties could also be explored. For instance, as forest cover strongly influences antecedent soil wetness and water input rates, particularly under snowmelt conditions, adding variation in the distribution of forest cover could provide some insight regarding the sensitivity of percolation-excess runoff generation to forest cover modification. Similar investigations incorporating variation in aspect, slope gradient, and topographic convergence/divergence would also be valuable.

The spatially intensive network of stratified randomly distributed hillslope monitoring sites that was employed in this study provided a unique opportunity to investigate spatial controls on groundwater response using statistical approaches, and a wealth of information was gained as a result. Extension of this approach to other regions and catchments would provide additional valuable insight regarding the persistence of controls on snowmelt runoff that were identified in this study. Moreover, the absence of information regarding groundwater transit times and measured rates of lateral flux created a missing link in the quest to fully characterize runoff source area dynamics. Future studies could address this limitation by coupling natural and/or artificial tracer

techniques with a similar network of distributed hillslope monitoring sites. Furthermore, extrapolation of ordinal logisitic regression models, like those developed in chapter 5, throughout catchments would provide a unique spatially-distributed assessment of groundwater response patterns and hillslope hydrologic connectivity. It would provide an alternative to using currently employed deterministic modelling techniques, which struggle to realistically represent highly variable and complex process behaviour in a distributed framework, to evaluate spatial hydrologic connectivity. Doing so would require extrapolating forest cover and soil parameters. Varying these parameters would allow further investigation of the sensitivity of groundwater response and hydrologic connectivity at different points in time to variations in the distributions of forest cover and soil K_s. The influences of forest cover modification on the occurrence, persistence, and timing of groundwater response for sites with different physiography (e.g. aspect, slope gradient, upslope drainage area, and deep soil K_s) could be examined. For instance, it is uncertain whether forested sites in the UEC catchment where groundwater responses were not observed during the period of record would experience significant responses after forest cover removal, and how any change in response behaviour would be influenced by topographic position and deep soil K_s.

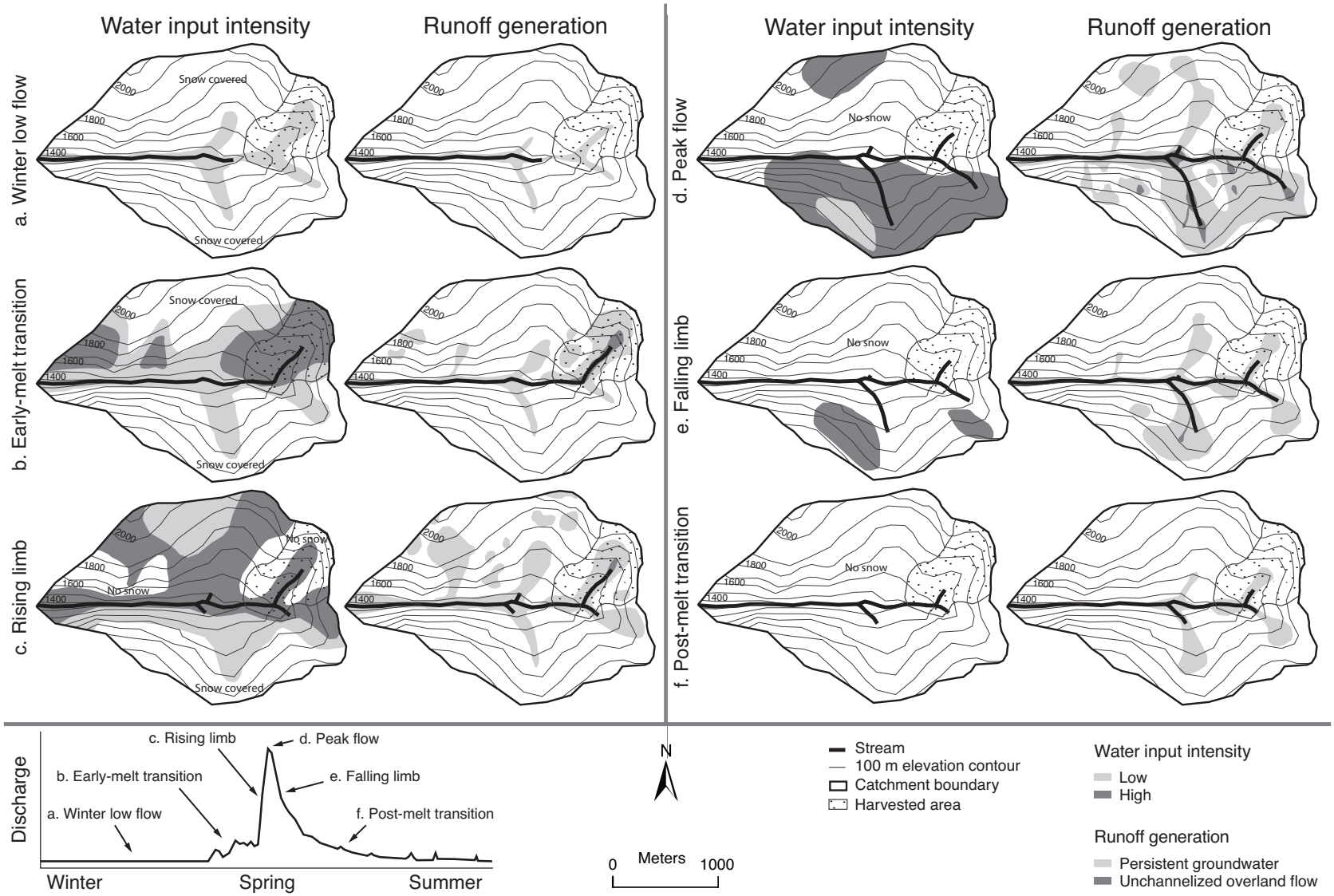
Water input intensity
Runoff generation
Water input intensity
Runoff generation
a. Winter low flow
b. Early-melt transition
c. Rising limb
d. Peak flow
e. Falling limb
f. Post-melt transition
Snow covered
No snow
2000
1800
1600
1400
Discharge
a. Winter low flow
b. Early-melt transition
c. Rising limb
d. Peak flow
e. Falling limb
f. Post-melt transition
Winter
Spring
Summer
N
0
Meters
1000
Stream
100 m elevation contour
Catchment boundary
Harvested area
Water input intensity
Low
High
Runoff generation
Persistent groundwater
Unchannelized overland flow

Figure 6.1. Previous page. Hydrogeomorphic conceptual model of runoff generation dynamics before, during, and after spring melt for a snowmelt-dominated montane catchment. Rows ‘a’ through ‘f’ correspond to the periods shown in the streamflow hydrograph. A water input intensity of approximately 2 mm/day differentiates low versus high values.

References

Akaike, H. (1987), Factor-analysis and AIC, *Psychometrika*, *52*(3), 317-332.

Albert, M. R., and W. R. McGilvary (1992), Thermal effects to to air-flow and vapor transport in dry snow, *Journal of Glaciology*, *38*(129), 273-281.

Anderson, M. G., and T. P. Burt (1978), The role of topography in controlling throughflow generation, *Earth Surface Processes and Landforms*, *3*(4), 331-344.

Anderton, S. P., S. M. White, and B. Alvera (2002), Micro-scale spatial variability and the timing of snow melt runoff in a high mountain catchment, *Journal of Hydrology*, *268*(1-4), 158-176.

Balk, B., and K. Elder (2000), Combining binary decision tree and geostatistical methods to estimate snow distribution in a mountain watershed, *Water Resources Research*, *36*(1), 13-26.

Beasley, R. S. (1976), Contribution of subsurface flow from upper slopes of forested watersheds to channel flow, *Soil Science Society of America Journal*, *40*(6), 955-957.

Bergstrom, S. (1995), The HBV model, in *Computer Models of Watershed Hydrology*, edited by V. P. Singh, pp. 443-476, Water Resources Publications, Highland Ranch, CO.

Berris, S. N., and R. D. Harr (1987), Comparative snow accumulation and melt during rainfall in forested and clear-cut plots in the Western Cascades of Oregon, *Water Resources Research*, *23*(1), 135-142.

Beschta, R. L., M. R. Pyles, A. E. Skaugset, and C. G. Surfleet (2000), Peakflow responses to forest practices in the western cascades of Oregon, USA, *Journal of Hydrology*, *233*(1-4), 102-120.

Beven, K. J., and M. J. Kirkby (1979), A physically-based variable contributing area model of basin hydrology, *Hydrological Sciences Bulletin*, *24*, 43-69.

Beven, K. J., K. Lamb, P. Quinn, R. Romanowicz, and J. Freer (1995), TOPMODEL, in *Computer models of watershed hydrology*, edited by V. P. Singh, pp. 627-668, Water Resources Publications, Highlands Ranch, CO.

Bishop, K. H. (1991), Episodic increases in stream acidity, catchment flow pathways and hydrograph separation, Ph.D. thesis, University of Cambridge.

Bonell, M. (1993), Progress in the understanding of runoff generation dynamics in forests, *Journal of Hydrology*, *150*(2-4), 217-275.

Bongartz, K. (2003), Applying different spatial distribution and modelling concepts in three nested mesoscale catchments of Germany, *Physics and Chemistry of the Earth*, *28*, 1343-1349.

Boyer, E. W., G. M. Hornberger, K. E. Bencala, and D. M. McKnight (1995), Variation of dissolved organic carbon during snowmelt in soil and stream waters of two headwater catchments, Summit County, Colorado, in *Biogeochemistry of Seasonally Snow-Covered Catchments*, edited by K. A. Tonnessen, M. W. Williams and M. Tranter, pp. 303-312.

Boyer, E. W., G. M. Hornberger, K. E. Bencala, and D. M. McKnight (1997), Response characteristics of DOC flushing in an alpine catchment, *Hydrological Processes*, *11*(12), 1635-1647.

Boyer, E. W., G. M. Hornberger, K. E. Bencala, and D. M. McKnight (2000), Effects of asynchronous snowmelt on flushing of dissolved organic carbon: a mixing model approach, *Hydrological Processes*, *14*(18), 3291-3308.

Brooks, R. H., and A. T. Corey (1966), Properties of porous media affecting fluid flow, *Journal of Irrigation and Drainage Division, ASCE*, *92*(IR2), 61-88.

Brubaker, K., A. Rango, and W. Kustas (1996), Incorporating radiation inputs into the snowmelt runoff model, *Hydrological Processes*, *10*(10), 1329-1343.

Burns, D. A., J. J. McDonnell, R. P. Hooper, N. E. Peters, J. E. Freer, C. Kendall, and K. Beven (2001), Quantifying contributions to storm runoff through end-member mixing analysis and hydrologic measurements at the Panola Mountain Research Watershed (Georgia, USA), *Hydrological Processes*, *15*, 1903-1924.

Buttle, J. M. (1994), Isotope hydrograph separations and rapid delivery of pre-event water from drainage basins, *Prog. Phys. Geogr.*, *18*(1), 16-41.

Buttle, J. M., P. J. Dillon, and G. R. Eerkes (2004), Hydrologic coupling of slopes, riparian zones and streams: an example from the Canadian Shield, *Journal of Hydrology*, *287*(1-4), 161-177.

Campbell, G. S. (1974), A simple method for determining unsaturated conductivity from moisture retention data, *Soil Science*, *117*(6), 311-314.

Campbell, G. S. (1977), *An introduction to environmental biophysics*, Springer-Verlag, New York.

Carey, S. K., and M. K. Woo (2001), Spatial variability of hillslope water balance, wolf creek basin, subarctic yukon, *Hydrological Processes*, *15*(16), 3113-3132.

Clapp, R. B., and G. M. Hornberger (1978), Empirical equestions for some soil hydraulic properties, *Water Resources Research*, *14*, 601-604.

Cline, D. W. (1997), Snow surface energy exchanges and snowmelt at a continental, midlatitude Alpine site, *Water Resources Research*, *33*(4), 689-701.

Daly, S. F., R. Davis, E. Ochs, and T. Pangburn (2000), An approach to spatially distributed snow modelling of the Sacramento and San Joaquin basins, California, *Hydrological Processes*, *14*(18), 3257-3271.

Deems, J. S., K. W. Birkeland, and K. J. Hansen (2002), Geographic variation in snow temperature gradients in a mountain snowpack, in *Proceedings of the 2002 Western Snow Conference*, edited, pp. 130-137, Granby, CO.

Deng, Y., G. N. Flerchinger, and K. R. Cooley (1994), Impacts of spatially and temporally varying snowmelt on subsurface flow in a mountainous watershed 2: Subsurface processes, *Hydrological Sciences Journal*, *39*(5), 521-533.

Detty, J. M., and K. J. McGuire (2010a), Threshold changes in storm runoff generation at a till-mantled headwater catchment, *Water Resources Research*, *46*.

Detty, J. M., and K. J. McGuire (2010b), Topographic controls on shallow groundwater dynamics: implications of hydrologic connectivity between hillslopes and riparian zones in a till mantled catchment, *Hydrological Processes*, *24*(16), 2222-2236.

Dunne, T. (1983), Relation of field studies and modeling in the prediction of storm runoff, *Journal of Hydrology*, *65*(1-3), 25-48.

Dunne, T., and R. D. Black (1970a), Partial area contributions to storm runoff in a small new-england watershed, *Water Resources Research*, *6*(5), 1296-1311.

Dunne, T., and R. D. Black (1970b), An experimental investigation of runoff production in permeable soils, *Water Resources Research*, *6*(2), 478-490.

Dunne, T., and R. D. Black (1971), Runoff processes during snowmelt, *Water Resources Research*, *7*(5), 1160-1172.

Durbin, J., and G. S. Watson (1950), Testing for serial correlation in least squares regression, I, *Biometrika*, *37*, 409-428.

Durbin, J., and G. S. Watson (1951), Testing for serial correlation in least squares regression, II, *Biometrika*, *38*, 159-179.

Engle, R. F. (1983), Wald, likelihood ratio, and Lagrange multiplier tests in econometrics, in *Handbook of Econometrics*, edited by M. D. Intriligator and Z. Griliches, pp. 796-801, Elsiever.

Erxleben, J., K. Elder, and R. Davis (2002), Comparison of spatial interpolation methods for estimating snow distribution in the Colorado Rocky Mountains, *Hydrological Processes*, *16*(18), 3627-3649.

Flerchinger, G. N. (2000), The Simultaneous Heat and Water (SHAW) Model: Technical documentation*Rep.*, 37 pp, USDA - Agricultural Research Service, Northwest Watershed Research Center, Boise, Idaho.

Flerchinger, G. N., and K. E. Saxton (1989a), Simultaneous heat and water model of a freezing snow-residue-soil system: II. field verification, *Trans. ASAE*, *32*(2), 573-578.

Flerchinger, G. N., and K. E. Saxton (1989b), Simultaneous heat and water model of a freezing snow-residue-soil system: I. theory and development, *Trans. ASAE*, *32*(2), 565-571.

Flerchinger, G. N., and F. B. Pierson (1991), Modeling plant canopy effects on variability of soil-temperature and water, *Agric. For. Meteorol.*, *56*(3-4), 227-246.

Flerchinger, G. N., and K. R. Cooley (2000), A ten-year water balance of a mountainous semi-arid watershed, *Journal of Hydrology*, *237*(1-2), 86-99.

Flerchinger, G. N., and Q. Yu (2007), Simplified expressions for radiation scattering in canopies with ellipsoidal leaf angle distributions, *Agric. For. Meteorol.*, *144*(3-4), 230-235.

Flerchinger, G. N., C. L. Hanson, and J. R. Wight (1996a), Modeling evapotranspiration and surface energy budgets across a watershed, *Water Resources Research*, *32*(8), 2539-2548.

Flerchinger, G. N., J. M. Baker, and E. J. A. Spaans (1996b), A test of the radiative energy balance of the SHAW model for snowcover, *Hydrological Processes*, *10*(10), 1359-1367.

Flerchinger, G. N., W. Xaio, D. Marks, T. J. Sauer, and Q. Yu (2009), Comparison of algorithms for incoming atmospheric long-wave radiation, *Water Resources Research*, *45*.

Flügel, W. (1997), Combining GIS with regional hydrological modelling using hydrological response units (HRUs): An application from Germany, *Mathematics and Computers in Simulation*, *43*, 297-304.

Freer, J., J. J. McDonnell, K. J. Beven, N. E. Peters, D. A. Burns, R. P. Hooper, B. Aulenbach, and C. Kendall (2002), The role of bedrock topography on subsurface storm flow, *Water Resources Research*, *38*(12).

Freeze, R. A. (1972), Role of subsurface flow in generating surface runoff 2: Upstream source areas, *Water Resources Research*, *8*(5), 1272-1283.

Goodrich, D. C., J. M. Faures, D. A. Woolhiser, L. J. Lane, and S. Sorooshian (1995), Measurement and analysis of small-scale convective storm rainfall variability, *Journal of Hydrology*, *173*(1-4), 283-308.

Graham, D. N., and M. B. Butts (2005), Flexible, integrated watershed modelling with MIKE SHE, in *Watershed Models*, edited by V. P. Singh and D. K. Frevert, pp. 245-272, CRC Press.

Grant, L., M. Seyfried, and J. McNamara (2004), Spatial variation and temporal stability of soil water in a snow-dominated, mountain catchment, *Hydrological Processes*, *18*(18), 3493-3511.

Guan, H., J. L. Wilson, and O. Makhnin (2005), Geostatistical mapping of mountain precipitation incorporating autosearched effects of terrain and climatic characteristics, *Journal of Hydrometeorology*, *6*(6), 1018-1031.

Harms, T. E., and D. S. Chanasyk (1998), Variability of snowmelt runoff and soil moisture recharge, *Nordic Hydrology*, *29*(3), 179-198.

Harr, R. D. (1977), Water flux in soil and subsoil on a steep forested slope, *Journal of Hydrology*, *33*(1-2), 37-58.

Hewlett, J. D., and A. R. Hibbert (1963), Moisture and energy conditions within a sloping soil mass during drainage, *Journal of Geophysical Research*, *68*(4), 1081-1087.

Hewlett, J. D., and A. R. Hibbert (1967), Factors affecting the response of small watersheds to precipitation in humid areas, paper presented at International

Symposium on Forest Hydrology, Pergamon, Oxford, August 29 - September 10, 1965.

Hock, R. (1999), A distributed temperature-index ice and snowmelt model including potential direct solar radiation, *Journal of Glaciology*, *45*(149), 101-111.

Hock, R. (2003), Temperature index melt modelling in mountain areas, *Journal of Hydrology*, *282*(1-4), 104-115.

Iwata, Y., and T. Hirota (2005), Monitoring over-winter soil water dynamics in a freezing and snow-covered environment using a thermally insulated tensiometer, *Hydrological Processes*, *19*(15), 3013-3019.

James, A. L., and N. T. Roulet (2007), Investigating hydrologic connectivity and its association with threshold change in runoff response in a temperate forested watershed, *Hydrological Processes*, *21*(25), 3391-3408.

Jencso, K. G., B. L. McGlynn, M. N. Gooseff, K. E. Bencala, and S. M. Wondzell (2010), Hillslope hydrologic connectivity controls riparian groundwater turnover: Implications of catchment structure for riparian buffering and stream water sources, *Water Resources Research*, *46*.

Jencso, K. G., B. L. McGlynn, M. N. Gooseff, S. M. Wondzell, K. E. Bencala, and L. A. Marshall (2009), Hydrologic connectivity between landscapes and streams: Transferring reach-and plot-scale understanding to the catchment scale, *Water Resources Research*, *45*.

Jost, G., M. Weiler, D. R. Gluns, and Y. Alila (2007), The influence of forest and topography on snow accumulation and melt at the watershed-scale, *Journal of Hydrology*, *347*(1-2), 101-115.

Jost, G., R. D. Moore, M. Weiler, D. R. Gluns, and Y. Alila (2009), Use of distributed snow measurements to test and improve a snowmelt model for predicting the effect of forest clear-cutting, *Journal of Hydrology*, *376*(1-2), 94-106.

Kattelmann, R. (1989), Spatial variability of snow-pack outflow at a site in Sierra Nevada, U.S.A, *Annals of Glaciology*, *13*, 124-128.

Keim, R. F., A. E. Skaugset, and M. Weiler (2005), Temporal persistence of spatial patterns in throughfall, *Journal of Hydrology*, *314*(1-4), 263-274.

Kendall, K. A., J. B. Shanley, and J. J. McDonnell (1999), A hydrometric and geochemical approach to test the transmissivity feedback hypothesis during snowmelt, *Journal of Hydrology*, *219*(3-4), 188-205.

Kendall, M. (1938), A new measure of rank correlation, *Biometrika*, *30*, 80-89.

Kim, J. K., R. C. Sidle, R. D. Moore, and R. Hudson (2004), Throughflow variability during snowmelt in a forested mountain catchment, coastal British Columbia, Canada, *Hydrological Processes*, *18*, 1219-1236.

Kirkby, M. J. (1969), Infiltration, throughflow, and overland flow, in *Water, Earth and Man*, edited by R. J. Chorley, pp. 215-227, Taylor & Francis, London.

Kirkby, M. J. (1975), Hydrograph modeling strategies., in *Processes in Physical and Human Geography*, edited by R. F. Peel, M. D. Chisholm and P. Haggett, Heinemann, London, UK.

Kuras, P. K., M. Weiler, and Y. Alila (2008), The spatiotemporal variability of runoff generation and groundwater dynamics in a snow-dominated catchment, *Journal of Hydrology*, *352*(1-2), 50-66.

Laudon, H., J. Seibert, S. Kohler, and K. Bishop (2004), Hydrological flow paths during snowmelt: Congruence between hydrometric measurements and oxygen 18 in meltwater, soil water, and runoff, *Water Resources Research*, *40*(3).

Lehmann, P., C. Hinz, G. McGrath, H. J. Tromp-van Meerveld, and J. J. McDonnell (2007), Rainfall threshold for hillslope outflow: an emergent property of flow pathway connectivity, *Hydrol. Earth Syst. Sci.*, *11*(2), 1047-1063.

Leuning, G. N. (2000), Estimation of scalar source/sink distributions in plant canopies using Lagrangian dispersion analysis: corrections for atmospheric stability and comparison with a multilayer canopy model, *Boundary-Layer Meteorology*, *96*, 293-314.

Leydecker, A., J. O. Sickman, and J. M. Melack (2001), Spatial scaling of hydrological and biogeochemical aspects of high-altitude catchments in the Sierra Nevada, California, USA, *Arctic Antarctic and Alpine Research*, *33*(4), 391-396.

Linderson, M. L. (2003), Spatial distribution of meso-scale precipitation in Scania, southern Sweden, *Geografiska Annaler Series A - Physical Geography*, *85A*(2), 183-196.

Lindstrom, G., K. Bishop, and M. O. Lofvenius (2002), Soil frost and runoff at Svartberget, northern Sweden - measurements and model analysis, *Hydrological Processes*, *16*(17), 3379-3392.

Link, T. E., G. N. Flerchinger, M. Unsworth, and D. Marks (2004), Simulation of water and energy fluxes in an old-growth seasonal temperate rain forest using the simultaneous heat and water (SHAW) model, *Journal of Hydrometeorology*, *5*(3), 443-457.

Lloyd, C. D. (2005), Assessing the effect of integrating elevation data into the estimation of monthly precipitation in Great Britain, *Journal of Hydrology*, *308*(1-4), 128-150.

Marks, D., A. Winstral, and M. Seyfried (2002), Simulation of terrain and forest shelter effects on patterns of snow deposition, snowmelt and runoff over a semi-arid mountain catchment, *Hydrological Processes*, *16*(18), 3605-3626.

Marks, D., J. Domingo, D. Susong, T. Link, and D. Garen (1999), A spatially distributed energy balance snowmelt model for application in mountain basins, *Hydrological Processes*, *13*(12-13), 1935-1959.

McCullagh, P. (1980), Regression models for ordinal data, *Journal of the Royal Statistical Society Series B - Methodological*, *42*(2), 109-142.

McDaniel, P. A., M. P. Regan, E. Brooks, J. Boll, S. Bamdt, A. Falen, S. K. Young, and J. E. Hammel (2008), Linking fragipans, perched water tables, and catchment-scale hydrological processes, *Catena*, *73*(2), 166-173.

McDonnell, J. J. (1990), A rationale for old water discharge through macropores in a steep, humid catchment, *Water Resources Research*, *26*(11), 2821-2832.

McDonnell, J. J., B. L. McGlynn, K. Kendall, J. Shanley, and C. Kendall (1998), The role of near-stream riparian zones in the hydrology of steep upland catchments, in *Hydrology, Water Resources and Ecology in Headwaters*, edited by K. Kovar, U. Tappeiner, N. E. Peters and R. G. Craig, pp. 173-180.

McGlynn, B. L., J. J. McDonnell, J. B. Shanley, and C. Kendall (1999), Riparian zone flowpath dynamics during snowmelt in a small headwater catchment, *Journal of Hydrology*, *222*(1-4), 75-92.

McGlynn, B. L., J. J. McDonnell, J. Seibert, and C. Kendall (2004), Scale effects on headwater catchment runoff timing, flow sources, and groundwater-streamflow relations, *Water Resources Research*, *40*(7).

McNamara, J. P., D. Chandler, M. Seyfried, and S. Achet (2005), Soil moisture states, lateral flow, and streamflow generation in a semi-arid, snowmelt-driven catchment, *Hydrological Processes*, *19*(20), 4023-4038.

Metcalfe, R. A., and J. M. Buttle (1998), Statistical model of spatially distributed snowmelt rates in a boreal forest basin, *Hydrological Processes*, *12*(10-11), 1701-1722.

Mitchell, J. K. (1993), *Fundamentals of soil behavior*, 2 ed., 437 pp., John Wiley & Sons, Inc., New York.

Molicova, H., and P. Hubert (1994), Canopy influence on rainfall fields' microscale structure in tropical forests, *Journal of Applied Meteorology*, *33*(12), 1464-1467.

Monteith, S. S., J. M. Buttle, P. W. Hazlett, F. D. Beall, R. G. Semkin, and D. S. Jeffries (2006a), Paired-basin comparison of hydrological response in harvested and undisturbed hardwood forests during snowmelt in central Ontario: I. Streamflow, groundwater and flowpath behaviour, *Hydrological Processes*, *20*(5), 1095-1116.

Monteith, S. S., J. M. Buttle, P. W. Hazlett, F. D. Beall, R. G. Semkin, and D. S. Jeffries (2006b), Paired-basin comparison of hydrologic response in harvested and undisturbed hardwood forests during snowmelt in central Ontario: II. Streamflow sources and groundwater residence times, *Hydrological Processes*, *20*(5), 1117-1136.

Montgomery, D. R., W. E. Dietrich, and J. T. Heffner (2002), Piezometric response in shallow bedrock at CB1: Implications for runoff generation and landsliding, *Water Resources Research*, *38*(12).

Montgomery, D. R., W. E. Dietrich, R. Torres, S. P. Anderson, J. T. Heffner, and K. Loague (1997), Hydrologic response of a steep, unchanneled valley to natural and applied rainfall, *Water Resources Research*, *33*(1), 91-109.

Moore, R. D. (2005), Slug injection using salt in solution, *Streamline Watershed Management Bulletin*, *8*(2), 1-6.

Mosley, M. P. (1979), Sstreamflow generation in a forested watershed, New Zealand, *Water Resources Research*, *15*(4), 795-806.

Motoya, K., T. Yamazaki, and N. Yasuda (2001), Evaluating the spatial and temporal distribution of snow accumulation, snowmelts and discharge in a multi basin scale: an application to the Tohoku Region, Japan, *Hydrological Processes*, *15*(11), 2101-2129.

Noguchi, S., Y. Tsuboyama, R. C. Sidle, and I. Hosoda (2001), Subsurface runoff characteristics from a forest hillslope soil profile including macropores, Hitachi Ohta, Japan, *Hydrological Processes*, *15*(11), 2131-2149.

Ocampo, C. J., M. Sivapalan, and C. Oldham (2006), Hydrological connectivity of upland-riparian zones in agricultural catchments: Implications for runoff generation and nitrate transport, *Journal of Hydrology*, *331*(3-4), 643-658.

Oke, T. R. (1987), *Boundary layer climates*, 2 ed., 435 pp., Routledge, New York.

Penna, D., H. J. Tromp-van Meerveld, A. Gobbi, M. Borga, and G. Dalla Fontana (2011), The influence of soil moisture on threshold runoff generation processes in an alpine headwater catchment, *Hydrol. Earth Syst. Sci.*, *15*(3), 689-702.

Pohl, S., B. Davison, P. Marsh, and A. Pietroniro (2005), Modelling spatially distributed snowmelt and meltwater runoff in a small Arctic catchment with a hydrology land-surface scheme (WATCLASS), *Atmosphere-Ocean*, *43*(3), 193-211.

Prevost, M., R. Barry, J. Stein, and A. P. Plamondon (1991), Snowmelt modeling in a balsam fir forest - comparison between an energy-balance model and other simplified models, *Canadian Journal of Forest Research*, *21*(1), 1-10.

Price, A. G., and L. K. Hendrie (1983), Water motion in a deciduous forest during snowmelt, *Journal of Hydrology*, *64*(1-4), 339-356.

Quinn, P. F., K. J. Beven, and R. Lamb (1995), The ln(A/tanB) index: how to calculate it and how to use it within the topmodel framework, *Hydrological Processes*, *9*(2), 161-182.

R Development Core Team (2010), R: a language and environment for statistical computing, edited, R Foundation for Statistical Computing, Vienna, Austria.

Redding, T. E., and K. J. Devito (2008), Lateral flow thresholds for aspen forested hillslopes on the Western Boreal Plain, Alberta, Canada, *Hydrological Processes*, *22*(21), 4287-4300.

Redding, T. E., and K. J. Devito (2010), Mechanisms and pathways of lateral flow on aspen-forested, Luvisolic soils, Western Boreal Plains, Alberta, Canada, *Hydrological Processes*, *24*(21), 2995-3010.

Schwarz, G. (1978), Estimating the dimension of a model, *Annals of Statistics*, *6*(2), 461-464.

Seibert, J., K. Bishop, A. Rodhe, and J. J. McDonnell (2003), Groundwater dynamics along a hillslope: A test of the steady state hypothesis, *Water Resources Research*, *39*(1).

Sensoy, A., A. A. Sorman, A. E. Tekeli, A. U. Sorman, and D. C. Garen (2006), Point-scale energy and mass balance snowpack simulations in the upper Karasu basin, Turkey, *Hydrological Processes*, *20*(4), 899-922.

Shapiro, S. S., and M. B. Wilk (1965), An analysis of variance test for normality (complete samples), *Biometrika*, *52*(3 and 4), 591-611.

Shoji, T., and H. Kitaura (2006), Statistical and geostatistical analysis of rainfall in central Japan, *Computers & Geosciences*, *32*(8), 1007-1024.

Sidle, R. C., Y. Tsuboyama, S. Noguchi, I. Hosoda, M. Fujieda, and T. Shimizu (1995), Seaonal hydrologic response at various spatial scales in a small forested catchment, Hitachi-Ohta, Japan, *Journal of Hydrology*, *168*(1-4), 227-250.

Sidle, R. C., Y. Tsuboyama, S. Noguchi, I. Hosoda, M. Fujieda, and T. Shimizu (2000), Stormflow generation in steep forested headwaters: a linked hydrogeomorphic paradigm, *Hydrological Processes*, *14*(3), 369-385.

Sklash, M. G., and R. N. Farvolden (1979), The role of groundwater in storm runoff, *Journal of Hydrology*, *43*(1-4), 45-65.

Soil Moisture Equipment Corp (1991), 2800 KI Guelph Permeameter operating instructions, edited, p. 28, Santa Barbara, CA.

Somers, R. H. (1962), A new asymmetric measure of association for ordinal variables, *American Sociological Review*, *27*(6), 799-811.

Sommerfeld, R. A., R. C. Bales, and A. Mast (1994), Spatial statistics of snowmelt flow: data from lysimeters and aerial photos, *Geophysical Research Letters*, *21*(25), 2821-2824.

Stadler, D., H. Wunderli, A. Auckenthaler, and H. Fluhler (1996), Measurement of frost-induced snowmelt runoff in a forest soil, *Hydrological Processes*, *10*(10), 1293-1304.

Staelens, J., A. De Schrijver, K. Verheyen, and N. E. C. Verhoest (2006), Spatial variability and temporal stability of throughfall water under a dominant beech (Fagus sylvatica L.) tree in relationship to canopy cover, *Journal of Hydrology*, *330*(3-4), 651-662.

Stein, J., S. Proulx, and D. Levesque (1994), Forest floor frost dynamics during spring snowmelt in a boreal forested basin, *Water Resources Research*, *30*(4), 995-1007.

Stewart, I. T. (2009), Changes in snowpack and snowmelt runoff for key mountain regions, *Hydrological Processes*, *23*(1), 78-94.

Stewart, I. T., D. R. Cayan, and M. D. Dettinger (2005), Changes toward earlier streamflow timing across western North America, *Journal of Climate*, *18*(8), 1136-1155.

Sturm, M., and J. B. Johnson (1991), Natural convection in the subarctic snow cover, *Journal of Geophysical Research-Solid Earth and Planets*, *96*(B7), 11657-11671.

Szeftel, P. (2010), Stream-catchment connectivity and streamflow dynamics in montane landscapes, 153 pp, Univeristy of British Columbia, Vancouver, Canada.

Szeftel, P., R. D. Moore, and M. Weiler (2011), Influence of distributed flow losses and gains on the estimation of transient storage parameters from stream tracer experiments, *Journal of Hydrology*, *396*, 277-291.

Tabachnick, B. G., and L. S. Fidell (2007), *Using multivariate statistics*, 5 ed., 980 pp., Pearson Education, Inc., Boston, USA.

Taupin, J. D. (1997), Characterization of rainfall spatial variability at a scale smaller than 1 km in a semiarid area (region of Niamey, Niger), *Comptes rendus de l'Académie des sciences. Série 2. Sciences de la terre et des planètes*, *325*(4), 251-256.

Thompson, J. C., and R. D. Moore (1996), Relations between topography and water table depth in a shallow forest soil, *Hydrological Processes*, *10*, 1513-1525.

Thyer, M., J. Beckers, D. Spittlehouse, Y. Alila, and R. Winkler (2004), Diagnosing a distributed hydrologic model for two high-elevation forested catchments based on detailed stand- and basin-scale data, *Water Resources Research*, *40*(1), 1-20.

Toews, D. A. A., and D. R. Gluns (1986), Snow accumulation and ablation on adjacent forested and clearcut sites in Southeastern British Columbia, paper presented at Proceedings, 54th Western Snow Conference, 1986.

Tromp-van Meerveld, I., and J. J. McDonnell (2005), Comment to "Spatial correlation of soil moisture in small catchments and its relationship to dominant spatial hydrological processes, Journal of Hydrology 286 : 113-134", *Journal of Hydrology*, *303*(1-4), 307-312.

Tromp-van Meerveld, I., and J. J. McDonnell (2006a), Threshold relations in subsurface stormflow: 1. A 147-storm analysis of the Panola hillslope, *Water Resources Research*, *42*(2).

Tromp-van Meerveld, I., and J. J. McDonnell (2006b), Threshold relations in subsurface stormflow: 2. The fill and spill hypothesis, *Water Resources Research*, *42*(2).

Tromp-van Meerveld, I., and M. Weiler (2008), Hillslope dynamics modeled with increasing complexity, *Journal of Hydrology*, *361*(1-2), 24-40.

Tromp-van Meerveld, I., N. E. Peters, and J. J. McDonnell (2007), Effect of bedrock permeability on subsurface stormflow and the water balance of a trenched hillslope at the Panola Mountain Research Watershed, Georgia, USA, *Hydrological Processes*, *21*(6), 750-769.

Tsuboyama, Y., R. C. Sidle, S. Noguchi, S. Murakami, and T. Shimizu (2000), A zero-order basin Ð its contribution to catchment hydrology and internal hydrological processes, *Hydrological Processes*, *14*, 387-401.

Tsukamoto, Y. (1963), Storm discharge from an experimental watershed, *Journal of Japanese Society of Forestry*, *45*, 186-190.

Walter, M. T., E. S. Brooks, D. K. McCool, L. G. King, M. Molnau, and J. Boll (2005), Process-based snowmelt modeling: does it require more input data than temperature-index modeling?, *Journal of Hydrology*, *300*(1-4), 65-75.

Watson, F. G. R., W. B. Newman, J. C. Coughlan, and R. A. Garrott (2006), Testing a distributed snowpack simulation model against spatial observations, *Journal of Hydrology*, *328*, 453-466.

Weiler, M., and F. Naef (2003), An experimental tracer study of the role of macropores in infiltration in grassland soils, *Hydrological Processes*, *17*, 477-493.

Weiler, M., and J. McDonnell (2004), Virtual experiments: a new approach for improving process conceptualization in hillslope hydrology, *Journal of Hydrology*, *285*(1-4), 3-18.

Whipkey, R. Z. (1965), Subsurface stormflow from forested slopes, *Bulletin of the International Association of Scientific Hydrology*, *10*(2), 74-85.

Whitaker, A. C., and H. Sugiyama (2005), Seasonal snowpack dynamics and runoff in a cool temperate forest: lysimeter experiment in Niigata, Japan, *Hydrological Processes*, *19*(20), 4179-4200.

Wigmosta, M. S., L. W. Vail, and D. P. Lettenmaier (1994), A distributed hydrology-vegetation model for complex terrain, *Water Resources Research*, *30*(6), 1665-1679.

Wigmosta, M. S., B. Nijssen, and P. Storck (2002), The distributed hydrology soil vegetation model, in *Mathematical Models of Small Watershed Hydrology and Applications*, edited by V. P. Singh and D. Frevert, pp. 7-42, Water Resources Publications, Highland Ranch, CO.

Williams, M. W., R. Sommerfeld, S. Massman, and M. Rikkers (1999), Correlation lengths of meltwater flow through ripe snowpacks, Colorado Front Range, USA, *Hydrological Processes*, *13*(12-13), 1807-1826.

Winkler, R. D., D. L. Spittlehouse, and D. L. Golding (2005), Measured differences in snow accumulation and melt among clearcut, juvenile, and mature forests in Southern British Columbia, *Hydrological Processes*, *19*(1), 51-62.

Yamanaka, T., A. Takeda, and J. Shimada (1998), Evaporation beneath the soil surface: some observational evidence and numerical experiments, *Hydrological Processes*, *12*(13-14), 2193-2203.

Zaslavsky, D., and G. Sinai (1981a), Surface Hydrology: V - In-surface transient flow, *Journal of the Hydraulics Division-ASCE*, *107*(1), 65-93.

Zaslavsky, D., and G. Sinai (1981b), Surface Hydrology: III - Causes of lateral flow, *Journal of the Hydraulics Division-ASCE*, *107*(1), 37-52.